AD_____

Award Number: DAMD17-98-1-8102

TITLE: Regulation of Apoptosis by Caspases

PRINCIPAL INVESTIGATOR: Junying Yuan, Ph.D.

CONTRACTING ORGANIZATION: Harvard College
Cambridge, Massachusetts 02138-3800

REPORT DATE: September 2001

TYPE OF REPORT: Final

PREPARED FOR: U.S. Army Medical Research and Materiel Command
Fort Detrick, Maryland 21702-5012

REPORT DOCUMENTATION PAGE

Form Approved
OMB No. 074-0188

1. AGENCY USE ONLY (Leave blank)	2. REPORT DATE	3. REPORT TYPE AND DATES COVERED
	September 2001	Final (1 Sep 98 - 31 Aug 01)

4. TITLE AND SUBTITLE
Regulation of Apoptosis by Caspases

5. FUNDING NUMBERS
DAMD17-98-1-8102

6. AUTHOR(S)
Junying Yuan, Ph.D.

7. PERFORMING ORGANIZATION NAME(S) AND ADDRESS(ES)

Harvard College
Cambridge, Massachusetts 02138-3800

E-Mail: jyuan@hms.harvard.edu

8. PERFORMING ORGANIZATION REPORT NUMBER

9. SPONSORING / MONITORING AGENCY NAME(S) AND ADDRESS(ES)

U.S. Army Medical Research and Materiel Command
Fort Detrick, Maryland 21702-5012

10. SPONSORING / MONITORING AGENCY REPORT NUMBER

11. SUPPLEMENTARY NOTES
Report contains color

12a. DISTRIBUTION / AVAILABILITY STATEMENT
Approved for Public Release; Distribution Unlimited

12b. DISTRIBUTION CODE

13. ABSTRACT *(Maximum 200 Words)*

Apoptosis is a cellular suicide mechanism critical for removing cells that may be harmful or no longer needed. Abnormal apoptosis may result in cancer and neural degenerative diseases such as Alzheimer's disease. Caspases are a family of cysteine proteases that play entral roles in mediating apoptosis. The goal of this idea award is to illustrate the mechanism of apoptosis regulated by caspases. In the past three years, this idea award allowed us 1) to identify an important caspase substrate, Bid, in mediating caspase signal transduction from cytoplasmic membrane to mitochondria (Li et al 1998); 2) to elucidate the functional role of a kinase, LKB1, in activating p53-dependent apoptosis (Karuman et al. 2001); 3) to develop a high throughput screen to identify small molecule inhibitors of BH3 domain mediated protein-protein interaction that are critical for Bcl-2 family of proteins to regulate apoptosis (Degterev et al. 2001).

14. SUBJECT TERMS	15. NUMBER OF PAGES
Breast Cancer	53
	16. PRICE CODE

17. SECURITY CLASSIFICATION OF REPORT	18. SECURITY CLASSIFICATION OF THIS PAGE	19. SECURITY CLASSIFICATION OF ABSTRACT	20. LIMITATION OF ABSTRACT
Unclassified	Unclassified	Unclassified	Unlimited

Table of Contents

Introduction

Apoptosis, or programmed cell death, is a cellular suicide mechanism critical for the well being of animals. Malfunction of this cell-intrinsic suicide pathway may result in cancer, neurodegenerative diseases, or other pathological conditions. My laboratory was the first to demonstrate the critical role of caspases in regulating apoptosis (Cryns and Yuan, 1998). The mammalian families of caspases and Bcl-2 proteins are homologues of C. elegans cell death gene products Ced-3 and Ced-9 which are critical for cells to undergo programmed cell death in C. elegans. To understand the mechanisms of apoptosis signal transduction, we initiated three separate projects closely related to the goals in the original proposal and they have been independently successful and resulted in four high profile publications (Li et al. 1998; Chou et al. 1998; Karuman et al. 2001; Degterev et al. 2001. Attached as Appendices).

Project I: Identification of a caspase-8 substrate that mediates the signal transduction from the cytoplasmic membrane to mitochondria.

Background: Caspase cascades have been implicated in both the initiation and execution of apoptosis (Cryns and Yuan, 1998). Fas induced apoptosis pathway is the best characterized example of such pathways. The Fas apoptosis pathway contributes to the deletion of unwanted mature T cells, cytotoxic T lymphocyte-mediated cytotoxicity, immune privilege in specific tissues and cancers, and autoimmune diseases. Cross-linking of the Fas receptor by engagement of the Fas ligand results in the formation of the so-called death-inducing signal complex (DISC), which consists of the adapter protein FADD (also known as MORT1) and caspase-8. The formation of DISC leads to the activation of caspase-8. In certain cells, activated caspase-8 directly cleaves caspase-3 and caspase-7 that then complete the execution of apoptosis. In other cell types, the activated protease-8 induces mitochondrial damage and then cell death. The study described here elucidated the mechanism by which the apoptotic signal transmits from cytoplasmic membrane to mitochondria.

Project II: Illustrating the molecular mechanism of a Ser/Thr kinase, LKB1, in regulating p53-dependent apoptosis.

Background: The LKB1 gene encodes a Ser/Thr kinase which functions as a tumor suppressor: loss-of-heterozygosity in this gene is responsible for majority of Peutz-Jegher patients who are heterozygous carriers of LKB1 loss-of-function mutation (Hemminki et al., 1998; Jenne et al., 1998). Peutz-Jegher disease is characterized by hamartomatous polyps in the small bowel, pigmented macules of the buccal mucosa, lips, fingers and toes and dramatically increased risks to develop cancers later in life (Giardiello et al., 1987; Jeghers et al., 1949; Peutz, 1921; Spigelman et al., 1989). LKB1 also functions to suppress breast cancer: patients with Peutz-Jegher syndrome have a significantly elevated risk for breast cancer (Boardman et al., 2000). The mechanism by which LKB1 regulates tumor formation was not clear at the time. The described here illustrates the mechanism of LKB1 function.

Project III: Identification of small molecule chemical inhibitors of BH3 domain interaction in Bcl-2 family.

Background: Antiapoptotic Bcl-2 family of proteins, which are frequently overexpressed in a variety of tumors such as prostate tumors, B cell lymphomas and

melanomas, were demonstrated by a wide variety of studies to protect cells from toxic effects of chemotherapeutic drugs and poor prognosis in treatment of various forms of cancer due to chemoresistance often correlates with the ratios of pro- and antiapoptotic proteins (Reed et al. 1995). On the other hand proapoptotic family members such as Bax (McCurrach et al. 1997; Miyashita et al. 1995) and Noxa (Oda et al. 2000) were shown to be direct transcriptional targets of most frequently mutated tumor suppressor protein p53. In addition recent genetic studies showed that inactivation of Bax directly contributes to tumorigenesis (McCurrach et al. 1997; Zhang et al. 2000). Consistent with these observations various antisense strategies (antisense oligonucleotides, dominant negative family members, ribozymes) targeting antiapoptotic Bcl-2 family members were found to show significant promise as novel anticancer agents both *in vitro* and *in vivo* in a variety of tumor models (Clarke et al. 1995; Baba et al. 2000; Miayake et al. 2000; Jansen et al. 1998; Gibson et al. 2000).

Dimerization of Bcl-2 family members through the BH3 domains was previously shown to be the central function of these proteins (Gross et al. 1998). Underscoring critical role of this interaction for the regulation of apoptosis synthetic BH3 domain containing peptide was shown to induce apoptosis in oocyte lysates, cultured cells and *in vivo* xenografts of human leukemia HL-60 cells (Holinger et al. 1999; Wang et al. 2000; Cosulich et al. 1997). The goal of this project is to identify small molecule inhibitors that can inhibit the BH3 domain interaction. Such molecules may be used as lead compounds to develop drugs that reduce chemoresistance of cancers.

Body

Project I: Identification of caspase-8 substrate that mediates the signal transduction from the cytoplasmic membrane to mitochondria.

Accomplished: We demonstrated that Bid is a critical intracellular signal transducer that mediates the death signal from cytoplasmic membrane to the mitochondria (Li et al. 1998) and we demonstrated the structural basis by which Bid functions (Chou et al. 1998). It was puzzling at time how caspase-8 activates the mitochondrial pathway of apoptosis as the activation of caspase-8 must be localized to the cytoplasmic membrane where Fas receptor is located. Our work (Li et al. 1998; Chou et al. 1998) provided the missing piece for the puzzle by demonstrating that activated caspase-8 cleaves Bid, which is diffusely present in the cytoplasm, and the cleaved Bid translocates to the mitochondria to induce mitochondrial damage.

Project II: Illustrating the molecular mechanism of a Thr/Ser kinase, LKB1, in regulating p53-dependent apoptosis.

Accomplished: We demonstrated that LKB1 is a mediator of p53 dependent apoptosis and involved in regulating spontaneous turnover of intestinal epithelial cells (Karuman et al., 2001). With the exception of PTEN, genes that are previously known to be involved in predisposition to breast cancer encode proteins, such as BRCA1, BRCA2 and p53, all function in the cellular response to DNA damage. There is no indication, however, that LKB1 is involved in the cellular response to DNA damage; in fact, we found that expression of a kinase-dead dominant negative mutant of LKB1 inhibited

apoptosis induced by agents that disrupt microtubule stability, such as taxol and vincristine, but not agents that cause DNA damage. Thus, LKB1 may represent a novel pathway which predisposes breast cancers through monitoring microtubule dynamics. This makes it mechanistically very interesting to examine the role of LKB1 in normal breast development, involution and tumorigenesis. Furthermore, this work may provide a critical missing link between the tumor suppression and spontaneous mammary epithelial cell turnover.

Project III: Identification of small molecule chemical inhibitors of BH3 domain interaction in Bcl-2 family.

Accomplished: We successfully identified two series of compounds that inhibit the BH3 domain interaction in vitro and in cultured cells (Degterev et al., 2001). Using high throughput screening of small molecule library we selected seven related inhibitors of the interaction between antiapoptotic Bcl-2 family member Bcl-xL and BH3 peptide from proapoptotic protein Bak. These compounds fall into two structural classes (4 BH3I-1 compounds and 3 BH3I-2 compounds) and therefore represent the perfect basis for further SAR studies. Using a variety of *in vitro* approaches (pulldown, mass spec, NMR, protein localization studies and cell-based FRET) we determined that these compounds are capable of specifically interfering with heterodimerization of both Bcl-2 and Bcl-xL *in vitro* and in living cells. Cell based studies further demonstrated that BH3Is are able to induce apoptosis in a broad range of cells and their ability to induce cell death is dependent on disruption of Bcl-2 interactions. Additional experiments demonstrated inactivation of the antiapoptotic function of Bcl-xL in the cells treated with BH3Is. NMR analyses undertaken in collaboration with the laboratory of Gerhard Wagner at the Department of Biological Chemistry and Molecular Pharmacology of Harvard Medical School provided the mechanistic basis for the BH3Is activity. BH3Is were found to bind to the same hydrophobic groove as the one occupied by BH3 peptide. Additional evidence suggested that the compounds might induce the same conformational change in Bcl-xL as the one induced by peptide binding. Overall, these results proved that BH3Is act as small molecule mimetics of the proapoptotic BH3 domain and induce cell death through inactivation of the heterodimerization-dependent antiapoptotic function of Bcl-2/Bcl-xL *in vitro* and in the cells.

Personnel supported by this award:
Junying Yuan (PI)
Alexei Degterev (Postdoctoral fellow)
Honglin Li (Postdoctoral fellow)
Philip Karuman (Graduate student)
Sungkwan An (Postdoctoral fellow)
Odmara Baretto-Chang (Research assistant)

Key Research Accomplishments

1. Identification of Bid as a key intracellular mediator of Fas/TNF induced apoptosis.

2. Elucidation of structural basis of Bid's action in inducing apoptosis.

3. Illustration of the molecular mechanism by which LKB1 regulates p53-dependent apoptosis.

4. Identification of small molecule inhibitors of the BH3 domain interaction in the Bcl-2 family.

Reportable Outcomes (papers attached as appendices)

Li H, Zhu H, Xu C-J, and Yuan J. Cleavage of BID by caspase 8 mediates the mitochondrial damage in the Fas pathway of apoptosis. Cell. 1998. 94, 491-501.

Chou JJ, Li H, Salveson G, Yuan J and Wagner G. Solution structure of Bid, an intracellular amplifier of apoptosis. 1999. Cell. 96, 615-624.

Karuman P, Gozani O, Odze RD, Zhou XC, Zhu H, Shaw R, Brien TP, Bozzuto CD, Ooi D, Cantley LC, and Yuan J. The Peutz-Jegher gene product LKB1 is a mediator of p53-dependent cell death. Molecular Cell. 2001. 7, 1307-1319.

Degterev A, Lugovskoy, Cardone M, Mulley B, Wagner G, Mitchison T and Yuan J. Identification of small molecular inhibitors of BH3 and Bcl-xL interaction. Nature Cell Biol. 2001. 3, 173-182.

Conclusions

This award has made it possible for us to characterize the molecular mechanism of signal transduction in apoptosis mediated by caspases using cellular, biochemical and chemical approaches. We showed that Bid is a critical intracellular signal transducer that mediates apoptotic signals from cytoplasmic membrane to mitochondria in Fas mediated apoptosis. LKB1, a tumor suppressor and Ser/Thr kinase, is involved in regulating p53-dependent apoptosis. Finally, we identified two series of small molecule inhibitors of protein-protein interaction mediated by the BH3 domain of the Bcl-2 family which may be used as lead compounds to develop drugs in reducing the chemoresistance of cancer cells. In summary, this idea award has allowed us to turn a number of our scientific "ideas" into scientific facts.

References

1. Baba, M., Iishi, H., and Tatsuta, M., In vivo electroporetic transfer of bcl-2 antisense oligonucleotide inhibits the development of hepatocellular carcinoma in rats, *Int J Cancer, 85*, 260 (2000).

2. Boardman LA, Pittelkow MR, Couch FJ, Schaid DJ, McDonnell SK, Burgart LJ, Ahlquist DA, Carney JA, Schwartz DI, Thibodeau SN, Hartmann LC. Association of Peutz-Jeghers-like mucocutaneous pigmentation with breast and gynecologic carcinomas in women. Medicine (Baltimore). 79, 293-8. (2000).

3. Chou JJ, Li H, Salveson G, Yuan J and Wagner G. Solution structure of Bid, an intracellular amplifier of apoptosis. 1999. Cell. 96, 615-624.

4. Clarke, M. F., Apel, I. J., Benedict, M. A., Eipers, P. G., Sumantran, V., Gonzalez-Garcia, M., Doedens, M., Fukunaga, N., Davidson, B., Dick, J. E., and et al., A

recombinant bcl-x s adenovirus selectively induces apoptosis in cancer cells but not in normal bone marrow cells, *Proc Natl Acad Sci U S A, 92*, 11024 (1995).

5. Cosulich, S. C., Worrall, V., Hedge, P. J., Green, S., and Clarke, P. R., Regulation of apoptosis by BH3 domains in a cell-free system, *Curr Biol, 7*, 913 (1997).

6. Cryns, V. L. and Yuan, J.. Proteases to die for. Gen. & Dev. *12*, 1551-1570. (1998).

7. Degterev, A., Lugovskoy, A., Cardone, M., Mulley, B., Wagner, G., Mitchison, T., and Yuan, J., Identification of small-molecule inhibitors of interaction between the BH3 domain and Bcl-xL, *Nat Cell Biol, 3*, 173 (2001).

8. Giardiello, F.M. *et al.* Increased risk of cancer in the Peutz-Jeghers syndrome. *N Engl J Med* **316**, 1511-1514 (1987).

9. Gibson, S. A., Pellenz, C., Hutchison, R. E., Davey, F. R., and Shillitoe, E. J., Induction of apoptosis in oral cancer cells by an anti-bcl-2 ribozyme delivered by an adenovirus vector, *Clin Cancer Res, 6*, 213 (2000).

10. Gross, A., Jockel, J., Wei, M. C., and Korsmeyer, S. J., Enforced dimerization of BAX results in its translocation, mitochondrial dysfunction and apoptosis, *Embo J, 17*, 3878 (1998).

11. Hemminki, A. *et al.* A serine/threonine kinase gene defective in Peutz-Jeghers syndrome. *Nature* **391**, 184-187 (1998).

12. Holinger, E. P., Chittenden, T., and Lutz, R. J., Bak BH3 peptides antagonize Bcl-xL function and induce apoptosis through cytochrome c-independent activation of caspases, *J Biol Chem, 274*, 13298 (1999).

13. Jansen, B., Schlagbauer-Wadl, H., Brown, B. D., Bryan, R. N., van Elsas, A., Muller, M., Wolff, K., Eichler, H. G., and Pehamberger, H., bcl-2 antisense therapy chemosensitizes human melanoma in SCID mice, *Nat Med, 4*, 232 (1998).

14. Jeghers, H., McKusick, V.A. & Karz, K.H. Generalized intestinal polyposis and melanin spots of the oral mucosa, lips and digits: a syndrome of disgnostic significance. *N. Engl. J. Med.* **241**, 992-1005 (1949).

15. Jenne, D.E. *et al.* Peutz-Jeghers syndrome is caused by mutations in a novel serine threonine kinase. *Nature* **391**, 184-187 (1998).

16. Karuman P, Gozani O, Odze RD, Zhou XC, Zhu H, Shaw R, Brien TP, Bozzuto CD, Ooi D, Cantley LC, and Yuan J. The Peutz-Jegher gene product LKB1 is a mediator of p53-dependent cell death. Molecular Cell. 2001. 7, 1307-1319.

17. Li H, Zhu H, Xu C-J, and Yuan J. Cleavage of BID by caspase 8 mediates the mitochondrial damage in the Fas pathway of apoptosis. Cell. 1998. 94, 491-501.

18. McCurrach, M. E., Connor, T. M., Knudson, C. M., Korsmeyer, S. J., and Lowe, S. W., bax-deficiency promotes drug resistance and oncogenic transformation by attenuating p53-dependent apoptosis, *Proc Natl Acad Sci U S A, 94*, 2345 (1997).

19. Miayake H, Tolcher A, Gleave ME. Chemosensitization and delayed androgen-independent recurrence of prostate cancer with the use of antisense Bcl-2 oligodeoxynucleotides. J Natl Cancer Inst. 92, 34-41. (2000).

20. Miyashita, T., and Reed, J. C., Tumor suppressor p53 is a direct transcriptional activator of the human bax gene, *Cell, 80*, 293 (1995).

21. Oda, E., Ohki, R., Murasawa, H., Nemoto, J., Shibue, T., Yamashita, T., Tokino, T., Taniguchi, T., and Tanaka, N., Noxa, a BH3-only member of the Bcl-2 family and candidate mediator of p53-induced apoptosis, *Science, 288*, 1053 (2000).

22. Peutz, J.L. On a very remarkable case of familial polyposis of the mucous membrane of the intestinal tract and nasopharynx accompanied by peculiar pigmentation of the skin and mucous membrane. *Ned. Tijdschr. Geneeskd.* **10**, 134-146 (1921).

23. Reed, J. C., Bcl-2: prevention of apoptosis as a mechanism of drug resistance, *Hematol Oncol Clin North Am, 9*, 451 (1995).

24. Spigelman, A.D., Murday, V. & Phillips, R.K. Cancer and the Peutz-Jeghers syndrome. *Gut* 30, 1588-1590 (1989).

25. Wang, J. L., Zhang, Z. J., Choksi, S., Shan, S., Lu, Z., Croce, C. M., Alnemri, E. S., Korngold, R., and Huang, Z., Cell permeable Bcl-2 binding peptides: a chemical approach to apoptosis induction in tumor cells, *Cancer Res, 60*, 1498 (2000).

26. Zhang, L., Yu, J., Park, B. H., Kinzler, K. W., and Vogelstein, B., Role of BAX in the apoptotic response to anticancer agents, *Science, 290*, 989 (2000).

Appendices

I. Li H, Zhu H, Xu C-J, and Yuan J. Cleavage of BID by caspase 8 mediates the mitochondrial damage in the Fas pathway of apoptosis. Cell. 1998. 94, 491-501.

II. Chou JJ, Li H, Salveson G, Yuan J and Wagner G. Solution structure of Bid, an intracellular amplifier of apoptosis. 1999. Cell. 96, 615-624.

III. Karuman P, Gozani O, Odze RD, Zhou XC, Zhu H, Shaw R, Brien TP, Bozzuto CD, Ooi D, Cantley LC, and Yuan J. The Peutz-Jegher gene product LKB1 is a mediator of p53-dependent cell death. Molecular Cell. 2001. 7, 1307-1319.

IV. Degterev A, Lugovskoy, Cardone M, Mulley B, Wagner G, Mitchison T and Yuan J. Identification of small molecular inhibitors of BH3 and Bcl-xL interaction. Nature Cell Biol. 2001. 3, 173-182.

Cell, Vol. 94, 491–501, August 21, 1998, Copyright ©1998 by Cell Press

Cleavage of BID by Caspase 8 Mediates the Mitochondrial Damage in the Fas Pathway of Apoptosis

Honglin Li, Hong Zhu, Chi-jie Xu, and Junying Yuan*
Department of Cell Biology
Harvard Medical School
Boston, Massachusetts 02115

Summary

We report here that BID, a BH3 domain–containing proapoptotic Bcl2 family member, is a specific proximal substrate of Casp8 in the Fas apoptotic signaling pathway. While full-length BID is localized in cytosol, truncated BID (tBID) translocates to mitochondria and thus transduces apoptotic signals from cytoplasmic membrane to mitochondria. tBID induces first the clustering of mitochondria around the nuclei and release of cytochrome c independent of caspase activity, and then the loss of mitochondrial membrane potential, cell shrinkage, and nuclear condensation in a caspase-dependent fashion. Coexpression of $Bclx_L$ inhibits all the apoptotic changes induced by tBID. Our results indicate that BID is a mediator of mitochondrial damage induced by Casp8.

Introduction

Caspase 8 (Casp8), a member of a mammalian caspase family, has been demonstrated to play a key role in mediating Fas-induced apoptosis (Boldin et al., 1996; Fernandes-Alnemri et al., 1996; Muzio et al., 1996; Cryns and Yuan, 1998). Cross-linking of the Fas receptor by engagement of the Fas ligand or agonistic antibodies results in the formation of so-called death-inducing signal complex (DISC), which includes adaptor protein FADD/MORT-1 and Casp8 (Kischkel et al., 1995). The formation of the DISC leads to the activation of Casp8, an initiator of the downstream apoptotic process that includes the activation of Casp3, −6, and −7 and mitochondrial damage (Salvesen and Dixit, 1997). Recently, Scaffidi et al. (1998) have shown that there may be two alternative Fas signaling pathways. In so-called Fas type I cells, a relatively large amount of Casp8 is recruited to DISC upon receptor cross-linking. The activated Casp8 propagates the apoptotic signal by activating downstream caspases through proteolytic cleavage, as well as by triggering mitochondrial damages that in turn activate a proteolytic cascade. In so-called Fas type II cells, a small amount of Casp8 is recruited to the DISC upon receptor cross-linking, and activated Casp8 mediates downstream apoptotic events mainly through inducing mitochondrial damage. These studies, however, did not reveal how active Casp8 induces mitochondrial damage.

A critical role of mitochondria in mediating apoptotic signal transduction pathway has been demonstrated recently (Vander Heiden et al., 1997). Biochemical and structural changes of mitochondria in apoptosis include mitochondrial swelling, disruption of mitochondrial outer membrane, mitochondrial depolarization, and the release of cytochrome c (Liu et al., 1996; Vander Heiden et al., 1997). The release of cytochrome c may trigger the interaction of Apaf1, a mammalian CED-4 homolog, and Casp9, which in turn results in the activation of Casp9 (Li et al., 1997c; Zou et al., 1997). Activated Casp9 then cleaves and activates pro-Casp3, an event that leads to the cleavage of other death substrates, cellular and nuclear morphological changes, and ultimately, cell death. An active site mutant of Casp9 (C287A) is able to block activation of Casp3 by Casp9 (Li et al., 1997c). Overexpression of $Bcl2/Bclx_L$ has been shown to block all apoptosis-induced mitochondrial changes (Kluck et al., 1997; Vander Heiden et al., 1997; Yang et al., 1997). Since mitochondrial damage is an obligatory step in mediating the Fas signaling in type II but not type I cells, $Bcl2/Bclx_L$ can inhibit Fas-induced apoptosis in type II but not type I cells (Scaffidi et al., 1998).

Bcl2 and $Bclx_L$, two members of the Bcl2 family, prevent apoptosis induced by a variety of death stimuli (Merry and Korsmeyer, 1997). They are localized mainly to the outer mitochondrial, nuclear membranes and endoplasmic reticular membrane through their carboxy-terminal membrane anchorage domains. Both of them contain the Bcl2 homology domains designated BH1, BH2, BH3, and BH4, all of which are essential for the antiapoptotic activity of $Bcl2/Bclx_L$ (Merry and Korsmeyer, 1997; Huang et al., 1998). The Bcl2 family also includes a class of BH3 domain–containing death agonists, which may promote apoptosis by inhibiting the death antagonist members of the Bcl2 family (Merry and Korsmeyer, 1997). Mutational analyses indicate that the BH3 domain of death agonists is required for their proapoptotic activity and their interactions with $Bcl2/Bclx_L$ (Chittenden et al., 1995; Wang et al., 1996; Kelekar et al., 1997). It was recently reported that in a cell-free *Xenopus* oocyte system, the BH3 domain alone can induce cytochrome c release and the activation of caspases that can be inhibited by Bcl2 (Cosulich et al., 1997). Thus, these BH3-containing death agonists may play an important regulatory role in mediating apoptotic mitochondrial damage. It is not clear, however, how these BH3 domain–containing proteins fit into the signal transduction pathway of apoptosis and how they act to induce mitochondrial damage.

In this study, we demonstrate that BID, a death agonist member of the $Bcl2/Bclx_L$ family (Wang et al., 1996), is a specific proximal substrate of Casp8 in the Fas signaling pathway. Cleavage of BID by Casp8 releases its potent proapoptotic activity, which in turn induces mitochondrial damage and, ultimately, cell shrinkage and nuclear condensation. Expression of $Bclx_L$ inhibits all the apoptotic phenotypes induced by truncated BID (tBID), whereas caspase inhibitors inhibit the loss of mitochondrial membrane potential, cell shrinkage, and nuclear condensation, but not mitochondrial clustering and cytochrome c release. Our study identified the first specific proximal substrate of Casp8 in the Fas pathway and a critical missing link between the activation of Casp8 and mitochondrial damage.

*To whom correspondence should be addressed.

Results

BID Is a Specific Substrate of Caspase 8 In Vitro

To identify the substrates of Casp8, we transcribed and translated in vitro a small pool mouse spleen cDNA library in the presence of ^{35}S-methionine, using the methods of Lustig et al. (1997). The radioactively labeled protein pools were incubated with either recombinant Casp8 in bacterial lysates or control lysates and analyzed by SDS-PAGE. cDNA small pools (1700) were screened, and the individual cDNA clones containing candidate Casp8 substrates were isolated from positive pools. In pool #814, a 24 kDa protein disappeared after incubation with Casp8 (Figure 1A). This pool was subdivided, and the cDNA encoding this 24 kDa protein was isolated and sequenced. The 24 kDa protein was identified to be murine BID, a proapoptotic Bcl2 family member whose homology to other members of the family is limited to a BH3 domain (Wang et al., 1996). N-terminal T7-tagged BID was cleaved by Casp8 into 15 kDa and 14 kDa fragments in vitro (due to the different contents of methionine in these two fragments, the two ^{35}S-Met-labeled fragments did not appear to be stoichiometric) (Figure 1B). As the majority of the caspase substrates identified so far are the substrates of Casp3, we determined the specificity of BID cleavage by Casp3 and −8, using PARP as a control. ^{35}S-labeled proteins were incubated with limited amounts of Casp3 and −8 for different lengths of time, and the cleavage efficiencies were evaluated by SDS-PAGE. As shown in Figure 1B, Casp8 cleaved most of BID but very little of PARP in 15 min, while the contrary was true for Casp3. This in vitro cleavage result indicates that BID is a much better substrate of Casp8 than of Casp3.

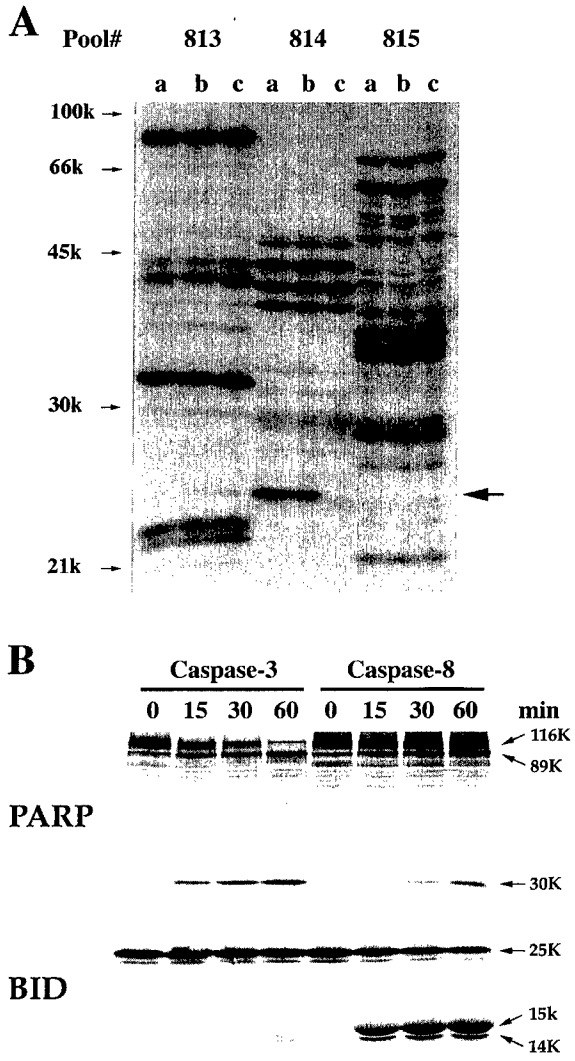

Figure 1. BID Is a Preferred Substrate of Caspase 8 In Vitro

(A) Primary screening of caspase substrates by small pool in vitro expression cloning. Different pools of ^{35}S-labeled proteins were incubated with bacterial lysates containing either no caspase (a), Casp2 (b), or Casp8 (c) for 2 hr at 37°C. The reactions were terminated and analyzed by 12% SDS-PAGE. An arrow points to a band, later identified as murine BID, that disappeared in the presence of Casp8.

(B) BID is a better substrate of Casp8 than of Casp3. ^{35}S-labeled N-terminal T7-tagged BID was incubated with either Casp3 or Casp8 for indicated time periods, and the cleavage products were analyzed by 15% SDS-PAGE.

BID Is Cleaved In Vivo during Fas- and TNFα-Induced Apoptosis

To examine the cleavage of BID in vivo, we generated a polyclonal antibody against human BID protein. Using this antibody for Western blots, we found that when Jurkat cells were induced to undergo apoptosis by anti-Fas antibody, BID was initially cleaved to a 15 kDa fragment and further to a 13 kDa fragment. The cleavage event occurred in the early stage of apoptosis and was comparable to the time courses of Casp7, -8 activation and PARP cleavage in Jurkat cells (Figure 2A). To rule out the possibility that the 15 kDa and 13 kDa BID fragments are newly synthesized novel protein products recognized by the BID antibody, we induced Jurkat cells to undergo apoptosis in the presence of cycloheximide (CHX), an inhibitor of protein synthesis, and anti-Fas antibody. The cleavage patterns of BID, Casp7, −8, and PARP were examined by immunoblotting. We found that the appearance of the BID fragments was not altered by the presence of CHX (data not shown). Thus, the 15 kDa and 13 kDa BID fragments are likely to be the cleavage products of full-length BID induced by apoptosis. The amount of the 15 kDa peptide was constant during the time course of apoptosis, possibly due to its rapid conversion to the 13 kDa peptide and subsequent degradation. The cleavage of BID in Fas-induced apoptosis was inhibitable by 100 μM of zVAD-fmk, a peptide inhibitor of caspases (Figure 2B). To confirm the cleavage of BID in vivo and to determine the approximate site of cleavage, we transiently transfected C-terminal Flag-tagged murine BID into HeLa cells, which were then treated by TNFα and CHX to induce the activation of Casp8 and apoptosis. A Western blot of the cell lysate was blotted by anti-FLAG antibody (Figure 2C). A 16 kDa Flag-tagged peptide was present in the apoptotic lysate and absent in the control lysate, confirming our in vivo cleavage data and suggesting that the cleavage site of BID is in the N-terminal portion of the protein.

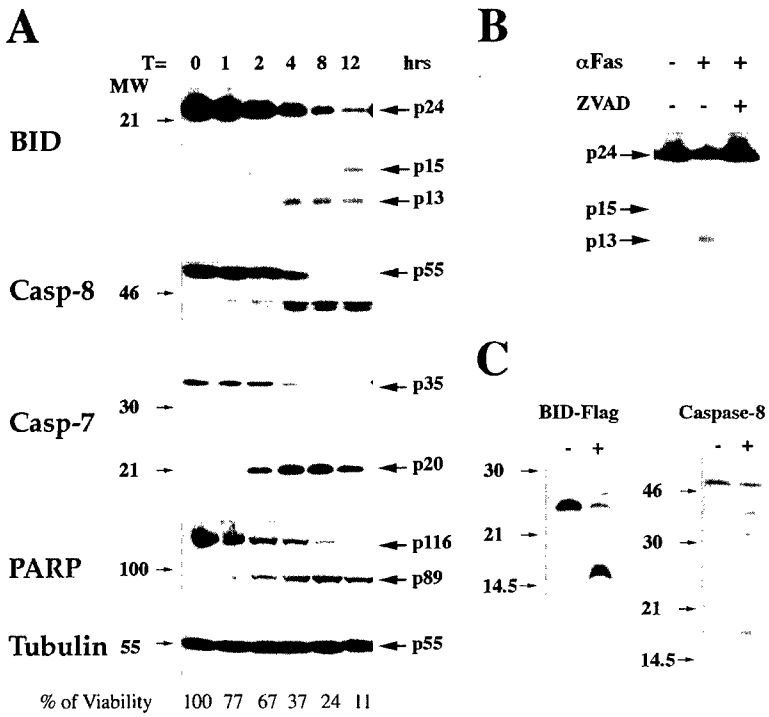

Figure 2. BID Is Cleaved In Vivo during Fas- and TNFα-Induced Apoptosis

(A) Time course of BID cleavage in Fas-induced apoptosis of Jurkat cells. The cell viability was determined by MTT assay and shown at the bottom of the figure.

(B) BID cleavage was inhibited with zVAD-fmk. Jurkat cells were preincubated with 100 μM of zVAD-fmk for 30 min and then incubated with anti-Fas antibody for 5 hr. Total cell lysates were prepared and blotted with anti-BID antibody. Arrows point to the full-length BID (p24) and two cleavage products, p15 and p13.

(C) C-terminal Flag-tagged BID was cleaved in TNFα-induced apoptosis of HeLa cells. Twenty-four hours after transient transfection of BID-Flag, HeLa cells were treated with either 1 μg/ml CHX alone (−) or 10 ng/ml TNFα and 1 μg/ml CHX (+) for 4 hr. Total cell lysates were subjected to Western blotting using either anti-Flag or anti-Casp8 antibodies. The molecular weight standard is shown on the left. A 16 kDa fragment is present specifically in the apoptotic HeLa cells transfected with BID-flag.

Determination of Cleavage Sites of BID

Two potential caspase cleavage sites reside in the N-terminal portion of murine BID: ^{56}Leu-Gln-Thr-Asp-Gly^{60} (LQTDG) and ^{72}Ile-Glu-Pro-Asp-Ser^{76} (IEPDS) (the corresponding sequences for human BID are ^{57}LQTDG^{61} and ^{72}IEADS^{76}). They match perfectly with the preferred cleavage sites for Casp8 and granzyme B, respectively, as determined by combinatorial peptide library screening (Thornberry et al., 1997). To confirm that they are indeed the cleavage sites for Casp8 and granzyme B, we mutated the two Asp residues to Glu either individually or both (namely mutant D59E, D75E, and DM). As shown in Figure 3A, N-terminal T7-tagged wild-type BID was completely cleaved by Casp1, -8, and granzyme B, and partially cleaved by Casp2 and −3. D59E BID mutant was only cleaved by granzyme B, not by caspases, while D75E BID mutant was cleaved efficiently by caspases, but not by granzyme B, suggesting that D75 is the cleavage site for granzyme B while D59 is the caspase cleavage site. As expected, the double mutant BID (DM BID) was cleaved by neither the caspases nor granzyme B. Two fragments of BID, a 15 kDa and a 14 kDa, were generated by caspase cleavage. The 14 kDa peptide was shifted to 13 kDa when a wild-type BID without N-terminal tag was cleaved by Casp8 (data not shown), suggesting that the 15 kDa peptide is the C-terminal part of BID and the 14 kDa peptide is the N-terminal portion with an anomalous mobility in SDS-PAGE. As an additional proof, the cleavage of BID by granzyme B generated a smaller C-terminal fragment and a larger N-terminal fragment that overlapped each other on SDS-PAGE (Figure 3A).

The Proapoptotic Activity of BID Strongly Depends upon Its Cleavage

BID was previously identified as a death agonist (Wang et al., 1996). Thus, it is interesting to examine whether its proapoptotic activity is enhanced by its cleavage. We cotransfected a *LacZ* construct with either wild-type BID or its cleavage-defective mutants into HeLa cells and then treated the cells with TNFα and CHX for 4 hr. The percentages of cell death expressing BID was determined by X-Gal staining. While 4 hr treatment of TNFα and CHX induced 54% of *LacZ*-transfected cells to die (*LacZ*-transfected control cells without treatment showed 3.8% of cell death, and WT BID–transfected cells without treatment showed 9.3% of cell death), the same TNFα and CHX treatment induced 91.5% of WT and 92.2% of D75E BID–transfected cells to die, respectively. Thus, the expression of wild-type and D75E BID increased TNFα-induced cell death by 69.4% and 69.5%, respectively, as shown in Figure 3B. In contrast, transfection of D59E and DM mutant BID had insignificant effects on TNFα-induced HeLa cell death (12.5% and 5.9%, respectively). The expression of BID and its mutants in transfected HeLa cells after TNFα treatment was also examined. Wild-type and D75E BID were cleaved into a 16 kDa fragment, but D59E and DM BID were not (Figure 3C). Thus, the proapoptotic activity of BID is strongly dependent upon its cleavage by Casp8 at D59.

The Cleaved BID Is a Potent Apoptosis-Inducing Agent

Most of the death agonists in the Bcl2 family contain a BH3 domain that is essential for their Bcl2 binding and proapoptotic activity (Chittenden et al., 1995; Wang et al., 1996; Kelekar et al., 1997) and capable of inducing caspase activation in a cell-free *Xenopus* oocyte system (Cosulich et al., 1997). It is possible that once BID is cleaved, the truncated portion containing the BH3 domain becomes lethal to cells. To investigate this possibility, we transiently transfected the C-terminal portion of BID (residue 60–195) (tBID) into Rat-1 fibroblast cells.

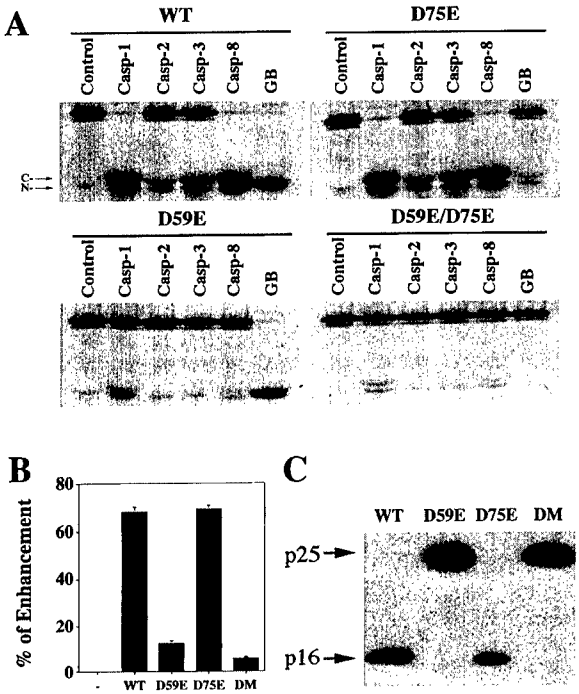

Figure 3. Proapoptotic Activity of BID Strongly Depends upon Its Cleavage

(A) Determination of cleavage sites of BID. ^{35}S-labeled wild-type BID or its mutants were incubated with either caspases or granzyme B and analyzed by SDS-PAGE. BID was cleaved by caspases into two fragments: the larger one (15 kDa) was the C-terminal fragment, and the smaller one (14 kDa) was the N-terminal fragment. The cleavage products of granzyme B overlapped each other.

(B) Wild-type BID and D75E mutant promoted TNFα-induced apoptosis of HeLa cells, while caspase cleavage–defective mutants (D59E and DM) did not. HeLa cells were transfected with either the expression constructs of Bid or its mutants with *LacZ* construct overnight and treated with 10 ng/ml TNFα and 1 μg/ml CHX for 4 hr. After fixation, X-Gal staining was performed, and the percentage of cell death was scored by cell morphology of blue cells (flat, well-attached versus round blue cells) as before (Miura et al., 1993).

(C) Cleavage of wild-type BID and its mutants in vivo. HeLa cells were transfected with the expression constructs of Bid or its mutants overnight and then treated with TNFα and CHX for 4 hr. The cell lysates were blotted with anti-Flag antibody. Arrows point to the full-length Flag-tagged BID (p25) and its cleavage product, p16.

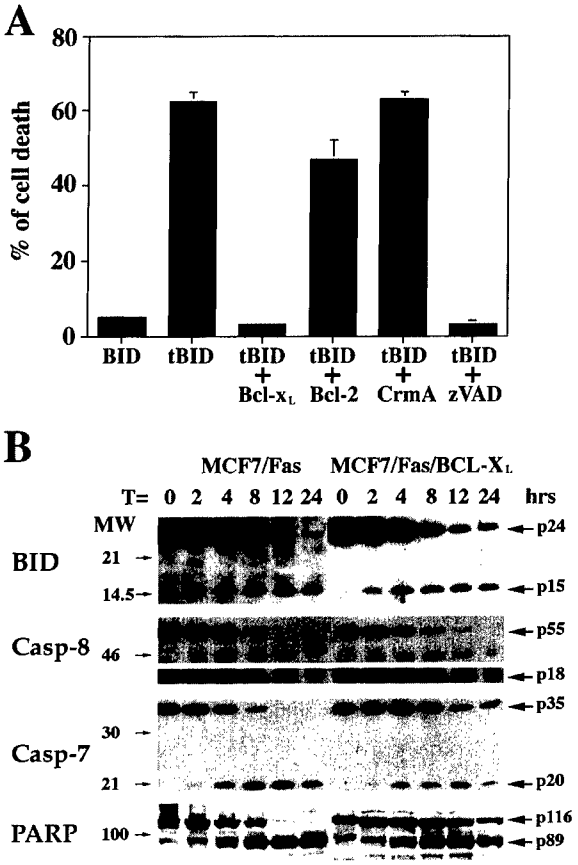

Figure 4. BID Acts Downstream of Casp8 and Upstream of $Bclx_L$ in Fas-Induced Apoptosis

(A) tBID-induced apoptosis of Rat-1 cells. Rat-1 cells seeded in 6-well plate were transfected with either 1 μg pcDNA-Bid or 0.25 μg pcDNA-tBid along with 1 μg *LacZ* construct. For different cell death inhibitors, 0.25 μg tBID was cotransfected with either 1 μg $Bclx_L$, 1 μg Bcl2, or 1 μg CrmA-expressing constructs, along with 1 μg *LacZ* construct. zVAD- fmk (100 μM) was added half an hour before transfection of tBid was performed. After 8 hr transfection, cells were fixed and X-Gal stained, and cell death percentage was scored by cell morphology of blue cells.

(B) Time course of BID cleavage in vivo. MCF7/Fas and MCF7/Fas/$Bclx_L$ cells were incubated with anti-Fas monoclonal antibody 7C11 (1:500) in the presence of 1 μg/ml CHX for different periods of time as indicated. Total cell lysates were then subjected to Western blotting analysis using antibodies against BID, Casp8, Casp7, and PARP. Arrows point to p24 (full-length BID), p15 (cleaved BID), p55 (full-length Casp8), p18 (cleaved Casp8), p35 (full-length Casp7), p20 (cleaved Casp7), p116 (full-length PARP), and p89 (cleaved PARP).

As shown in Figure 4A, full-length BID could not induce apoptosis, while tBID induced apoptosis very rapidly and efficiently. tBID-induced cell death was inhibited completely by $Bclx_L$ and zVAD-fmk, partially by Bcl2, but not at all by CrmA. This result suggests that the N terminus of BID has an inhibitory effect to its proapoptotic activity, and its removal by caspase cleavage yields tBID that is an effective inducer of downstream apoptotic events. The apoptosis-inducing activity of tBID is completely inhibited by $Bclx_L$, suggesting that BID may function upstream of $Bclx_L$/Bcl2. As CrmA can inhibit Casp1 and Casp8, but not other caspases (Zhou et al., 1997), the failure of CrmA to inhibit tBID-induced apoptosis is consistent with the hypothesis that BID acts downstream of Casp8.

BID Acts Downstream of Caspase 8 and Upstream of $Bclx_L$ in Fas-Induced Apoptosis

To examine whether BID is a specific proximal substrate of Casp8 and whether it operates upstream of $Bclx_L$/Bcl2, we used MCF7/Fas and its $Bclx_L$ stable cell lines. It has been shown that in MCF7 cells, $Bclx_L$ can prevent Fas- and TNFα-induced cell death and inhibit downstream caspase activation even though Casp8 is activated (Medema et al., 1998; Srinivasan et al., 1998). As shown in Figure 4B, the cleavage profile of BID correlated perfectly with the activation of Casp8, both of

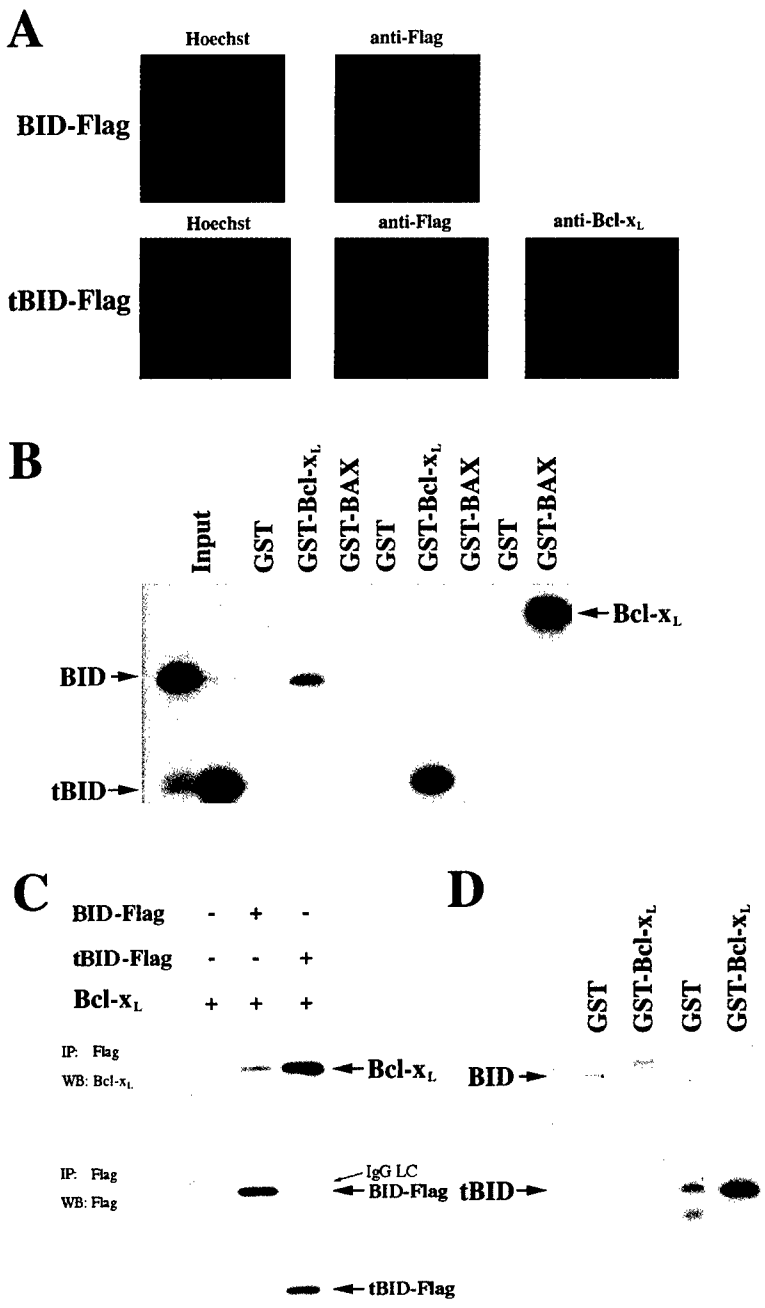

Figure 5. Truncated BID Has a Stronger Affinity for $Bclx_L$ than Its Precursor

(A) tBID was colocalized with $Bclx_L$. Constructs expressing BID-Flag or tBID-Flag fusion proteins were transiently transfected into HeLa/$Bclx_L$ stable cells. Immunohistochemistry was performed using anti-Flag antibody M2 and anti-$Bclx_L$ antibody.

(B) In vitro interactions between BID and $Bclx_L$ or Bax. ^{35}S-labeled BID or its cleaved form was incubated with either GST-$Bclx_L$ or GST-Bax bound to glutathione-agarose beads. After 3 hr incubation and three washes, the bound BID or tBID was analyzed by SDS-PAGE and autoradiography.

(C) In vivo interactions between BID and $Bclx_L$. Constructs expressing BID-Flag or tBID-Flag were cotransfected with $Bclx_L$ construct into HEK 293T cells. BID-Flag or tBID-Flag was immunoprecipitated by anti-Flag M2 affinity gel in the presence of 0.25% nonionic detergent IGEPAL CA-630 and Western blotted using anti-$Bclx_L$ antibody and M2 anti-Flag antibody, respectively.

(D) In vitro interaction between BID and $Bclx_L$ in the absence of nonionic detergent. ^{35}S-labeled BID or tBID was incubated with GST-$Bclx_L$ in a binding buffer without any nonionic detergent, and the bound BID or tBID was subjected to SDS-PAGE and autoradiography.

which were not altered by expression of $Bclx_L$. In contrast, the activation of Casp7 and the cleavage of PARP were delayed and partially inhibited by overexpression of $Bclx_L$. This result strongly supports our hypothesis that BID is a specific proximal substrate of Casp8 during Fas-induced apoptosis that functions upstream of $Bclx_L$.

Truncated BID Has a Stronger Affinity for $Bclx_L$ than the Full-Length BID

How does tBID induce apoptosis? It was proposed that BID, which localizes in cytoplasmic as well as in membrane fractions, acts as a ligand to Bcl2/$Bclx_L$ and Bax (Wang et al., 1996). We examined whether tBID behaves the same as its precursor. When tBID was overexpressed in HeLa/$Bclx_L$ stable cells, tBID colocalized with $Bclx_L$ (Figure 5A), suggesting that BID is translocated from cytoplasm to the membrane compartments when cleaved by Casp8. In contrast, the full-length BID was evenly distributed in every cellular compartment (Figure 5A). As BID does not have a membrane anchorage domain, one possible mechanism of translocation is that tBID has a stronger affinity to $Bclx_L$ than its precursor. To test this hypothesis, we examined the interaction between tBID and $Bclx_L$ in vitro and in vivo. We incubated ^{35}S-labeled BID or tBID with GST-$Bclx_L$ in vitro in the presence of 0.25% nonionic detergent IGEPAL CA-630,

and the amount of bound BID or tBID was analyzed by SDS-PAGE. As estimated by intensities of the corresponding bands, tBID has approximately 10-fold higher affinity toward GST-Bclx$_L$ fusion protein compared to its full-length precursor (Figure 5B), while the interaction between tBID and GST-Bax was undetectable. To examine the interaction of BID with Bclx$_L$ in vivo, we cotransfected the C-terminal Flag-tagged BID or its truncated form with Bclx$_L$ into HEK 293T cells and immunoprecipitated with anti-Flag M2 affinity gel in the presence of 0.25% nonionic detergent IGEPAL CA-630. The expression level of tBID was much lower than that of its precursor (data not shown). As shown in Figure 5C, much more Bclx$_L$ was coimmunoprecipitated with tBID than with full-length BID, and the difference was estimated around 20-fold by phosphoimager. It was reported that the presence of detergent in coimmunoprecipitation experiments affects the conformation of Bax and its interaction with Bcl2/Bclx$_L$ (Hsu and Youle, 1997), so we examined the interaction between BID and Bclx$_L$ in the absence of detergent. The interaction between the full-length BID and GST-Bclx$_L$ in the absence of detergent was not significantly different from the background, while the tBID C-terminal fragment, but not the N-terminal fragment, still bound effectively to Bclx$_L$ (Figure 5D). Thus, our in vivo and in vitro data indicate that the N-terminal domain of BID may have an inhibitory function, and the removal of the N-terminal domain exposes BID's BH3 domain to allow efficient interactions with other proteins.

Truncated BID Induces Mitochondrial Damage, Cell Shrinkage, and Nuclear Condensation

Mitochondrial damage and release of cytochrome c have been identified as key events in mediating activation of downstream caspases in apoptosis (Liu et al., 1996; Shimizu et al., 1996; Susin et al., 1996). Occurrence of these events is prevented by overexpression of Bcl2/Bclx$_L$ (Kluck et al., 1997; Vander Heiden et al., 1997; Yang et al., 1997). We postulated that tBID may be able to mediate mitochondrial damage that is inhibitable by Bclx$_L$. To illustrate the downstream events resulting from the cleavage of BID, we used an ecdysone-inducible system in which the tBID-GFP fusion gene was placed under the control of an ecdysone-inducible promoter. After transient transfection of tBID-GFP and transactivator pVgRXR overnight, the expression of tBID-GFP was induced by addition of 1 μM of muristerone A, an ecdysone analog, and examined by appearance of green fluorescence. Green fluorescence of tBID-GFP could be detected as early as 2 hr after induction (data not shown). Mitochondrial integrity was examined by fluorescent dye mitotracker, whose uptake depends on mitochondrial membrane potential, immunostaining of cytochrome c, which resides between inner and outer mitochondrial membranes, and cytochrome c oxidase subunit VIc (COX VIc), which resides within the inner mitochondrial membrane. The change of nuclear morphology was monitored by Hoechst dye staining. In the early stage of tBID-induced apoptosis, when nuclear morphology was largely normal, the signals of mitotracker, immunostaining of cytochrome c, and COX VIc began to fade in the periphery of the cells and became clustered around nuclei forming a ring (data not shown). As the apoptotic process proceeded, cells shrank and nuclei began to condense and fragment, and both signals of mitotracker and cytochrome c immunostaining became diffused, while immunostaining of COX VIc became intensified around shrunk nuclei (Figure 6A). This result suggests that tBID induces the clustering of mitochondria, release of cytochrome c, loss of mitochondrial membrane potential, cell shrinkage, and nuclear condensation. Green fluorescence of tBID-GFP exactly overlapped with COX VIc immunostaining in the early and late stages, further suggesting that tBID is targeted to the mitochondria.

Bclx$_L$ and Caspase Inhibitors Inhibit Distinct Steps in Apoptosis Induced by Truncated BID

To elucidate the mechanism of tBID-induced apoptosis, we examined the effects of various cell death inhibitors, such as CrmA, p35, zVAD-fmk, Casp9 (C287A) dominant negative mutant (DN), and Bclx$_L$, on tBID-induced mitochondrial damage, cell shrinkage, and nuclear condensation. Ninety-eight percent of MCF7/Fas cells underwent cell shrinkage and nuclear condensation and fragmentation at 4 hr after induction of tBID-GFP (Figures 6A and 6B). Among caspase inhibitors, CrmA had no effect, and p35 had a modest effect (32% inhibition), while zVAD-fmk inhibited most of tBID-induced cell shrinkage and nuclear condensation (90% inhibition) (Figures 6B and 6C), indicating that the caspase activity is required for tBID-induced cell shrinkage and nuclear condensation. Casp9 DN mutant also inhibited tBID-induced cell shrinkage and nuclear condensation, but was less effective than zVAD-fmk (71% inhibition) (Figure 6B), suggesting that BID acts upstream of Casp9/cytochrome c/Apaf1 pathway. Thirty hours after induction, most of the cells remained normal in the presence of zVAD-fmk (85%), while only 30% of nuclei were normal in the presence of Casp9 DN mutant (data not shown), indicating that Casp9 DN mutant can only delay, not block, the apoptotic process induced by tBID. Compared to other inhibitors, Bclx$_L$, which completely inhibited tBID-induced cell shrinkage and nuclear condensation, was the most effective antagonist of tBID's function (Figures 6B and 6D).

Although zVAD-fmk, Casp9 DN, and Bclx$_L$ have comparable effects on tBID-induced cell shrinkage and nuclear condensation, they had very different effects on tBID-induced mitochondrial damage. As shown in Figure 6D, the distribution of mitotracker, cytochrome c, and COX VIc in tBID/Bclx$_L$–expressing cells was the same as that in normal cells where green fluorescence of tBID-GFP overlapped with mitotracker signals and immunostaining of cytochrome c and COX VIc. In contrast, in the presence of zVAD-fmk, the signal of mitotracker disappeared from the peripheral region of cytoplasm and became aggregated around the nuclei, while immunostaining of cytochrome c completely disappeared (Figure 6C), suggesting that zVAD-fmk inhibits the loss of mitochondrial inner membrane potential but not the release of cytochrome c induced by tBID. The Casp9 DN mutant has a similar but less effective inhibitory activity (data not shown). As COX is an enzyme

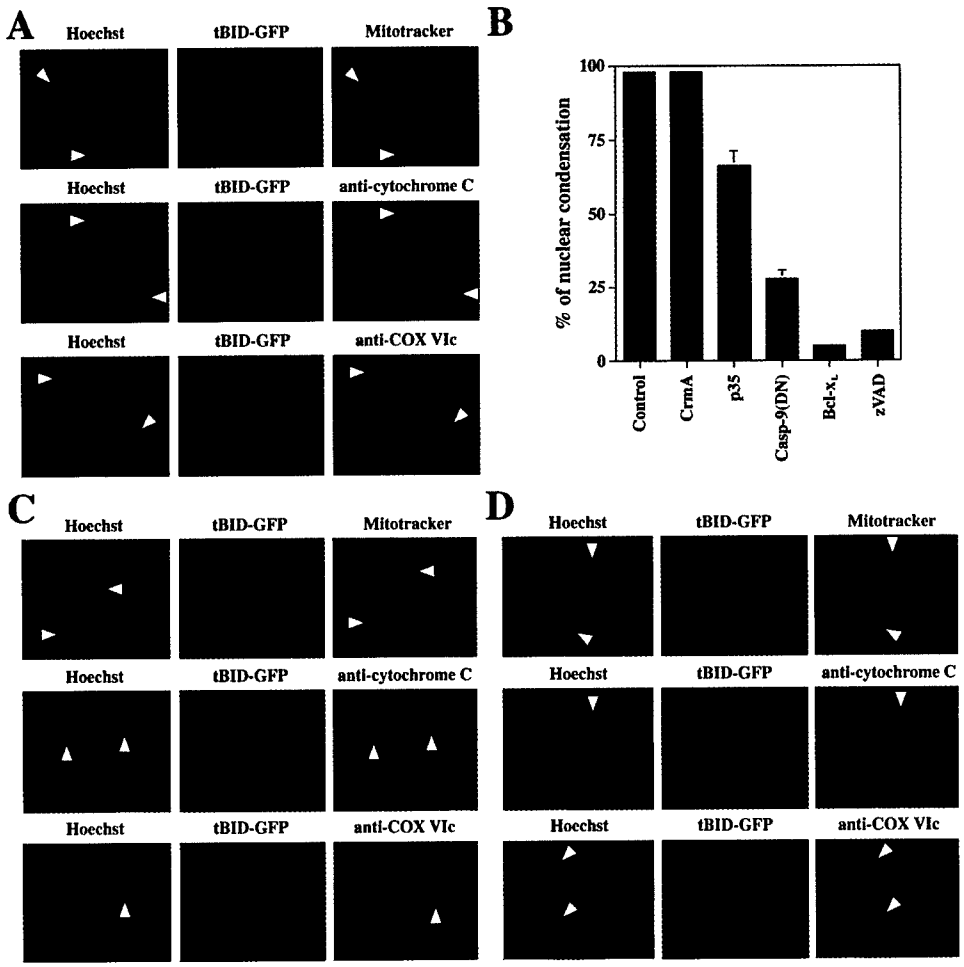

Figure 6. Differential Effects of $Bclx_L$ and zVAD-fmk on Truncated BID–Induced Apoptosis

(A) tBID-induced mitochondrial depolarization and the release of cytochrome c. MCF7/Fas cells were transfected with pIND-tBID-GFP and pVgRxR overnight and induced with muristerone A for 4 hr. For mitotracker staining, 300 nM Mitotracker CMTMRos was added into medium and then cells were fixed. For immunohistochemistry, cells were then fixed and immunostained with either anti-cytochrome c antibody or anti-COX VIc antibody. Arrows indicate the cells expressing tBID-GFP fusion protein.

(B) Effects of different cell death inhibitors on tBID-induced nuclear condensation. pIND-tBID-GFP and pVgRxR were transfected into MCF7/Fas or in combinations with different cell death inhibitors: CrmA, p35, Casp9 DN mutant, and $Bclx_L$. After overnight transfection, 1 μM of muristerone A was added into medium (for zVAD-fmk, cells were incubated with 100 μM of zVAD-fmk for half an hour prior to the addition of muristerone A). After 4 hr induction, cells were fixed and washed with PBS and then incubated with 1 ng/ml of Hoechst dye. Percentage of nuclear condensation was scored by nuclear morphology.

(C) zVAD-fmk–inhibited tBID-induced loss of mitochondrial membrane potential, indicated by the ability of mitochondria to uptake mitotracker, cell shrinkage, and nuclear condensation, but not mitochondrial clustering and cytochrome c release. Cells were incubated with 100 μM of zVAD-fmk for half an hour prior to addition of muristerone A. Similar experiments described in (B) were performed. Arrows indicate the cells expressing tBID-GFP fusion protein.

(D) $Bclx_L$ completely inhibited all apoptotic morphological changes induced by tBID. $Bclx_L$ construct was cotransfected into MCF7/Fas cells along with pIND-tBID-GFP and pVgRxR. After overnight transfection, similar experiments described in (B) were performed. Arrows indicate the cells expressing tBID-GFP fusion protein.

localized in the inner membrane of mitochondria, immunostaining of COX VIc is an indication of mitochondrial distribution. In contrast to the disappearance of cytochrome c immunostaining in the presence of zVAD-fmk, the signal of COX VIc immunostaining remained largely clustered around nuclei and overlapped with the tBID-GFP signal (Figure 6C). Taken together, these results suggest that tBID induces the redistribution of mitochondria and the release of cytochrome c in a caspase-independent process but does not cause a complete disruption of mitochondrial inner membrane in the presence of caspase inhibitors.

Truncated BID Induces the Release of Cytochrome c from Purified Mitochondria In Vitro

To examine the mechanism by which BID mediates mitochondrial damage, we evaluated its ability to induce cytochrome c release from partially purified mitochondria in a cell-free system. Partially purifed mitochondria were incubated with purified full-length BID or its truncated form, and the release of cytochrome c was examined. As shown in Figure 7, both full-length and tBID were able to induce the release of cytochrome c from mitochondria, but tBID was much more efficient than

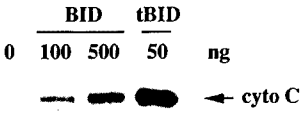

Figure 7. Truncated BID Induced the Release of Cytochrome c from Partially Purified Mitochondria In Vitro

Purified recombinant BID or tBID were incubated with partially purified mitochondria from mouse liver, and the released cytochrome c was examined by immunoblotting.

full-length BID. This result is consistent with our in vivo observation that tBID is more potent in its proapoptotic activity than its precursor.

Discussion

A number of BH3-containing death agonists of the Bcl2 family have been recently identified. Among them, a group of so-called "BH3-only" death agonists, including Bik/Bbk, BID, Hrk/DP5, and newly identified Blk and Bim, seem to be more potent in their apoptosis-inducing activity than other death agonists in the family that contains additional BH1 and BH2 domains such as Bad. Identification of *C. elegans egl-1* as a general component of programmed cell death machinery indicates that BH3-containing death agonists are important regulators in apoptosis (Conradt and Horvitz, 1998). The BH3 domain is the only homologous region shared by these BH3-only death agonists, indicating that they may use a common BH3 domain-mediated mechanism to induce apoptosis, although the regulation of their activities may be different from each other. BID differs from other BH3-only molecules by two characteristics: the absence of a C-terminal hydrophobic membrane anchor, and the presence of two perfect cleavage sites for Casp8 and granzyme B, respectively, which are not found in other BH3-only molecules. Although overexpression of full-length BID can induce apoptosis in certain cells (data not shown; Wang et al., 1996), its truncated form is much more potent, indicating that caspase cleavage is one of the mechanisms to regulate its proapoptotic activity. It was recently reported that death antagonists of the Bcl2 family, such as CED-9, Bcl2, and $Bclx_L$, can be cleaved by caspases (Cheng et al., 1997; Xue and Horvitz, 1997; Clem et al., 1998), indicating that caspase cleavage of Bcl2 family members is evolutionarily conserved and diversified.

We presented the evidence of BID translocation from cytosol to mitochondria during propagation of a death signal. Such translocation during apoptosis has been observed for two additional members of the Bcl2 family, Bax and BAD. It was reported that Bax moves from cytosol to mitochondria during apoptosis, although the regulatory mechanism of Bax translocation is unclear (Wolter et al., 1997). BAD exhibits a similar behavior when FL5.12 cells are starved for IL-3 and the translocation is regulated by protein phosphorylation (Zha et al., 1996). Translocation from cytosol to mitochondria may be an important activating mechanism for the proapoptotic members of the Bcl2 family and the propagation of apoptotic signals intracellularly. Caspase cleavage–induced BID translocation represents a novel mechanism to release the proapoptotic potential of BID, perhaps by removing the inhibitory N-terminal domain, exposing BH3 domain and allowing tBID to interact with its receptor on the mitochondria.

Availability of different cell death inhibitors allowed us to map accurately the position of BID in the Fas signaling pathway and to study the downstream events after BID cleavage. The first detectable morphological change induced by tBID is the clustering of mitochondria around the nuclei at a stage when cytochrome c appears to remain largely within the mitochondria and mitotracker uptake is normal. Such movement of mitochondria has not been detected previously during the Fas-induced apoptosis, which may be because of two reasons. First, Fas-induced apoptosis can activate multiple apoptotic downstream events that occur very fast, and thus it may be difficult to capture such an intermediate step. Second, caspase inhibitors such as CrmA, p35, and zVAD-fmk are all effective inhibitors of Casp8, and thus they inhibit the activation of Casp8 itself and prevent the activation of downstream events altogether. Truncated BID allows us to bypass the requirement of Casp8 to dissect the downstream events of the Fas pathway. Why do mitochondria appear to be clustering around nuclei in the early stage of tBID-induced apoptosis? One possible explanation is that mitochondria are damaged sequentially, with mitochondria closest to the cytoplasmic membrane being damaged first. Alternatively, tBID may be able to induce not only mitochondrial leakage but also their detachment from cytoskeletal structure, resulting in their collapsing around nuclei. More experiments will be done to distinguish these two possibilities.

The second detectable morphological change in tBID-induced apoptosis appears to be the release of cytochrome c while mitotracker uptake is still normal. In the presence of zVAD-fmk, we can see rings of mitochondria that are mitotracker-positive and COX VIc–positive, while cytochrome c immunostaining has disappeared. Since cytochrome c resides between the inner and outer mitochondrial space, mitotracker uptake depends upon mitochondrial membrane potential, and COX VIc resides in the inner mitochondrial membrane, our results suggest that tBID may be able to cause disruption of the outer mitochondrial membrane directly, while the disruption of inner mitochondrial membrane needs the help from caspase. Our results are consistent with the observation of Vander Heiden et al. (1997), who have suggested that in apoptosis the disruption of outer mitochondrial membrane occurs before the loss of mitochondrial membrane potential, which is mainly an indication of the inner mitochondrial membrane integrity. Our results are also consistent with the observation of Bossy-Wetzel et al. (1998), who showed that the loss of mitochondrial membrane potential, but not cytochrome c release of CEM and HeLa cells induced by UVB irradiation or staurosporine treatment, can be inhibited by zVAD-fmk. We suggest that BID or related BH3 domain–containing proteins may be involved in inducing mitochondrial damage in apoptosis induced by other stimuli as well, although the mechanism of activation may be different.

Although caspase inhibitors such as Casp9 DN, p35, and zVAD-fmk are unable to inhibit the early mitochondrial damages induced by tBID, they can inhibit the loss of mitochondrial membrane potential, cell shrinkage, and nuclear condensation induced by tBID with different effectiveness. While CrmA does not inhibit tBID-induced cell death, and p35 has a modest effect, zVAD-fmk is very effective in inhibiting tBID-induced nuclear condensation and in halting apoptotic process at an early stage when mitochondria cluster around normal-looking nuclei. The inhibitory activity of Casp9 DN mutant is similar to that of zVAD-fmk but less effective. Although this spectrum of inhibitor profile does not allow us to identify positively the critical caspase(s) involved in this process, it does suggest, however, that the release of cytochrome c may not be the only critical event downstream from the mitochondrial damage induced by tBID, since Casp9 DN is only partially effective in inhibition of tBID-induced cell death. This conclusion is also supported by the fact that tBID induces apoptosis of MCF7/Fas cells effectively, while microinjection of cytochrome c to MCF7/Fas cells does not induce apoptosis (Li et al., 1997a). Alternatively, tBID may activate downstream caspases by a cytochrome c–independent pathway in which tBID simply competes $Bclx_L$ from $Bclx_L$/Apaf1/caspase complex and activates downstream caspases. The observation that the Apaf1/Casp9/$Bclx_L$ complex exists (Hu et al., 1998; Pan et al., 1998) provides additional support for this model. These two mechanisms, however, are not mutually exclusive, and the mechanism by which tBID acts may be cell type–specific.

In contrast to caspase inhibitors, $Bclx_L$ can fully block the tBID's activity. Thus, the interaction of tBID with $Bclx_L$ must be the key to its ability to induce apoptosis. Kelakar et al. (1997) reported recently that wild-type BAD fails to induce apoptosis in response to growth factor withdrawal when cells are protected by a $Bclx_L$ mutant that does not bind to the BAD BH3 domain, suggesting that the interaction between the BH3 domain and Bcl2/$Bclx_L$ is critical for BH3 domain's proapoptotic activity. tBID may behave as an intracellular ligand for $Bclx_L$, which acts as the receptor in the Fas pathway. Unlike the conventional ligand–receptor interactions at cytoplasmic membrane, where such interactions usually result in the activation of the receptor, the interaction of tBID with $Bclx_L$ results in the inactivation of protective functions of $Bclx_L$ (or may we call it the activation of apoptotic-inducing functions of $Bclx_L$?). Alternatively, tBID may be capable of triggering apoptosis on its own, which may be Bcl2/$Bclx_L$–inhibitable, or Bcl2/$Bclx_L$ may simply act as a neutralizer of its death-inducing activity. These are interesting questions for future experiments. The dimeric interactions of antiapoptotic members of the Bcl2 family with proapoptotic members of the Bcl2 have been hypothesized to be an important mechanism of regulation (Oltvai and Korsmeyer, 1994). Recently, however, this view has been questioned mainly because of two works. First, Knudson and Korsmeyer (1997) reported that, in a genetic analysis, Bcl2 and Bax are able to act independently. Second, Hsu and Youle (1997) reported that the dimeric interaction of Bcl2 and Bax can only be detected in the presence of detergent, suggesting that detergent may induce specific conformational changes, exposing the interacting domain of Bcl2 and Bax and allowing such dimerization to occur. Interestingly, while we can detect the interaction of full-length BID with $Bclx_L$ in the presence of detergent, such interaction appears to be largely absent in the absence of detergent. In contrast, the interaction of tBID with $Bclx_L$ is still very strong in the absence of detergent. Our results indicate that the interaction of tBID with $Bclx_L$ is not induced by detergent. On the other hand, nonionic detergent appears to enhance the binding of full-length BID with $Bclx_L$, suggesting that detergent may be able to induce the conformational change of BID by removing the inhibition of N-terminal domain, a hypothesis that can be examined directly by further experimentation.

Experimental Procedures

Construction of Mouse Spleen cDNA Small Pool Library and In Vitro Expression Cloning

A mouse spleen cDNA library of 2×10^5 independent clones was constructed by using a Stratagene cDNA synthesis and cloning kit (Stratagene, La Jolla, CA), and cDNAs were inserted into EcoRI and XhoI sites of pCS2. Pools of cDNAs and in vitro translations were done as described by Lustig et al. (1997). The caspase cleavage assay was performed as described previously (Li et al., 1997b). The individual positive cDNA was identified using 96-well plates as described (Lustig et al., 1997), was sequenced, and compared with known sequences by searching the GenBank database.

Bacterial and Mammalian Expression Constructs of Murine and Human Bid and Generation of Anti-BID Antibody

The original clone of murine *Bid* obtained from the small pool library contained the full-length open reading frame of Bid. The standard molecular cloning methods and PCR were used to construct various mammalian expression vectors of murine Bid.

The full-length human BID gene was amplified by PCR from EST cDNA clone 52055 (Research Genetics, Inc., Huntsville, AL) and then cloned into the BamHI site of pGEX-2T. GST-BID fusion protein was purified by GST beads, GST was removed by thrombin digestion, and the purified BID protein was injected into rats to generate polyclonal antibody.

To establish an inducible expression system of tBid, tBid was inserted into BamHI site in frame with GFP (green fluorescence protein) in pEGFP-N1 vector (CLONTECH, Palo Atlo, CA), generating tBID-GFP fusion gene. The cassette of tBID-GFP was then cloned into EcoRI and NotI sites of pIND (Invitrogen, San Diego, CA).

Site-Directed Mutagenesis of the Cleavage Sites of Bid

Aspartic acid residues at positions 59 and 75 of Bid were mutated to glutamic acid individually or in combination, using QuickChange site-directed mutagenesis kit (Stratagene), following the supplier's instruction. Mutated sites were verified by DNA sequencing.

Tissue Culture Cells

Jurkat cells were cultured in RPMI 1640 supplemented with 10% fetal bovine serum (FBS), and HeLa and HEK 293T cells were cultured in DMEM containing 10% FBS. MCF7/Fas and MCF7/Fas/$Bclx_L$ stable cells were cultured in RPMI 1640 containing 10% FBS, 200 μg/ml G418, and 100 μg/ml hygromycin (Srinivasan et al., 1998).

Immunohistochemistry

For Mitotracker staining, Mitotracker CMTMRos (Molecular Probes Inc., Eugene, OR) was added to medium in a final concentration of 300 nM, and cells were further cultured for 30 min and fixed in 4% paraformadehyde for 15 min. Immunohistochemistry of cytochrome c and COX VIc was done according to Srinivasan et al. (1998), with minor modifications.

In Vitro and In Vivo Binding Assays

^{35}S-labeled BID or its cleaved form was incubated with 10 μg GST-$Bclx_L$ in 100 μl of the binding buffer (10 mM HEPES [pH 7.5], 150 mM KCl, 5 mM $MgCl_2$, 1 mM EDTA, and 0.25% IGEPAL CA-630) at

4°C for 3 hr with agitation. After brief centrifugation, beads were washed three times with 400 μl of binding buffer and resuspended in protein sample buffer. The samples were subjected to SDS-PAGE and autoradiography.

For in vivo binding assay, constructs expressing BID-Flag or tBID-Flag fusion protein were cotransfected with the construct expressing $Bclx_L$ into HEK 293T cells by a calcium-phosphate method. After 24 hr, cells were lysed in 1 ml of binding buffer, and total cell lysates were centrifuged at 10,000 × g for 15 min. M2 anti-Flag affinity gel (30 μl) was added into the supernatant, and the resulting mixture was incubated at 4°C for 3 hr with agitation. Following three washes, the beads were resuspended in appropriate amounts of protein sample buffer. The samples were subjected to Western blotting analysis.

Cell-Free Assay for the Release of Cytochrome c from Purified Mouse Liver Mitochondria

Mitochondria were purified as described by Shimizu et al. (1998). For in vitro assay, 5 μl of purified mitochondria was incubated with purified BID or tBID at 37°C for 1 hr. The reaction mixture was then centrifuged at 10,000 × g for 10 min, and the supernatant was subjected to SDS-PAGE and immunoblotting using anti-cytochrome c antibody.

Acknowledgments

We thank Dr. Marc Kirschner and the members of his laboratory for helpful advice on constructing and using the small pool expression library, which was critical for the success of this project. We thank Kevin Welch, Xun Clare Zhou, and members of the Yuan laboratory for a joint effort in preparing the small pool cDNA library, which was a lot of work. We thank Dr. Arnold Greenberg for providing granzyme B; Dr. Vishva Dixit for permission to use MCF7/Fas and MCF7/Fas/$Bclx_L$ cells; Dr. Emad Alnemri for Casp9 DN; Drs. Yoshihide Tsujimoto and Xiaodong Wang for protocols and advice on preparation of mitochondria; and Dr. Zhi-Jun Lu for GST-Bax. We also thank Xun Clare Zhou, Roberto Sanchez-Olea, Suyue Wang, Louise Bergeron, and Qiang Yu for their critical reading of the manuscript. This work was supported in part by a postdoctoral fellowship from National Institute of Aging (to H. L.), a grant from the Army's Breast Cancer Program (to J. Y.), and an American Heart Established Investigatorship (to J. Y.).

Received May 19, 1998; revised July 20, 1998.

References

Boldin, M.P., Goncharov, T.M., Goltsev, Y.V., and Wallach, D. (1996). Involvement of MACH, a novel MORT1/FADD-interacting protease, in Fas/APO-1- and TNF receptor-induced cell death. Cell *85*, 803–815.

Bossy-Wetzel, E., Newmeyer, D.D., and Green, D.R. (1998). Mitochondrial cytochrome C release in apoptosis occurs upstream of DEVD-specific caspase activation and independent of mitochondrial transmembrane depolarization. EMBO J. *17*, 37–49.

Cheng, E.H., Kirsch, D.G., Clem, R.J., Ravi, R., Kastan, M.B., Bedi, A., Ueno, K., and Hardwick, J.M. (1997). Conversion of Bcl-2 to a Bax-like death effector by caspases. Science *278*, 1966–1968.

Chittenden, T., Flemington, C., Houghton, A.B., Ebb, R.G., Gallo, G.J., Elangovan, B., Chinnadurai, G., and Lutz, R.J. (1995). A conserved domain in Bak, distinct from BH1 and BH2, mediates cell death and protein binding functions. EMBO J. *14*, 5589–5596.

Clem, R.J., Cheng, E.H., Karp, C.L., Kirsch, D.G., Ueno, K., Takahashi, A., Kastan, M.B., Griffin, D.E., Earnshaw, W.C., Veliuona, M.A., et al. (1998). Modulation of cell death by $Bcl\text{-}x_L$ through caspase interaction. Proc. Natl. Acad. Sci. USA *95*, 554–559.

Conradt, B., and Horvitz, H.R. (1998). The *C. elegans* protein EGL-1 is required for programmed cell death and interacts with the Bcl-2-like protein CED-9. Cell *93*, 519–529.

Cosulich, S.C., Worrall, V., Hedge, P.J., Green, S., and Clarke, P.R. (1997). Regulation of apoptosis by BH3 domains in a cell-free system. Curr. Biol. *7*, 913–920.

Cryns, V., and Yuan, J. (1998). Proteases to die for. Genes Dev. *12*, 1551–1570.

Fernandes-Alnemri, T., Armstrong, R.C., Krebs, J., Srinivasula, S.M., Wang, L., Bullrich, F., Fritz, L.C., Trapani, J.A., Tomaselli, K.J., Litwack, G., et al. (1996). In vitro activation of CPP32 and Mch3 by Mch4, a novel human apoptotic cysteine protease containing two FADD-like domains. Proc. Natl. Acad. Sci. USA *93*, 7464–7469.

Hsu, Y.-T., and Youle, R.J. (1997). Nonionic detergents induces dimerization among members of the Bcl-2 family. J. Biol. Chem. *272*, 13829–13834.

Hu, Y., Benedict, M.A., Wu, D., Inohara, N., and Nunez, G. (1998). $Bcl\text{-}x_L$ interacts with Apaf-1 and inhibits Apaf-1-dependent caspase-9 activation. Proc. Natl. Acad. Sci. USA *95*, 4386–4391.

Huang, D.C.S., Adams, J.M., and Cory, S. (1998). The conserved N-terminal BH4 domain of Bcl-2 homologues is essential for inhibition of apoptosis and interaction with CED-4. EMBO J. *17*, 1029–1039.

Kelekar, A., Chang, B.S., Harlan, J.E., and Thompson, C.B. (1997). Bad is a BH3 domain–containing protein that forms an inactivating dimer with $Bcl\text{-}X_L$. Mol. Cell. Biol. *17*, 7040–7046.

Kischkel, F.C., Hellbardt, S., Behrmann, I., Germer, M., Pawlita, M., Krammer, P.H., and Peter, M.E. (1995). Cytotoxicity-dependent APO-1 (Fas/CD95)-associated proteins form a death-inducing signaling complex (DISC) with the receptor. EMBO J. *14*, 5579–5588.

Kluck, R.M., Bossy-Wetzel, E., Green, D.R., and Newmeyer, D.D. (1997). The release of cytochrome c from mitochondria: a primary site for Bcl-2 regulation of apoptosis. Science *275*, 1132–1136.

Knudson, C.M., and Korsmeyer, S.J. (1997). Bcl-2 and Bax function independently to regulate cell death. Nat. Genet. *16*, 358–363.

Li, F., Srinivasan, A., Wang, Y., Armstrong, R.C., Tomaselli, K.J., and Fritz, L.C. (1997a). Cell-specific induction of apoptosis by microinjection of cytochrome c. $Bcl\text{-}x_L$ has activity independent of cytochrome c release. J. Biol. Chem. *272*, 30299–30305.

Li, H., Bergeron, L., Cryns, V., Pasternack, M.S., Zhu, H., Shi, L., Greenberg, A., and Yuan, J. (1997b). Activation of caspase-2 in apoptosis. J. Biol. Chem. *272*, 21010–21017.

Li, P., Nijhawan, D., Brudihardjo, I., Srinivasula, S.M., Ahmad, M., Alnemri, E.S., and Wang, X. (1997c). Cytochrome C and dATP-dependent formation of Apaf-1/caspase-9 complex initiates an apoptotic protease cascade. Cell *91*, 479–489.

Liu, X., Kim, C.N., Yang, J., Jemmerson, R., and Wang, X. (1996). Induction of apoptotic program in cell free extracts: requirement for dATP and cytochrome C. Cell *86*, 147–157.

Lustig, K.D., Stukenberg, P.T., McGarry, T.J., King, R.W., Cryns, V.L., Mead, P.E., Zon, L.I., Yuan, J., and Kirschner, M.W. (1997). Small pool expression screening: identification of genes involved in cell cycle control, apoptosis, and early development. Methods Enzymol. *283*, 83–99.

Medema, J.P., Scaffidi, C., Krammer, P.H., and Peter, M.E. (1998). $Bcl\text{-}x_L$ acts downstream of caspase-8 activation by the CD95 death-inducing signaling complex. J. Biol. Chem. *273*, 3388–3393.

Merry, D.E., and Korsmeyer, S.J. (1997). Bcl-2 gene family in the nervous system. Annu. Rev. Neurosci. *20*, 245–267.

Miura, M., Zhu, H., Rotello, R., Hartwieg, E.A., and Yuan, J. (1993). Induction of apoptosis in fibroblasts by IL-1β-converting enzyme, a mammalian homolog of the *C. elegans* cell death gene *ced-3*. Cell *75*, 653–660.

Muzio, M., Chinnaiyan, A.M., Kischkel, F.C., O'Rourke, K., Shevchenko, A., Ni, J., Scaffidi, C., Bretz, J.D., Zhang, M., Gentz, R., et al. (1996). FLICE, a novel FADD-homologous ICE/CED-3-like protease, is recruited to the CD95 (Fas/APO-1) death-inducing signaling complex. Cell *85*, 817–827.

Oltvai, Z.N., and Korsmeyer, S.J. (1994). Checkpoints of dueling dimers foil death wishes. Cell *79*, 189–192.

Pan, G., O'Rourke, K., and Dixit, V.M. (1998). Caspase-9, $Bcl\text{-}x_L$, and Apaf-1 form a ternary complex. J. Biol. Chem. *273*, 5916–5922.

Salvesen, G.S., and Dixit, V.M. (1997). Caspases: intracellular signaling by proteolysis. Cell *91*, 443–446.

Scaffidi, C., Fulda, S., Srinivasan, A., Friesen, C., Li, F., Tomaselli,

K.J., Debatin, K.M., Krammer, P.H., and Peter, M.E. (1998). Two CD95 (APO-1/Fas) signaling pathways. EMBO J. *17*, 1675–1687.

Shimizu, S., Eguchi, Y., Kamiike, W., Waguri, S., Uchiyama, Y., Matsuda, H., and Tsujimoto, Y. (1996). Bcl-2 blocks loss of mitochondrial membrane potential while ICE inhibitors act a different step during inhibition of death induced by respiratory chain inhibitors. Oncogene *13*, 21–29.

Shimizu, S., Eguchi, Y., Kamiike, W., Funahashi, Y., Mignon, A., Lacronique, V., Matsuda, H., Tsujimoto, Y. (1998). Bcl-2 prevents apoptotic mitochondrial dysfunction by regulating proton flux. Proc. Natl. Acad. Sci. USA *95*, 1455–1459.

Srinivasan, A., Li, F., Wong, A., Kodandapani, L., Smidt, R., Jr., Krebs, J.F., Fritz, L.C., Wu, J.C., and Tomaselli, K.J. (1998). Bcl-x_L functions downstream of caspase-8 to inhibit Fas- and tumor necrosis factor receptor 1-induced apoptosis of MCF7 breast carcinoma cells. J. Biol. Chem. *273*, 4523–4529.

Susin, S.A., Zamzami, N., Castedo, M., Hirsch, T., Marchetti, P., Macho, A., Daugas, E., Geuskens, M., and Kreomer, G. (1996). Bcl-2 inhibits the mitochondrial release of an apoptogenic protease. J. Exp. Med. *184*, 1331–1341.

Thornberry, N.A., Rano, T.A., Peterson, E.P., Rasper, D.M., Timkey, T., Garcia-Calvo, M., Houtzager, V.M., Nordstrom, P.A., Roy, S., Vaillancourt, J.P., et al. (1997). A combinatorial approach defines specificities of members of the caspase family and granzyme B. Functional relationships established for key mediators of apoptosis. J. Biol. Chem. *272*, 17907–17911.

Vander Heiden, M.G., Chandel, N.S., Williamson, E.K., Schmacker, P.T., and Thompson, C.B. (1997). Bcl-x_L regulates the membrane potential and volume homeostasis of mitochondria. Cell *91*, 627–637.

Wang, K., Yin, X.-M., Chao, D.T., Milliman, C.L., and Korsmeyer, S.J. (1996). BID: a novel BH3 domain-only death agonist. Genes Dev. *10*, 2859–2869.

Wolter, K.G., Hsu, Y., Smith, C.L., Nechushtan, A., Xi, X., and Youle, R.J. (1997). Movement of Bax from the cytosol to mitochondria during apoptosis. J. Cell. Biol. *139*, 1281–1292.

Xue, D., and Horvitz, H.R. (1997). *Caenorhabditis elegans* CED-9 protein is a bifunctional cell-death inhibitor. Nature *390*, 305–308.

Yang, E., Zha, J., Jockel, J., Boise, L.H., Thompson, C.B., and Korsmeyer, S.J. (1995). Bad, a heterodimeric partner for Bcl-xl and Bcl-2, displaces Bax and promotes cell death. Cell *80*, 285–291.

Yang, J., Liu, X., Bhalla, K., Kim, C.N., Ibrado, A.M., Cai, J., Peng, T.I., Jones, D.P., and Wang, X. (1997). Prevention of apoptosis by Bcl-2: release of cytochrome C from mitochondria blocked. Science *275*, 1129–1132.

Zha, J., Harada, H., Yang, E., Jockel, J., and Korsmeyer, S.J. (1996). Serine phosphorylation of death agonist BAD in response to survival factor results in binding to 14–3–3 not BCL-X_L. Cell *87*, 619–626.

Zhou, Q., Snipas, S., Orth, K., Muzio, M., Dixit, V.M., and Salvesen, G.S. (1997). Target protease specificity of the viral serpin CrmA. Analysis of five caspases. J. Biol. Chem. *272*, 7797–7800.

Zou, H., Henzel, W.J., Liu, X., Lutschg, A., and Wang, X. (1997). Apaf-1, a human protein homologous to *C. elegans* CED-4, participates in cytochrome c-dependent activation of caspase-3. Cell *90*, 405–413.

Cell, Vol. 96, 615–624, March 5, 1999, Copyright ©1999 by Cell Press

Solution Structure of BID, an Intracellular Amplifier of Apoptotic Signaling

James J. Chou,*† Honglin Li,‡
Guy S. Salvesen,§ Junying Yuan,‡
and Gerhard Wagner*†‖
*Committee on Higher Degrees in Biophysics
Harvard University
Cambridge, Massachusetts 02138
†Department of Biological Chemistry and Molecular Pharmacology
‡Department of Cell Biology
Harvard Medical School
Boston, Massachusetts 02115
§The Burnham Institute
San Diego, California 92037

Summary

We report the solution structure of BID, an intracellular cross-talk agent that can amplify FAS/TNF apoptotic signal through the mitochondria death pathway after Caspase 8 cleavage. BID contains eight α helices where two central hydrophobic helices are surrounded by six amphipathic ones. The fold resembles pore-forming bacterial toxins and shows similarity to BCL-X_L although sequence homology to BCL-X_L is limited to the 16-residue BH3 domain. Furthermore, we modeled a complex of BCL-X_L and BID by aligning the BID and BAK BH3 motifs in the known BCL-X_L–BAK BH3 complex. Additionally, we show that the overall structure of BID is preserved after cleavage by Caspase 8. We propose that BID has both BH3 domain–dependent and –independent modes of action in inducing mitochondrial damage.

Introduction

The intracellular FAS signal transduction pathway of apoptosis is initiated when Procaspase 8 is recruited to the death-induced signaling complex (DISC) through interaction with the adapter molecule FADD/MORT1 (Boldin et al., 1996; Muzio et al., 1996). The local aggregation of Procaspase 8 is sufficient to allow auto- or transprocessing to produce active Caspase 8 (reviewed by Green, 1998; Muzio et al., 1998; Yang et al., 1998), which can subsequently activate executioners such as Caspases 3, 6, and 7. An alternative amplification pathway leading to large-scale activation of downstream caspases is through mitochondrial damage. This pathway is initiated upon cytochrome c release from mitochondria. Cytochrome c, in the presence of dATP, triggers the activation of Caspase 9 through Apaf1/Caspase 9 complex formation (Li et al., 1997). For the mitochondria pathway, Caspase 9 is the central initiator that activates the downstream executioners such as Caspases 3, 6, and 7. Although activated Caspase 8 can lead directly to downstream caspase activation in certain cell types, mitochondria are the essential mediators in others (Scaffidi et al., 1998). In cell-free *Xenopus* egg extracts, the ability of small amounts of Caspase 8 to trigger activation of downstream caspases was dependent on the presence of mitochondria (Kuwana et al., 1998). In extracts devoid of mitochondria, high concentrations of Caspase 8 were required to activate downstream caspases. However, when mitochondria were present, the trigger of downstream caspase activation from low concentration of Caspase 8 was vastly amplified through cytochrome c release after mitochondrial damage.

While mitochondrial damage is the major amplification step in the apoptotic pathway, the mitochondrion is also the principal site of action for pro- and antiapoptotic members of the BCL2 superfamily. The BCL2 family of proteins shares amino acid sequence homology in one to four regions designated the BCL2 homology (BH) domains: BH1, BH2, BH3, and BH4 (reviewed by Kelekar and Thompson, 1998). The two well-known antiapoptotic members BCL2 and BCL-X_L are usually localized on the cytoplasmic face of the mitochondrial outer membrane. Overexpression of BCL2 or BCL-X_L blocks the release of cytochrome c and aborts the apoptotic response (Kluck et al., 1997; Yang et al., 1997). The survival function of BCL2 has also been implicated in its binding to the CED4-like portion of Apaf1 to thereby prevent the activation of Procaspase 9 (Hu et al., 1998; Pan et al., 1998). In addition, both BCL2 and BCL-X_L have been shown to form selective ion channels in lipid membranes (Minn et al., 1997), which may regulate the mitochondrial membrane potential and thus prevent cytochrome c release. The proapoptotic members of the BCL2 family include BAX, which contains multiple BH homology domains (BH1, BH2, and BH3), as well as a class of molecules sharing only the BH3 homology, such as BIK, BAD, BID, and EGL1 (reviewed by Adams and Cory, 1998). The BH3 domain of the proapoptotic members of the BCL2 superfamily has been shown to interact with antiapoptotic members of the family (see review by Kelekar and Thompson, 1998). Furthermore, the BH3 domains from proapoptotic, but not antiapoptotic, members of the BCL2 family can induce the release of cytochrome c from isolated mitochondria (Cosulich et al., 1997). These results suggest that the heterodimerization of pro- and antiapoptotic members of the BCL2 family may be critical for killing induced by BAX-like molecules. Recently, however, multiple lines of evidence suggest that proapoptotic functions of BAX-like molecules go beyond its ability to bind BCL2 or BCL-X_L through the BH3 domains. Genetic studies indicated that BCL2 and BAX function independently to regulate apoptosis in nonlymphoid cell lineages as well as lymphoid cell lineages other than thymocytes (Knudson and Korsmeyer, 1997). Mutagenesis of the BAX BH3 domain, which eliminated the ability of BAX to interact with BCL2 and BCL-X_L, did not perturb its ability to induce apoptosis (Wang et al., 1998). These results suggest that BAX-like molecules have an important mechanism of killing that is independent of the BH3

‖To whom correspondence should be addressed (e-mail: wagner@wagner.med.harvard.edu).

domain, although the structural basis of this mechanism is unclear.

BID is a proapoptotic member of the BCL2 family that shares only the BH3 domain homology with other members of the family in its amino acid sequence. It has recently been established as an intracellular messenger connecting the FAS receptor and the death-inducing complex at the cytoplasmic membrane to the mitochondrial death machinery (Li et al., 1998; Luo et al., 1998). The full-length BID is inactive and present in the cytosolic fraction of living cells. Upon cleavage by Caspase 8, the COOH-terminal part of BID then translocates to mitochondria and is sufficient to trigger cytochrome c release in isolated mitochondria. BID demonstrates some very unique and important properties after cleavage by Caspase 8. In addition to the ability of truncated BID to translocate from cytosol to mitochondria, truncated BID has at least a 10-fold higher affinity toward BCL-X_L and is 100 times more efficient in inducing cytochrome c release from mitochondria compared to its full-length precursor (Li et al., 1998). Though BAX has also been shown to induce cytochrome c release both in vivo and in vitro (Jurgensmeier et al., 1998; Rosse et al., 1998), the cleaved BID is a much more potent cytochrome c–releasing factor than BAX (Luo et al., 1998). Mutagenesis studies have also shown that translocation of truncated BID onto mitochondria is independent of its BH3 domain (Luo et al., 1998). Due to its unique (or nonhomologous) sequence, BID has not been related to any known structures other than its BH3 domain. It remains to be a puzzle as to what conformational feature of BID allows it to acquire so much more potency in promoting cytochrome c release after Caspase 8 cleavage.

In this study, we have determined the solution structure of BID using NMR spectroscopy. It consists of eight α helices arranged in a compact fold in resemblance to transmembrane and pore-forming proteins of bacterial toxins, such as diphtheria toxin and the colicins, suggesting its potential to form selective ion channels on the mitochondrial membrane. Helices 6 and 7 are primarily hydrophobic and function as two central pillars, which are surrounded by six amphipathic helices. The structure of BID shows striking similarity to BCL-X_L despite the fact that the amino acid sequences of these two antagonists share only a 16-residue BH3 domain and are otherwise unrelated. Based on a structure of BCL-X_L–BAK BH3 peptide complex (Sattler et al., 1997) and the position of the BH3 domain–containing helix in BID, we modeled the interaction between BCL-X_L and the full-length BID. We also found that the four highly conserved hydrophobic residues of the BH3 domain that are responsible for heterodimerization are surface exposed in BID, suggesting their readiness to bind BCL-X_L. Additionally, we monitored the conformation change in BID during Caspase 8 cleavage and found that the overall structural integrity of BID is preserved after it is cleaved. Analyzing ^{15}N–^{1}H cross peak changes upon cleavage, conformational changes are localized and the role of Caspase 8 cleavage in the dramatic enhancement of proapoptotic activity of BID is elucidated. Finally, based on structure comparison of BID and BCL-X_L, along with the recent finding that BID can promote mitochondrial apoptosis independent of heterodimerization with BCL2 members, we propose that BID can induce mitochondrial damage through both BH3 domain–dependent and –independent mechanisms.

Results and Discussion

Structure Determination

The structure of full-length BID was defined by a total of 2202 NMR-derived distance constraints. For residues 42–78, no long-range NOEs were observed. The local sequential NOE patterns and transverse ^{15}N relaxation rates (data not shown) of this region are characteristic of an unstructured and flexible loop. Interestingly, BCL-X_L also has a long flexible loop (consisting of approximately 64 residues) near the N terminus (Muchmore et al., 1996). In addition to residues 42–78, the N-terminal 12 residues of BID, including Gly-1 and Ser-2 (which are part of the thrombin cleavage site in the GST fusion protein), are not defined in the structure. However, this is because the resonances of the amide protons of residues 3–9 were not observed due to either fast amide proton exchange with solvent (at pH 7.0) or conformational exchange on an intermediate time scale. In all other regions, the structure is well determined. The entire protein (including the loops) consists of 60% helices (Figure 1).

Overall, the structure determination employed the simple "local to global" strategy, which puts emphasis on stabilizing the local order prior to determination of the global fold. This approach is very efficient, especially for solving structures of helical proteins (see Experimental Procedures). First, the backbone NH resonances were rigorously confirmed by three pairs of triple-resonance experiments, selective ^{15}N labeling of Lys, Phe, Ser, Tyr, Leu, Val, Ile, and Ala residues, and sequential short-range NOEs. The ^{1}H and ^{13}C resonances of the side chains were determined by various TOCSY experiments. Second, helices were identified by both $^{13}C^{\alpha}$ chemical shift values (Wishart and Sykes, 1994) and NH(i)–HA (i − 3) and NH(i)–NH(i ± 1) NOE patterns. Additionally, using the short- and medium-range NOE patterns, some of the helix-turn-helix configurations were determined. The stabilization of local orders greatly reduced the conformation search space. Finally, the global fold was determined by identifying key NOEs between hydrophobic side chains. This was confirmed by analyzing 3D ^{15}N- and ^{13}C-dispersed NOESY and 2D homonuclear ^{1}H NOESY experiments. Complete structural statistics and root-mean-square deviation values are presented in Table 1. The precision of this structure can also be assessed from the dispersion of the 15 superimposed backbone traces shown in Figure 2A.

Structure Overview

The three-dimensional structure of BID is illustrated in Figure 2. Loops 1–12 and 43–77 are not displayed in the figure because they are completely disordered. The structured portion of BID consists of eight α helices arranged in a compact fold (Figures 2 and 5C). The primarily hydrophobic helices H6 and H7 are arranged in an antiparallel manner in the core of the protein. The

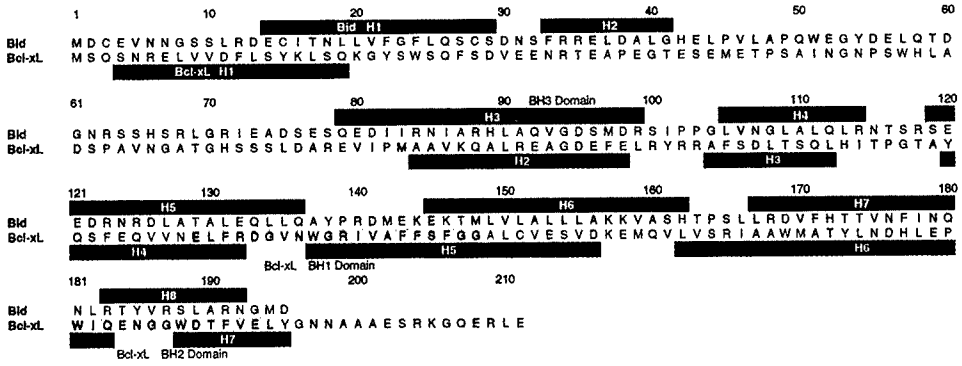

Figure 1. Amino Acid Sequences of BID and BCL-X_L Aligned at the BH3 Domains (Shaded in Yellow)

There is no sequence homology between the two proteins outside the BH3 domain. Red and blue bars indicate helices identified in BID and BCL-X_L, respectively. The BH1 and BH2 domains of BCL-X_L are shaded in light blue.

other six helices are amphipathic and packed around the two central helices. Helix H3 contains the BH3 domain and is fixed by hydrophobic contacts with helix H1 and helix H8. Structure comparison of BID and BCL-X_L (Figure 2C) shows extensive conformation homology between the two proteins (Muchmore et al., 1996) although their sequences are completely unrelated outside the 16-residue BH3 domain (Figure 1). The major difference between the two structures is that BID has an extra helix (H2) in its N-terminal region. Additionally, the flexible loop in BCL-X_L between the BH3 domain–containing helix (H2) and N-terminal helix (H1) is almost twice as long as that in BID. By matching the structurally homologous regions between these two molecules, we found that H1, H3, H4, H5, H6, H7, and H8 of BID correspond to H1, H2, H3, H4, H5, H6, and H7 of BCL-X_L, respectively (Figure 1).

The surface electrostatic potential of BID shown in Figure 3A does not reveal any unusually charged regions. However, BID has large hydrophobic patches on the surface (Figure 3B). Since BID and BCL-X_L are structurally similar, it is informative to compare their hydrophobic surfaces. Interestingly, four partially conserved hydrophobic residues of the BH3 domain (I82, I86, L90, and M97) are exposed in BID (Figures 1 and 3B), whereas those of BCL-X_L are buried (Figures 1 and 3C). As illustrated in Figure 3B, the surface of BID also has a large hydrophobic cleft formed by L105, Y140, V150, L151, and L154. This region remotely resembles the hydrophobic cleft (F105, L108, and L130) of BCL-X_L, which has been shown to bind BH3 death ligand (Sattler et al., 1997). However, biological implication of the BID hydrophobic cleft remains to be investigated. Thus far, neither BID homodimerization nor interaction between BID and BH3 ligand has been reported.

Structural Similarity to BCL-X_L Implies the Function of BID

Interaction between pro- and antiapoptotic members of the BCL2 family has long been considered a crucial mechanism for cell death induced by BAX-like members. However, multiple lines of recent evidence suggest that proapoptotic activities of BAX-like proteins are independent of the heterodimerization via the BH3 domain (discussed in Introduction). Studies have also shown that BID does not only function through heterodimerization with BCL2. A mutant of the truncated BID, which cannot bind BCL-X_L, can still target mitochondria and induce apoptosis very efficiently (H. L. and J. Y., unpublished results). In a separate study, Luo et al. showed that the BH3 mutant of the truncated BID (G94E) associated with mitochondria to the same extent as the wild type (Luo et al., 1998). On the other hand, heterodimerization may be important for the functions of BID. It has been proposed that heterodimerization with other prosurvival members of the BCL2 family is essential for the proapoptotic activity of the BH3 members (reviewed in Adams and Cory, 1998; Kelekar and Thompson, 1998). As the BH3 domain is the only homologous region that BID shares with other members of the family, heterodimerization would involve this domain. The above controversies may be resolved by the structural similarity between BID and BCL-X_L. Since the structure of BID is remarkably similar to BCL-X_L, we propose that BID is able to interact with mitochondria in a very similar way as to BCL-X_L and BAX, either by forming a selective ion channel or interacting with some unknown receptors on the membrane. BCL2 has been shown to bind the CED4-like portion of Apaf1, dependent on its N-terminal BH4 domain (helix H1 in Figures 1 and 2C), and thereby prevent the activation of Procaspase 9 (Hu et al., 1998; Pan et al., 1998). Since the truncated BID does not have the BH4 domain, one possible proapoptotic mechanism is that BID, upon cleavage by Caspase 8, can partially mimic BCL-X_L in interacting with mitochondria while not inhibiting proapoptotic molecules such as Apaf1. Indeed, this is in line with the previous finding, which was not well understood at the time, that cleavage of the N-terminal BH4 domain of BCL2 by Caspase 3 can convert BCL2 into a proapoptosis protein (Cheng et al., 1997). An equally possible mechanism would be that the cleaved BID can target the mitochondrial membrane and form selective ion channels that counter the effect of those formed by BCL-X_L.

Model for Heterodimerization between Full-Length BID and BCL-X_L

As mentioned previously, one of the proapoptotic mechanisms adopted by BAX and BH3 proteins is to bind BCL2 proteins and inhibit their antiapoptotic action via

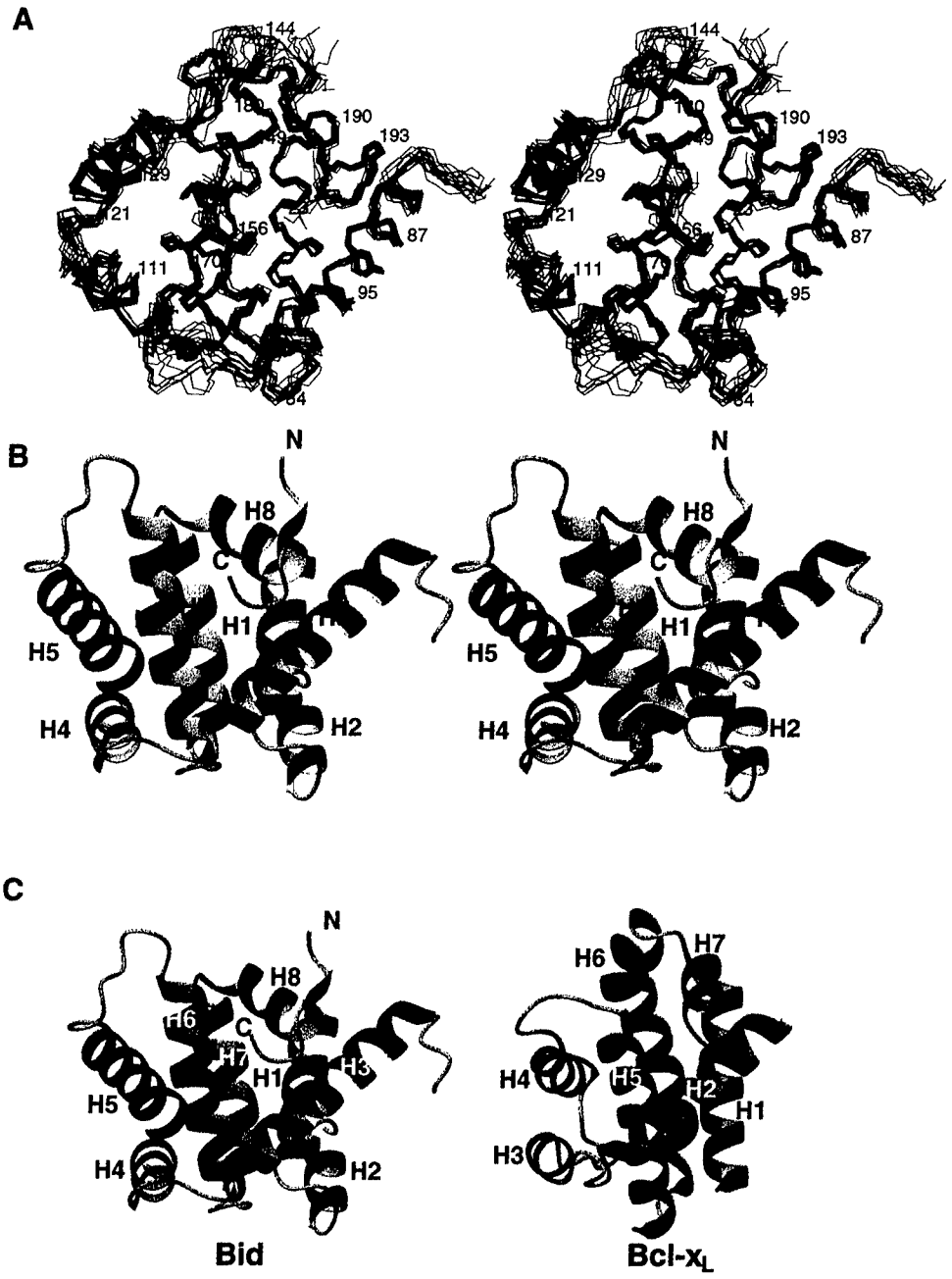

Figure 2. Solution Structure of BID

The flexible regions of BID (1–12 and 43–78) are not displayed.

(A) Stereoview of an ensemble of 15 out of 20 calculated structures representing the models with lowest energy (see Experimental Procedures). Only backbone atoms (N, C^{α}, C′) are shown.

(B) Ribbons stereodrawing of BID showing the eight helices, labeled H1–H8. This view emphasizes the position of the BH3 domain–containing H3 and the two hydrophobic helices H6 and H7.

(C) Ribbons drawings of BID (displayed in blue) and BCL-X_L (displayed in brown) showing the comparison of the two structures. The coordinates of BCL-X_L were obtained from the Protein Data Bank with the ID code 1MAZ. The figure was generated with MOLMOL (Koradi et al., 1996).

their BH3 "death ligands." This heterodimerization can either prevent BCL2 from interacting with Apaf1 or affect its ion channel formation on the mitochondria membrane that maintains the membrane potential (reviewed by Adams and Cory, 1998; Kelekar and Thompson, 1998). Now we know that BID and BAX members are structurally related and should interact with BCL2 in a similar fashion. The structure of BCL-X_L in complex with the BH3 amphipathic helix of BAK revealed that the insertion of the BH3 helix of BAK into the hydrophobic cleft of BCL-X_L (formed by its BH1 and BH2 domains) is a key event in the heterodimerization between death agonist and antagonist (Sattler et al., 1997). According to the structure and mutagenesis studies (Sattler et al., 1997),

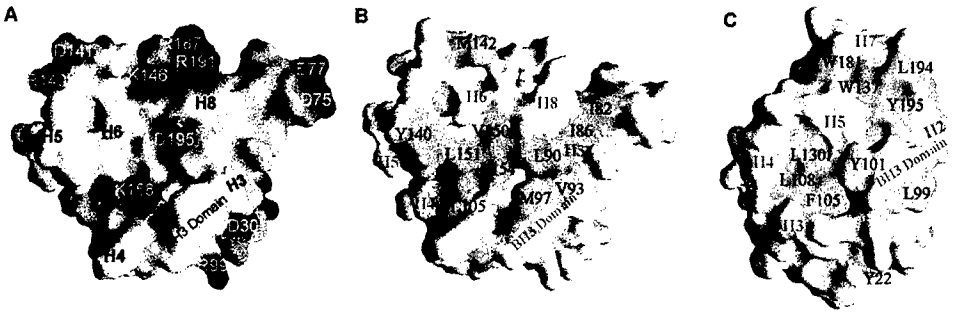

Figure 3. Surface Diagrams of BID and BCL-X_L

The BCL-X_L coordinates were obtained from the Protein Data Bank with ID code 1MAZ. In (A), the surface electrostatic potential is color coded such that regions with electrostatic potentials <-8 k_BT are red, while those $>+8$ k_BT are blue; k_B and T are the Boltzmann constant and temperature, respectively. In (B) and (C), surface-exposed hydrophobic residues, including Leu, Val, Ile, Met, Trp, Phe, and Tyr, are colored in light green. (A) Electrostatic potential surface of BID, showing no distinct charged regions. (B) Hydrophobic surface of BID formed primarily by residues in H6 and H3. (C) The elongated hydrophobic cleft of BCL-X_L to which the BAK BH3 peptide binds. This cleft is formed primarily by residues in H5 and H7. The figure was generated using GRASP (Nicholls et al., 1991).

four highly conserved hydrophobic side chains of the BAK BH3 helix point into the hydrophobic cleft of BCL-X_L and stabilize complex formation. These four residues are V74, L78, I81, and I85, and they are aligned with residues I86, L90, V93, and M97 of the BID BH3–containing helix (H3), respectively (Figure 1). Based on the homology model of BAK, derived from the structure of BCL-X_L, Sattler et al. found that the above four hydrophobic residues of the BAK BH3 domain point toward the interior of the BAK protein, making these residues unavailable to interact with BCL-X_L (Sattler et al., 1997). This is expected, since the corresponding residues are also buried in BCL-X_L (Figure 3C), which was the structural template for BAK modeling. As a result, the authors suggested that binding to BCL-X_L would necessitate a conformational change near the BAK BH3 helix to expose the hydrophobic surface of that helix. Furthermore, it was pointed out that such a conformational change is facilitated by the presence of the highly flexible loop preceding the BH3 helix.

Interestingly, residues I86, L90, V93, and M97 of the BID BH3 domain are surface exposed and ready to bind to a hydrophobic cleft. The surface representation of BID (Figure 3B) shows that these residues form an elongated hydrophobic patch on H3, adjacent to H8. Among these four residues, V93 and M97 completely point outward, whereas I86 and L90 are partially exposed and make contact with the hydrophobic residues on H8 (Figure 4A). Based on the information from the BCL-X_L–BAK peptide complex (Sattler et al., 1997), it is likely that I86 and L90 of BID are released from H8 and turn completely into the binding groove during heterodimerization. Additionally, the side chain of a highly conserved charged residue D95 (which corresponds to D83 of the BAK BH3 domain) leans toward the BID interior, yet is partially surface exposed. It is in a position to form a salt bridge with R100 and possibly R103 of BCL-X_L. This orientation is similar to that of D83 in the BCL-X_L–BAK complex structure. Since the BH3 helix of BID seems to be readily inserted into the hydrophobic cleft of BCL-X_L, we tested whether BID can be docked to BCL-X_L without any stereochemical conflict. By superimposing precisely the BH3 helix of BID and that of BAK (in complex with BCL-X_L), we were able to obtain a heterodimer model in which the binding surfaces of the two molecules complement each other reasonably well (Figure 4B). The model showed only minor stereochemical conflicts between the two molecules that can be readily eliminated by slight outward movement of BID H3 during the docking process.

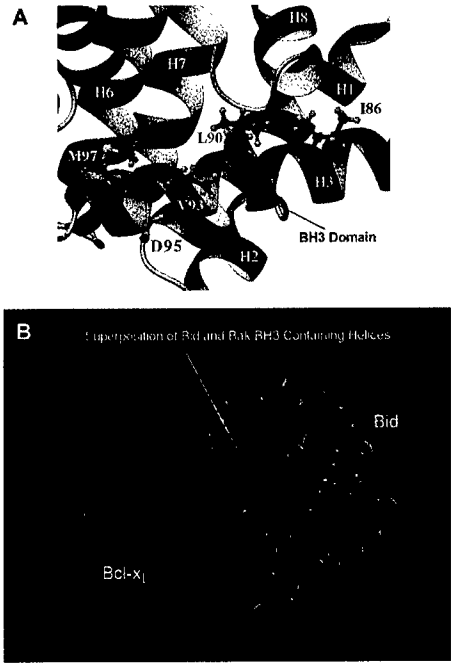

Figure 4. Model of the BID–BCL-X_L Heterodimer

(A) Ribbon diagram showing the BH3 domain of BID and its environment. The surface-exposed side chains of four highly conserved hydrophobic residues—I86, L90, V93, and M97—and the charged residue D95 are displayed.

(B) Overall view of the model for the BID–BCL-X_L heterodimer. The docking was performed using the InsightII program (Biosym, San Diego) by superimposing the BH3 domains of BAK and BID. Note that the red and blue BH3 helices of BAK and BID coincide almost completely. The rotational orientation around the BH3-helix axis was achieved by superimposing the conserved residues of the BH3 domains. The coordinates of BCL-X_L–BAK BH3 peptide complex were obtained from the Protein Data Bank (ID code 1BXL).

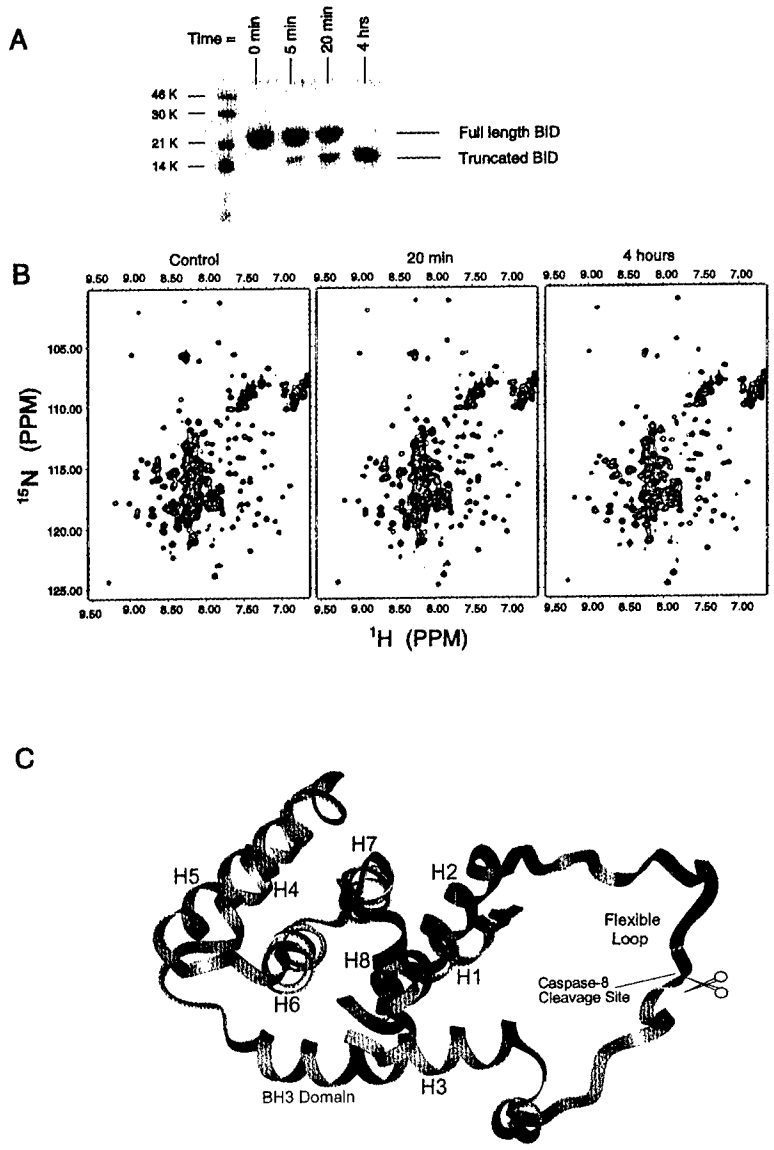

Figure 5. Monitoring the Conformation Change in BID during Caspase 8 Cleavage

The proteolytic reaction is initiated by mixing ^{15}N-labeled BID with unlabeled and active Caspase 8 at the ratio of 100:1.

(A) SDS-PAGE showing the fraction of cleaved BID. Four time points—0 min, 5 min, 20 min, and 4 hr—were recorded.

(B) ^{15}N–^{1}H HSQC spectrum of BID in the absence of Caspase 8 (control), BID after 20 min of Caspase 8 reaction, and BID after 4 hr of Caspase 8 reaction.

(C) Ribbon diagram of BID highlighting the residues whose local chemical environments are changed due to Caspase 8 cleavage. In this representation, residues of which NH chemical shift changes are greater than 0.1 and 0.02 ppm in ^{15}N and ^{1}H dimension, respectively (based on the spectra shown in [B]), are colored in red. Otherwise, they are illustrated in gray.

Mechanism of BID Activation by Caspase 8

Inasmuch as cleavage by Caspase 8 can greatly enhance the proapoptotic activity of BID, it has been hypothesized that such a dramatic activation is accompanied by major conformation changes after cleavage. To test this hypothesis, we monitored structural changes in BID during Caspase 8 proteolytic reaction using ^{15}N–^{1}H heteronuclear single quantum coherence correlation (HSQC) experiments (Bax et al., 1990; Cavanagh et al., 1996). The ^{15}N–^{1}H HSQC spectrum is characteristic of the protein conformation and is thus sensitive to structural changes. We initiated the proteolytic reaction by mixing full-length BID and active Caspase 8 at the ratio of 100:1 at room temperature. Then, ^{15}N–^{1}H HSQC spectra were recorded after 20 min and 4 hr. The fraction of cleaved BID at these two time points can be assessed from SDS-PAGE, shown in Figure 5A. The SDS-PAGE shows almost complete cleavage of BID after 4 hr of reaction (Figure 5A). The times above the HSQC spectra shown in Figure 5B are the times at which the individual experiment was started. Since each ^{15}N–^{1}H HSQC experiment took 1 hr and 10 min, the line shapes of the cross peaks that change upon cleavage are modulated in the spectrum started at 20 min. However, the spectrum recorded after 4 hr represents the fully cleaved product. Interestingly, the latter spectrum resembles very closely that of BID in the absence of Caspase 8 (the control) (Figure 5B), suggesting that the overall structural integrity of BID is preserved upon Caspase 8 cleavage. However, there are many small changes in resonance positions, which are a result of minor conformation changes, and can be easily traced in the spectra. Residues that showed significant chemical shift changes are highlighted in the ribbon drawing of BID (Figure 5C). As expected, the changes predominantly occurred in the loop region near the cleavage site, the N-terminal helices H1 and H2, H3 (containing the BH3 domain), H7, and H8. In the top view of the BID ribbon representation

shown in Figure 5C, it can be readily seen that H3, H7, and H8 all have close contacts with the N-terminal H1 and H2. Hence, small chemical shift changes are expected for these regions due to small rearrangements of H1 and H2 upon Caspase 8 cleavage.

The finding that the N-terminal domain remains intact at approximately the same position and orientation shows that the loop between H3 and H2 has no tension and plays no part in the folding of the eight helices in the uncleaved molecule. The unexpected result of this study is that the uncleaved and cleaved BID have approximately the same conformation. On the other hand, though the flexible loop is not important for the maintenance of BID structure, its cleavage has a profound effect on the proapoptotic activity. Upon cleavage, BID can target mitochondria and induce apoptosis independent of its BH3 domain (H. L. and J. Y., unpublished results). Additionally, truncated BID can bind approximately ten times stronger to BCL-X_L via its BH3 domain (Li et al., 1998). One possible mechanism for the activation of BID is that the N-terminal segment may serve as an internal inhibitor of proapoptotic activity. We propose that the proapoptotic activity of BID requires dissociation of the N-terminal segment including H1 and H2. While the N-terminal segment remains associated with the core of BID at the high concentrations used for the NMR experiment (Figure 5), at low cellular concentrations of BID this segment may detach after Caspase 8 cleavage and render the protein active. Even in the uncleaved BID, the N-terminal helices H1 and H2 may temporarily detach from the protein core, leading to some (although much lower) activity of the uncleaved protein.

The effect of Caspase 8 cleavage should be discussed with respect to the two models for the mechanism of BID function, formation of selective ion channels, like BCL-X_L and BAX, and/or inhibition of the interaction of BCL-X_L with Apaf1. Channel formation by BID could be promoted by Caspase 8 cleavage, since dissociation of the N-terminal segment would expose the hydrophobic face of helices H6 and H7 (Figure 5C). The two helices resemble closely the two central pore-forming helices H5 and H6 of BCL-X_L (Minn et al., 1997; Matsuyama et al., 1998), which have been considered important for channel formation. Figure 5C shows that dissociation of the N-terminal H1 and H2 can expose the central hydrophobic helices H6 and H7. Acquisition of channel-formation capabilities after cleavage may be the switch that enables the molecule to vigorously target mitochondria and promote cytochrome c release. However, the mechanism of cytochrome c release by pore formation is still unclear.

BID cleavage by Caspase 8 may also enhance heterodimerization with BCL-X_L and prevent the formation of the antiapoptotic complex between BCL-X_L and Apaf1. Dissociation of the N-terminal domain in BID is expected to loosen the contact of H3 and H8 with the protein core, and the H3 helix is less restricted to rearrange upon binding BCL-X_L. The putative binding site for BCL-X_L on helix H3 of BID and the contact area on H3 for the N-terminal helix H1 are on opposite faces of this H3 helix, and both interactions may have a competitive element. If cleaved BID is initially associated with the N-terminal domain, insertion of BH3 into the hydrophobic cleft of BCL-X_L could promote dissociation of H1 and H2. Thus, heterodimerization efficiency of the BH3 domain would depend on the local concentration of BCL-X_L and BID N-terminal domain. However, in full-length BID, the flexible loop can function as a chemical cross-link that can oppose heterodimerization with BCL-X_L by maintaining a much higher local concentration of the N-terminal domain.

Conclusion

We have determined the solution structure of BID, a proapoptosis member of the BCL2 regulatory family that has recently been established as a cross-talk agent for relaying the FAS/TNF apoptotic signal to the mitochondria death pathway. It consists of eight α helices arranged in a compact fold homologous to BCL-X_L. The structure of BID also revealed that the BH3 domain–containing helix is in a position ready for interaction with the hydrophobic cleft of BCL-X_L that has been shown to bind the BAK BH3 domain. Using the available structural data on the BCL-X_L–BAK BH3 peptide complex, we modeled the heterodimerization between BCL-X_L and the full-length BID by superimposing the BH3 domains of BAK and BID. Since BID becomes truly active in promoting cytochrome c release only after cleavage by Caspase 8, we monitored the conformation change in BID during Caspase 8 reaction using NMR spectroscopy. Analysis of the ^{15}N–^{1}H cross peaks of full-length and cleaved BID concluded that the overall structural integrity of BID is preserved after it is cleaved by Caspase 8. Additionally, based on the cleavage study, the role of Caspase 8 cleavage in the dramatic enhancement of proapoptotic activity of BID is elucidated. Although the BH3 domain of BID is critical for its heterodimerization with BCL-X_L, truncated BID is capable of targeting mitochondria and promoting mitochondria damage independent of its BH3 domain (Luo et al., 1998; H. L. and J. Y., unpublished results). In this study, we have provided a structural basis for truncated BID–induced mitochondrial damage. We propose that BID may have two modes of proapoptotic actions. First, BID can interact with proapoptotic members of the BCL2 family through their respective BH3 domains. We showed that although the full-length BID can interact reasonably well with BCL-X_L, cleavage by Caspase 8 and removal of H1 and H2 of BID may eliminate H1 as a competitive binder of the BH3 domain, making it more available for interacting with BCL-X_L. Second, BID also contains the structural motifs for pore formation and is potentially able to form selective ion channels similar to BAX and may promote apoptosis in a way other than inhibiting BCL2 proteins. Cleavage by Caspase 8 and dissociation of the N-terminal H1 and H2 expose the central hydrophobic helices H6 and H7, which remarkably resemble the two central pore-forming helices H5 and H6 of BCL-X_L (Minn et al., 1997; Matsuyama et al., 1998). The central hydrophobic helices H6 and H7 may be responsible for mitochondrial targeting after cleavage by Caspase 8 as well as potential pore-forming ability of BID. Overall, we

Table 1. Structural Statistics for the 15 Structures of Lowest Energy Obtained from 20 Starting Structures[a]

NOE distance restraints		
All	2202	
Intraresidue	610	
Interresidue	1592	
Sequential ($\|i - j\| = 1$)	760	
Medium	287	
i, i + 2	63	
i, i + 3	150	
i, i + 4	74	
Long ($\|i - j\| > 4$)	405	
Hydrogen bonds[b]	140	
Dihedral angle restraints		
ϕ ($C'_{(i-1)} - N_i - C_{\alpha i} - C'_i$)	93	
ψ ($N_i - C_{\alpha i} - C'_i - N_{(i+1)}$)	94	
$\chi 1$ ($N_i - C_{\alpha i} - C_{\beta i} - C_{\gamma 1 i}$ or $O_{\gamma 1 i}$)	74	
Ramachandrian plot[c]	Residues 13–44, 77–197	Secondary Structure
Most favorable region	70.2	81.1
Additionally allowed region	21.7	15.4
Generously allowed region	7.3	3.3
Disallowed region	0.8	0.2
Average rms deviations from experimental distance restraints (Å) all (2102)		0.044 ± 0.001
Average rms deviations from experimental dihedral restraints (°) all (261)		0.32 ± 0.04
Average rms deviations from idealized covalent geometry		
Bonds (Å)		0.003 ± 0.0001
Angles (°)		0.48 ± 0.006
Impropers (°)		0.42 ± 0.010
Average rms deviations of atomic coordinates between 15 structures[d]	Residues 13–44, 77–197	Secondary Structure
Backbone (Å)	0.92	0.54
Heavy atoms (Å)	1.44	0.93

[a] None of these structures exhibited distance violations greater than 0.4 Å or dihedral angle violations greater than 5°.
[b] During structure calculation, hydrogen bond restraints were added only for α helices, identified based on backbone $^{13}C\alpha$ resonances (Wishart and Sykes, 1994) and NH(I)–HA(I − 3, I − 4) NOE observed in the 3D ^{15}N-NOESY-HSQC spectrum.
[c] The program PROCHECK_nmr (Laskowski et al., 1993) was used to assess the quality of the structures.
[d] The precision of the atomic coordinates is defined as the average rms differences between the 15 final calculated structures and the mean coordinates.

propose that although there is only very limited sequence homology between BID and BAX, BID acts very similarly to BAX and may have multiple modes of action in inducing mitochondrial damage.

The conformational similarity between BID and BCL-X_L is rather surprising, since the two proteins are unrelated in their amino acid sequences. This has been independently shown by McDonnell et al. (1999 [this issue of *Cell*]), who have solved the BID structure at 45°C. However, this phenomenon was also observed for proteins involved in caspase recruitment. The FAS death domain (DD), FADD death effector domain (DED), and caspase recruitment domain (CARD) are unrelated in sequence yet adopt the similar six-helix bundle conformations (Huang et al., 1996; Chou et al., 1998; Eberstadt et al., 1998). The recurrence of this phenomenon of different sequences yielding similar structures suggests that apoptosis is an ancient process that involves a limited number of evolutionarily highly conserved structural motifs. In order for them to construct an intricate network of regulatory pathways, a high degree of specificity must be employed. For instance, BCL-X_L, BID, and BAX are structurally similar yet functionally nonredundant. Still, little is known about the detailed molecular mechanisms that allow them to take different roles in apoptosis.

Experimental Procedures

Expression and Purification of BID

Human full-length BID gene was amplified by PCR from EST cDNA clone 52055 using primers HL176 (5′ CCGGATCCATGGACTGTGAG GTCAAC) and HL178 (5′ GGGGATCCCTGAGTCAGTCCATCCCATTT CTG) and then cloned into the BamHI site of pGEX-2T vector. BID was expressed in *Escherichia coli* with GST fused at the N terminus. The transformed cells were grown in either LB-rich media (for unlabeled protein) or M9-minimal media (for labeled protein). For isotope labeling, the M9 media were substituted with ^{15}N-labeled ammonia (1 g l^{-1}) or ^{13}C glucose (2 g l^{-1}). For triple-resonance experiments, uniformly ^{15}N, ^{13}C, ^{2}H-labeled protein was prepared by growing the cells in 90% D_2O with ^{15}N-labeled ammonia and ^{13}C glucose. A 50% deuterated and ^{15}N, ^{13}C-labeled sample was prepared by growing the cells in 50% D_2O with ^{15}N ammonia and ^{13}C glucose. For selective amino acid labeling, the plasmid was transformed into DL39 cell line (cell that lacks aminotransferase) to minimize cross labeling between different amino acids. Selective ^{15}N labeling was done by growing the cells in M9 media supplemented with selected ^{15}N-labeled amino acids.

After cell lysis, the GST-fusion recombinant protein was first separated from other *E. coli* proteins by GST affinity chromatography at pH 7 and then cleaved off GST with thrombin (Biotech Pharmacia). The eluted BID was purified to homogeneity using gel filtration (Sephadex G-50). The identity of the protein was confirmed by N-terminal sequencing, amino acid composition analysis, and SDS-PAGE. NMR samples contained 1 mM protein in 20 mM Tris (pH 7.0) and 5 mM NaCl in H_2O/D_2O (9/1) or D_2O. For the homonuclear NOESY experiment, the sample contained 1 mM protein in 50 mM

$NaPO_4$ (pH 7.0) in D_2O. The NMR sample used for monitoring Caspase 8 cleavage was prepared by mixing 1 mM ^{15}N-labeled BID with unlabeled Caspase 8 at the ratio of 100:1.

NMR Spectroscopy

All NMR spectra were acquired at 25°C on Varian Unity 500, Varian UnityPlus 500, Bruker 600, or Varian UnityPlus 750 spectrometers. For assignment of the backbone ^1H, ^{13}C, and ^{15}N resonances, three pairs of triple-resonance experiments were recorded using uniformly ^{15}N, ^{13}C-labeled and 90% deuterated protein in H_2O. These are [HNCA, HN(CO)CA], [HNCO, HN(CA)CO], and [HN(CA)CB, HN(COCA)CB] (for overviews, see Clore and Gronenborn, 1993; Yamazaki et al., 1994; Matsuo et al., 1996a, 1996b). $^{13}C^\beta$ decoupling was used in HNCA and HN(CO)CA for higher $^{13}C^\alpha$ resolution and better signal sensitivity (Matsuo et al., 1996b). In addition, amino acid–selective ^{15}N labeling of Lys, Phe, Ser, Tyr, Val, Leu, Ile, and Ala was used to confirm the sequential assignment of amide protons. Side-chain proton resonances were mostly assigned using 3D Cbd-HCCH-TOCSY (Clore and Gronenborn, 1994; Matsuo et al., 1997) and 3D ^{15}N-dispersed TOCSY-HSQC spectra, recorded using uniformly ^{15}N, ^{13}C-labeled protein in D_2O and uniformly ^{15}N-labeled protein in H_2O, respectively. The assignment of aromatic side chains was accomplished using homonuclear TOCSY and NOESY experiments, acquired with the nonlabeled protein in D_2O. Stereospecific assignment of methyl groups of Val and Leu residues was obtained from ^{13}C-HSQC spectrum of a 10% ^{13}C-labeled protein (Szyperski et al., 1992). Transverse ^{15}N relaxation rates were measured with experiments as described by Peng and Wagner (1992) and Farrow et al. (1994).

Distance restraints between amide protons and side chains were obtained from two ^{15}N-dispersed NOESY spectra, acquired with mixing times of 60 and 120 ms. Long-range distance restraints between side chains (especially those of Val, Leu, and Ile) were obtained from a ^{13}C-dispersed NOESY experiment with a mixing time of 100 ms. NOE connectivities between aromatics and from aromatics to nonaromatic side chains were assigned with the combination of homonuclear 2D NOESY and ^{13}C-dispersed NOESY spectra. NOE distance restraints used for the structure calculations are summarized in Table 1. Hydrogen bond distance restraints were imposed only for the helical region, identified on the basis of $^{13}C^\alpha$ chemical shift values (Wishart and Skyes, 1994) and NH(i)-HA(i − 3, i − 4) NOE cross peaks. The backbone torsion angles ϕ and ψ were obtained using a method for measuring proton splitting in ^{15}N-HSQC spectrum by J doubling (del Rio-Portilla et al., 1994). The torsion angles $\chi 1$ of side chains in helical regions were restrained within the ranges found in refined crystal structure using the rotamer libraries of Dunbrack and Karplus (1993).

Structure calculations were performed following simulated annealing protocols of Nilges et al. (1988) using X-PLOR 3.851 (Brünger, 1993) on R10000 IndigoII Silicon Graphics work stations. Out of 20 starting structures, 19 had no violations larger than 0.4 Å or dihedral angle violations greater than 5°. The 15 structures with the lowest energy were selected for display (superimposed in Figure 2A). Structures were displayed and analyzed using the InsightII program (Biosym, San Diego), GRASP (Nicholls et al., 1991), MOLMOL (Koradi et al., 1996), and PROCHECK_nmr (Laskowski et al., 1993). The structural statistics are presented in Table 1.

Acknowledgments

We thank Greg Heffron for help with the use of spectrometers and Alexey Lugovskoy for kind assistance in making the figures. This research was supported in part by a grant from the NIH (GM 38608 and GM 47467) to G. W., a grant from the Breast Cancer Program of the US Army to J. Y., and a postdoctoral fellowship to H. L. Acquisition and maintenance of spectrometers and computers used for this work were supported by NSF (MCB 9527181) and the Harvard Center for Structural Biology and the Giovanni Armenise-Harvard Foundation for Advanced Scientific Research.

Received December 24, 1998; revised January 20, 1999.

References

Adams, J.M., and Cory, S. (1998). The Bcl-2 protein family: arbiters of cell survival. Science *281*, 1322–1326.

Bax, A., Ikura, M., Kay, L.E., and Torchia, D.A. (1990). Comparison of different modes of two dimensional reverse correlation NMR for the study of proteins. J. Magn. Reson. *86*, 304–318.

Boldin, M.P., Goncharov, T.M., Goltsev, Y.V., and Wallach, D. (1996). Involvement of MACH, a novel MORT1/FADD-interacting protease, in Fas/APO-1- and TNF receptor–induced cell death. Cell *85*, 803–815.

Brünger, A.T. (1993). XPLOR Version 3.1 (New Haven, CT: Yale University Press).

Cavanagh, J., Fairbrother, W.J., Palmer, A.G., III, and Skelton, N.J. (1996). Protein NMR Spectroscopy (San Diego, CA: Academic Press).

Cheng, E.H., Kirsch, D.G., Clem, R.J., Ravi, R., Kastan, M.B., Bedi, A., Ueno, K., and Hardwick, J.M. (1997). Conversion of Bcl-2 to a Bax-like death effector by caspases. Science *278*, 1966–1968.

Chou, J.J., Matsuo, H., Duan, H., and Wagner, G. (1998). Solution structure of the RAIDD CARD and model for CARD/CARD interaction in Caspase-2 and Caspase-9 recruitment. Cell *94*, 171–180.

Clore, G.M., and Gronenborn, A.M. (1994). Multidimensional heteronuclear nuclear magnetic resonance of proteins. Methods Enzymol. *239*, 349–363.

Cosulich, S.C., Worrall, V., Hedge, P.J., Green, S., and Clarke, P.R. (1997). Regulation of apoptosis by BH3 domains in a cell-free system. Curr. Biol. *7*, 913–920.

del Rio-Portilla, F., Blechta, V., and Freeman, R. (1994). Measurement of poorly-resolved splittings by J-doubling in the frequency domain. J. Magn. Reson. *A111*, 132–135.

Dunbrack, R., and Karplus, M. (1993). Backbone-dependent rotamer library for proteins. Application to side-chain prediction. J. Mol. Biol. *230*, 543–574.

Eberstadt, M., Huang, B., Chen, Z., Meadows, R.P., Ng, S., Zheng, L., Lenardo, M.J., and Fesik, S.W. (1998). NMR structure and mutagenesis of the FADD (Mort1) death-effector domain. Nature *392*, 941–945.

Farrow, N.A., Muhandiram, R., Singer, A.U., Pascal, S.M., Kay, C.M., Gish, G., Shoelson, S.E., Pawson, T., Forman-Kay, J.D., and Kay, L.E. (1994). Backbone dynamics of a free and a phosphopeptide-complexed Src homology 2 domain studied by ^{15}N NMR relaxation. Biochemistry *33*, 5984–6003.

Green, D.R. (1998). Apoptotic pathways: the roads to ruin. Cell *94*, 695–698.

Hu, Y., Benedict, M.A., Wu, D., Inohara, N., and Nunez, G. (1998). Bcl-x_L interacts with Apaf-1 and inhibits Apaf-1-dependent caspase-9 activation. Proc. Natl. Acad. Sci. USA. *95*, 4386–4391.

Huang, B., Eberstadt, M., Olejniczak, E.T., Meadows, R.P., and Fesik, S.W. (1996). NMR structure and mutagenesis of the FAS (APO-1/CD95) death domain. Nature *384*, 638–641.

Jurgensmeier, J.M., Xie, Z., Deveraux, Q., Ellerby, L., Bredesen, D., and Reed, J.C. (1998). Bax directly induces release of cytochrome c from isolated mitochondria. Proc. Natl. Acad. Sci. USA *95*, 4997–5002.

Kelekar, A., and Thompson, C.B. (1998). Bcl-2-family proteins: the role of the BH3 domain in apoptosis. Trends Cell Biol. *8*, 324–329.

Kluck, R.M., Bossy-Wetzel, E., Green, D.R., and Newmeyer, D.D. (1997). The release of cytochrome c from mitochondria: a primary site for bcl-2 regulation of apoptosis. Science *275*, 1132–1136.

Knudson, C.M., and Korsmeyer, S.J. (1997). Bcl-2 and Bax function independently to regulate cell death. Nat. Genet. *16*, 358–363.

Koradi, R., Billeter, M., and Wüthrich, K. (1996). MOLMOL: a program for display and analysis of macromolecular structures. J. Mol. Graph. *14*, 51–55.

Kuwana, T., Smith, J.J., Muzio, M., Dixit, V., Newmeyer, D.D., and Kornbluth, S. (1998). Apoptosis induction by Caspase-8 is amplified through the mitochondrial release of cytochrome c. J. Biol. Chem. *273*, 16589–16594.

Laskowski, R.A., MacArthur, M.W., Moss, D.S., and Thornton, J.M. (1993). PROCHECK: a program to check the stereochemical quality of protein structures. J. Appl. Crystallogr. *26*, 283–291.

Li, P., Nijhawan, D., Budihardjo, I., Srinivasula, S.M., Ahmad, M.,

Alnemri, E.S., and Wang, X. (1997). Cytochrome c and dATP-dependent formation of Apaf-1/Caspase-9 complex initiates an apoptotic protease cascade. Cell *91*, 479–489.

Li, H., Zhu, H., Xu, C.-J., and Yuan, J. (1998). Cleavage of BID by Caspase 8 mediates the mitochondrial damage in the Fas pathway of apoptosis. Cell *94*, 491–501.

Luo, X., Budihardjo, I., Zou, H., Slaughter, C., and Wang, X. (1998). Bid, a Bcl2 interacting protein, mediates cytochrome c release from mitochondria in response to activation of cell surface death receptors. Cell *94*, 481–490.

Matsuo, H., Li, H., and Wagner, G. (1996a). A sensitive HN(CA)CO experiment for deuterated proteins. J. Magn. Reson. B *110*, 112–115.

Matsuo, H., Kupce, E., Li, H., and Wagner, G. (1996b) Increased sensitivity in HNCA and HN(CO)CA experiments by selective C^{β} decoupling. J. Magn. Reson. B *113*, 91–96.

Matsuo, H., Li, H., McGuire, A.B., Fletcher, C.M., Gingras, A., Sonenberg, N., and Wagner, G. (1997). Structure of translation factor eIF4E bound to m^7GDP and interaction with 4E-binding protein. Nat. Struct. Biol. *4*, 717–724.

Matsuyama, S., Schendel, S.L., Xie, Z., and Reed, J.C. (1998). Cytoprotection by Bcl-2 requires the pore-forming α5 and α6 helices. J. Biol. Chem. *273*, 30995–31001.

McDonnell, J.M., Fushman, D., Milliman, C.L., Korsmeyer, S.J., and Cowburn, D. (1999). Solution structure of the proapoptotic molecule BID: a structural basis for apoptotic agonists and antagonists. Cell *96*, this issue, 625–634.

Minn, A.J., Velez, P., Schendel, S.L., Liang, H., Muchmore, S.W., Fesik, S.W., Fill, M., and Thompson, C.B. (1997). Bcl-x_L forms an ion channel in synthetic lipid membranes. Nature *385*, 353–357.

Muchmore, S.W., Sattler, M., Liang, H., Meadows, R.P., Harlan, J.E., Yoon, H.S., Nettesheim, D., Chang, B.S., Thompson, C.B., Wong, S.L., et al. (1996). X-ray and NMR structure of human Bcl-x_L, an inhibitor of programmed cell death. Nature *381*, 335–341.

Muzio, M., Chinnaiyan, A.M., Kischkel, F.C., O'Rourke, K., Shevchenko, A., Ni, J., Scaffidi, C., Bretz, J.D., Zhang, M., Gentz, R., et al. (1996). FLICE, a novel FADD-homologous ICE/CED-3 like protease, is recruited to the CD95 (Fas/APO-1) death-inducing signaling complex. Cell *85*, 817–827.

Muzio, M., Stockwell, B.R., Stennicke, H.R., Salvesen, G.S., and Dixit, V.M. (1998). An induced proximity model for caspase-8 activation. J. Biol. Chem. *273*, 2926–2930.

Nicholls, A., Sharp, K.A., and Honig, B. (1991). Protein folding and association: insights from the interfacial and thermodynamic properties of hydrocarbons. Proteins *11*, 281–296.

Nilges, M., Clore, G.M., and Gronenborn, A.M. (1998). Determination of three-dimensional structures of proteins from interproton distance data by dynamical simulated annealing from a random array of atoms. FEBS Lett. *239*, 129–136.

Pan, G., O'Rourke, K., and Dixit, V.M. (1998). Caspase-9, Bcl-x_L, and Apaf-1 form a ternary complex. J. Biol. Chem. *273*, 5841–5845.

Peng, J.W., and Wagner, G. (1992). Mapping of spectral density functions using heteronuclear NMR relaxation measurements. J. Magn. Reson. *98*, 308–332.

Rosse, T., Olivier, R., Monney, L., Rager, M., Conus, S., Fellay, I., Jansen, B., and Bomer, C. (1998). Bcl-2 prolongs cell survival after Bax-induced release of cytochrome c. Nature *391*, 496–499.

Sattler, M., Liang, H., Nettesheim, D., Meadows, R.P., Harlan, J.E., Eberstadt, M., Yoon, H.S., Shuker, S.B., Chang, B.S., Minn, A.J., et al. (1997). Structure of Bcl-x_L-Bak peptide complex: recognition between regulators of apoptosis. Science *275*, 983–986.

Scaffidi, C., Fulda, S., Srinivasan, A., Friesen, C., Li, F., Tomaselli, K.J., Debatin, K.M., and Krammer, P.H. (1998). Two CD95 (APO-1/Fas) signaling pathways. EMBO J. *17*, 1675–1687.

Szyperski, T., Neri, D., Leithing, B., Otting, G., and Wüthrich, K. (1992). Support of 1H NMR assignments in proteins by biosynthetically directed fractional ^{13}C-labeling. J. Biomol. NMR *2*, 323–334.

Wang, K., Gross, A., Waksman, G., and Korsmeyer, S.J. (1998). Mutagenesis of the BH3 domain of BAX identifies residues critical for dimerization and killing. Mol. Cell. Biol. *18*, 6083–6089.

Wishart, D.S., and Sykes, B.D. (1994). The ^{13}C chemical-shift index: a simple method for the identification of protein secondary structure using ^{13}C chemical-shift data. J. Biomol. NMR *4*, 171–180.

Yamazaki, T., Lee, W., Arrowsmith, C.H., Muhandiram, D.R., and Kay, L.E. (1994). A suite of triple resonance NMR experiments for the backbone assignment of ^{15}N, ^{13}C, ^{2}H labeled proteins with high sensitivity. J. Am. Chem. Soc. *116*, 11655–11666.

Yang, J., Liu, X., Bhalla, K., Kim, C.N., Ibrado, A.M., Cai, J., Peng, T.I., Jones, D.P., and Wang, X. (1997). Prevention of apoptosis by bcl-2 release of cytochrome c from mitochondria blocked. Science *275*, 1129–1132.

Yang, X., Chang, H.Y., and Baltimore, D. (1998). Autoproteolytic activation of pro-caspases by oligomerization. Mol. Cell *1*, 319–325.

Protein Data Bank ID Code

The coordinates for the human BID structure were deposited in the Protein Data Bank under ID code 2bid.

Molecular Cell, Vol. 7, 1307–1319, June, 2001, Copyright ©2001 by Cell Press

The Peutz-Jegher Gene Product LKB1 Is a Mediator of p53-Dependent Cell Death

Philip Karuman,[1] Or Gozani,[1] Robert D. Odze,[2] Xun Clare Zhou,[1] Hong Zhu,[1] Reuben Shaw,[1,3] Tom P. Brien,[2] Christopher D. Bozzuto,[1] Danny Ooi,[1] Lewis C. Cantley,[1,3] and Junying Yuan[1,4]
[1]Department of Cell Biology
Harvard Medical School
Boston, Massachusetts 02115
[2]Department of Pathology
Brigham and Women's Hospital
Boston, Massachusetts 02115
[3]Department of Medicine
Beth Israel Hospital
Boston, Massachusetts 02115

Summary

Here, we investigate the mechanism and function of LKB1, a Ser/Thr kinase mutated in Peutz-Jegher syndrome (PJS). We demonstrate that LKB1 physically associates with p53 and regulates specific p53-dependent apoptosis pathways. LKB1 protein is present in both the cytoplasm and nucleus of living cells and translocates to mitochondria during apoptosis. In vivo, LKB1 is highly upregulated in pyknotic intestinal epithelial cells. In contrast, polyps arising in Peutz-Jegher patients are devoid of LKB1 staining and have reduced numbers of apoptotic cells. We propose that a deficiency in apoptosis is a key factor in the formation of multiple benign intestinal polyps in PJS patients, and possibly for the subsequent development of malignant tumors in these patients.

Introduction

Peutz-Jegher syndrome (PJS) is an autosomal dominant disease. Early manifestations of PJS include melanocytic macules of the lips and multiple hamartomatous polyps in the gastrointestinal tract (Jeghers et al., 1949; Peutz, 1921). Later in life, PJS patients have a dramatically increased incidence of cancers in a wide variety of tissues (Giardiello et al., 1987; Spigelman et al., 1989). The genetic locus responsible for the majority of PJS cases was mapped to chromosome 19p13.3 and found to encode a Ser/Thr protein kinase named LKB1/STK11 (Hemminki et al., 1997, 1998; Olschwang et al., 1998; Jenne et al., 1998).

LKB1 is widely expressed in all tissues (Hemminki et al., 1998). Analysis of the sequence revealed that the LKB1 kinase domain (codons 50–337) contains weak homology to the conserved catalytic core of the kinase domain common to both Ser/Thr and tyrosine protein kinase family members (Hanks and Hunter, 1995), while the C-terminal domain is not homologous to any known protein. A mouse homolog (mLKB1) and a putative *Xenopus* homolog (XEEK1) of LKB1 have been identified and share 88% and 83.7% amino acid sequence identity, respectively, to human LKB1 (Smith et al., 1999; Su et al., 1996). XEEK1 is a kinase with apparent narrow substrate specificity and is enriched in the cytoplasm of oocytes and fertilized eggs.

Most of the LKB1 mutations in PJS patients result in the complete loss of protein product. Rare missense mutations that disrupt kinase function have been identified in the kinase domain (Hemminki et al., 1998; Jenne et al., 1998; Mehenni et al., 1998; Nakagawa et al., 1998). This is consistent with the proposal that LKB1 acts as a recessive tumor suppressor gene and that the formation of hamartomas and tumors is the result of somatic inactivation of the wild-type LKB1 allele in PJS patients (Hemminki et al., 1997).

Disruption of the homeostatic balance between cell proliferation and cell death is a key to cancer development (Hanahan and Weinberg, 2000). Tumor cells not only proliferate without regard to environmental clues, but also evade apoptosis. The cellular tumor suppressor gene p53 plays a prominent role in this process through its potent ability to inhibit cell proliferation and activate apoptosis (Bates and Vousden, 1996). While it is clear that p53 plays a critical role in regulating apoptosis, the mechanism by which p53 induces apoptosis remains controversial.

Our results suggest that the Peutz-Jegher syndrome gene product LKB1 may be one of the signal transduction molecules regulating p53-dependent apoptosis. We propose that the loss of LKB1 function in PJS leads to a deficiency in intestinal epithelial cell apoptosis. This defect may be a primary cause of benign hamartoma formation in PJS patients, and ultimately may render tissues highly susceptible to malignant transformation.

Results

The Expression Patterns of LKB1 in Normal Small Intestine and Peutz-Jegher Polyps

To characterize endogenous LKB1 activity, we generated a rat anti-LKB1 polyclonal antibody that specifically recognizes the murine and human 55 kDa LKB1 protein on Western blot (Figure 1A). Anti-LKB1 immunostaining of small intestinal samples from normal adult human biopsies is shown in Figure 1B. LKB1 is expressed in both the nucleus and cytoplasm of small intestinal epithelial cells. The expression of LKB1 in the cytoplasm shows a gradient pattern: epithelial cells near the luminal end of the villus tip contain more cytoplasmic LKB1 than cells elsewhere in the villus (Figure 1B, first panel). The staining is specific, as no staining was observed when the primary antibody was omitted (Figure 1C, second panel). Adult small intestinal epithelial cells are generated through divisions of multipotent stem cells anchored near the base of crypts. These cells migrate in a vertical band from the crypt up to the villus tip where they die. Thus, the spatial position of epithelial cells along the villus reflects their age: cells close to the villus tip are older than those distal to it (Potten, 1997). Accordingly, LKB1 expression is higher in older epithelial cells than in younger epithelial cells.

[4]Correspondence: jyuan@hms.harvard.edu

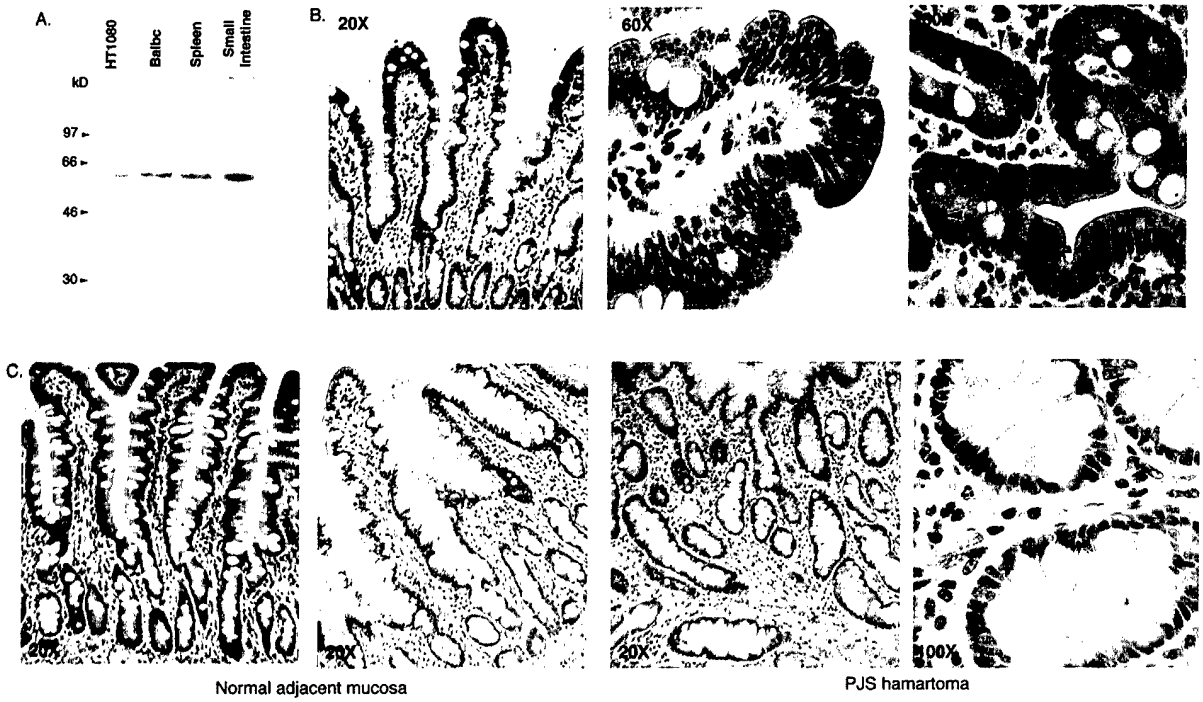

Figure 1. The Expression of LKB1 in Normal and Peutz-Jegher Small Intestinal Samples

(A) A Western blot of indicated cell and mouse tissue lysates was probed with a polyclonal rat anti-LKB1 antibody.

(B) Immunostaining of LKB1 in normal biopsy small intestinal samples by the polyclonal rat anti-LKB1 antibody. Elevated LKB1 expression in the cytoplasm of pyknotic epithelial cells (arrowheads).

(C) The expression of LKB1 in a small intestinal sample from a Peutz-Jegher patient. The apparent normal region between polyps still immunostained positive for LKB1 (first panel), while the polyps are negative for LKB1 staining (last two panels). The second panel is a control without the primary antibody.

In addition to the gradual increase of LKB1 expression along the villus, individual dying cells with pyknotic nuclei exhibited very high levels of cytoplasmic LKB1 staining (Figure 1B, second and third panels). These pyknotic cells were found in the epithelial cell region in both the crypts and villi, suggesting that upregulation of LKB1 expression may be involved in the apoptosis of epithelial cells.

To characterize the expression of LKB1 in Peutz-Jegher disease, we immunostained polypectomy samples from Peutz-Jegher patients with anti-LKB1. As expected, LKB1 expression is found in the areas of normal intestinal epithelium adjacent to or between polyps (Figure 1C, first panel). In contrast, LKB1 immunostaining is absent within the polyps (Figure 1C, last two panels). These results are consistent with mutations in the LKB1 gene of PJS patients, generally resulting in the loss of LKB1 protein expression (Hemminki et al., 1998; Jenne et al., 1998; Mehenni et al., 1998; Nakagawa et al., 1998).

A Model for LKB1-Induced Apoptosis

The observation that LKB1 expression increases in dying cells suggests that LKB1 may function as an inducer of apoptosis. To directly test this possibility, we established a cellular model to mimic LKB1 upregulation in vivo. We transfected GFP-tagged wild-type LKB1 (LKB1) into HT1080 cells, a fibrosarcoma cell line that expresses wild-type p53 (Labrecque and Matlashewski, 1995). Overexpression of LKB1 induced cell death (Figure 2A). As the kinase domain of LKB1 is often mutated in PJS, we asked whether this domain alone is sufficient for the apoptosis activity of LKB1. Expression of the kinase domain alone (amino acids 1–309; KDA) in HT1080 cells induced apoptosis more efficiently than full-length LKB1 (Figure 2A). This suggests that the C-terminal domain negatively regulates LKB1 apoptotic activity. To determine whether the kinase activity of LKB1 is required for the induction of apoptosis, we analyzed two LKB1 mutants predicted to be deficient in kinase activity, an invariant nucleotide binding site mutant (K78M LKB1) and a deletion mutant missing the first 88 amino acids (Δ88 LKB1). Neither mutant induced apoptosis (Figure 2A). Thus, we conclude that the kinase activity of LKB1 is likely required for the induction of apoptosis by LKB1.

To determine whether caspase activation is involved in LKB1-induced apoptosis, LKB1-transfected cells were treated with the pan-caspase inhibitor z-VAD-fmk (zVAD). LKB1-induced cell death was blocked by zVAD treatment (Figure 2A), indicating that caspases are critical for mediating the apoptosis triggered by LKB1. In addition, LKB1-overexpressing cells stained positive for activated caspase-3, and zVAD treatment or coexpression of Bcl-x_L blocked this staining (data not shown). Thus, LKB1 overexpression triggers caspase activation, and inhibitors of apoptosis block this activation. We also observed a significant reduction in LKB1-induced cell

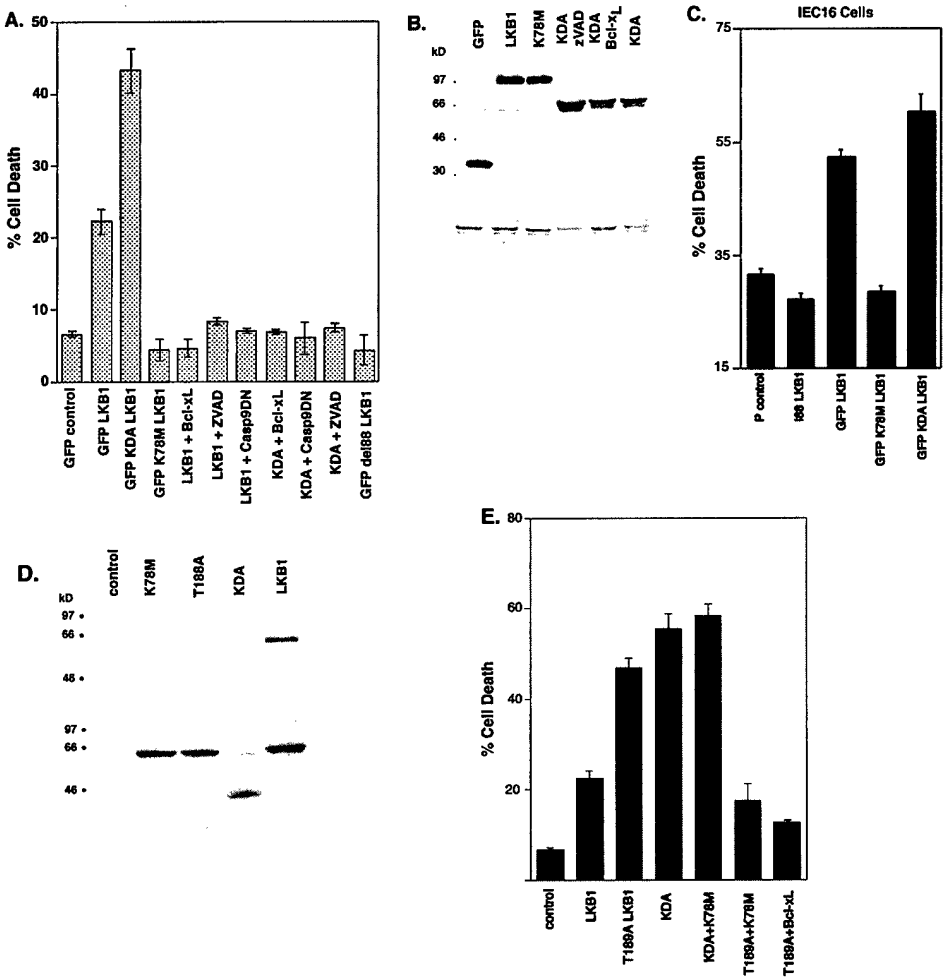

Figure 2. Apoptosis Induced by LKB1, Phosphorylation of LKB1, and Identification of a Dominant-Negative LKB1 Mutant

Indicated expression constructs were transfected into HT1080 cells (A) or IEC16 cells (C) alone or in combination with Bcl-x_L, the C287A caspase-9 dominant negative (Casp9DN), or the pan-caspase inhibitor zVAD-fmk (100 μM). At least 100 cells were scored for a total of three times for each data point. The percentages of cell death were quantified by morphological criteria. 2 μg of LKB1 DNA was used and the total amount of DNA was normalized to 4 μg of DNA. The results are exhibited as the means ± s.e.m. from at least three experiments.

(B) Loading control. Western blots of lysates from HT1080 cells transfected with the indicated plasmids were probed with an anti-GFP antibody (upper panel) and an anti-tubulin control (bottom panel).

(D) Phosphorylation of LKB1. The expression constructs of Flag alone (control), the Flag-tagged ATP binding site mutant K78M, the T189A mutant (T189A), the kinase domain alone (KDA), and wild-type LKB1 (LKB1) were transfected into HT1080 cells and immunoprecipitations were carried out 12–14 hr posttransfection. Immunocomplexes were incubated with in vitro kinase reaction buffer and analyzed by SDS-PAGE (top) and Western blot for the levels of LKB1 protein expression (bottom).

(E) Identification of an activating mutation and a dominant-negative mutation. HT1080 cells were transfected with expression constructs of control (GFP alone), GFP-LKB1 (LKB1), the GFP-kinase domain alone LKB1 (KDA), and the GFP-T189A LKB1 mutant (T189A) with or without the ATP binding site mutant (K78M) and Bcl-x_L. Cell death was assessed at 24 hr posttransfection. The results are exhibited as the means ± s.e.m. from at least three experiments.

death when LKB1 KDA was cotransfected with either Bcl-x_L or caspase-9 dominant-negative expression vectors (Li et al., 1997; Figure 2A). The protection conferred by Bcl-x_L and caspase-9 dominant negative suggests that LKB1-mediated cell death likely functions via the mitochondrial pathway of apoptosis.

To determine whether LKB1-induced apoptosis is a general phenomenon that can occur in epithelial cells, we overexpressed LKB1 in the epithelial cell line IEC16 and measured for cell death (Figure 2C). Similar to HT1080 cells, in response to LKB1 overexpression, IEC16 cells underwent apoptosis in a kinase-dependent manner (compare Figures 2A and 2C). Thus, we conclude that LKB1 can induce apoptosis in epithelial cells.

To characterize the LKB1 kinase activity and its phosphorylation pattern, we transfected HT1080 cells with wild-type and derivative constructs of LKB1. Expressed proteins were immunoprecipitated and incubated in an in vitro kinase assay. We found that the wild-type LKB1 was heavily phosphorylated whereas the phosphorylation of K78M LKB1 was greatly reduced, suggesting that LKB1 undergoes autophosphorylation (Figure 2D). In

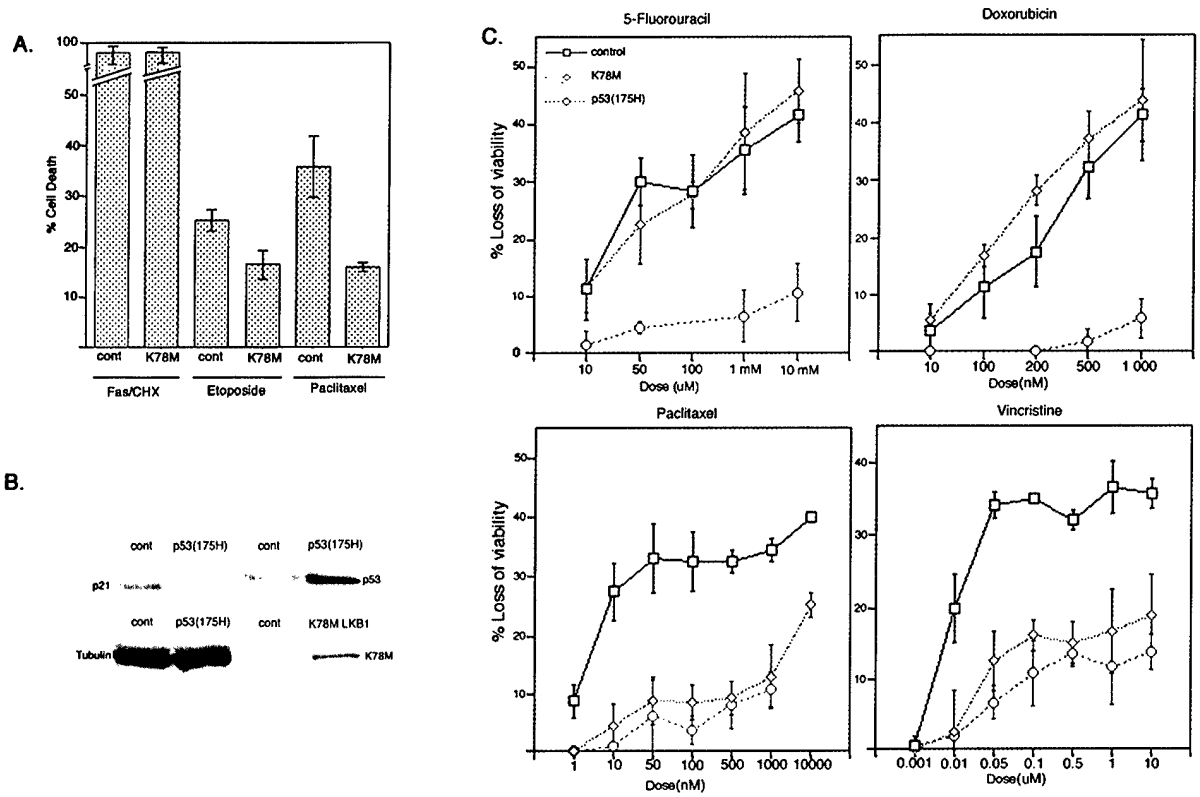

Figure 3. Inhibition of Specific Apoptosis by a Dominant-Negative Mutant of LKB1

(A) Inhibition of apoptosis by the K78M LKB1 mutant. HT1080 cells were transfected with 1 μg of GFP vector or GFP-K78M LKB1. Apoptosis was induced by treatment of Fas (7C11; 1/500 dilution) plus cycloheximide (CHX; 1 μg/ml) for 4 hr, etoposide (40 nM) for 24 hr, and paclitaxel (100 nM) for 24 hr. Dead or dying cells with nuclear apoptotic changes by Hoechst dye were counted. The difference between the control and K78M in the paclitaxel treatment group was very significant ($p < 0.0002$).

(B) The expression levels of p21, p53, and tubulin in control and p53.175H retrovirus-infected cells, and that of K78M LKB1 in K78M LKB1 retrovirus-infected cells.

(C) HT1080 cells were infected with retrovirus expressing K78M LKB1, p53.175H, or control virus. Cells were selected for 4–6 days and treated with 5-fluorouracil, doxorubicin, paclitaxel, or vincristine at the doses indicated. Apoptosis was determined 24 hr later by MTT assay. The data were collected from at least three data points. The error bars are s.e.m.

Xenopus, the Thr-197 residue of XEEK1 has been shown to be autophosphorylated (Su et al., 1996). To test whether the equivalent residue in mammalian LKB1, Thr-189, is phosphorylated (Hemminki et al., 1998), we mutated Thr-189 to Ala-189. The phosphorylation of the T189A LKB1 mutant was significantly reduced when compared to the wild-type (Figure 2D). These data suggest that like XEEK1, LKB1 is phosphorylated at Thr-189. This phosphorylation is most likely due to autophosphorylation by LKB1, although we have not ruled out the possible involvement of a coimmunoprecipitating kinase. In either case, the regulatory domain appears to be required for phosphorylation, as the KDA protein is not phosphorylated (Figure 2D). In addition, LKB1 kinase activity is also needed for phosphorylation, as the K78M LKB1 protein is not phosphorylated to any significant amount (Figure 2D).

To determine the functional role of Thr-189 phosphorylation, we transfected T189A into HT1080 cells. Interestingly, we found that the T189A LKB1 mutant is much more active in inducing apoptosis than LKB1 in HT1080 cells (Figure 2E). These data suggest that the phosphorylation of Thr-189 negatively regulates LKB1 activity. Since K78M LKB1 is kinase inactive and does not induce apoptosis, we tested to see whether it could function as a dominant negative of LKB1. Cotransfecting the constitutively active T189A LKB1 with K78M LKB1 significantly reduced the apoptosis induced by T189A LKB1. In contrast, K78M LKB1 had no effect on the apoptosis induced by the KDA construct (Figure 2E), suggesting that K78M LKB1 can function as a dominant-negative mutant, and that this activity relies on the presence of the regulatory domain in the functioning protein.

Inhibition of Apoptosis by K78M LKB1

The K78M LKB1 mutant functions as a dominant negative of wild-type LKB1 in coexpression studies (Figure 2). To test the role of endogenous LKB1 in apoptosis pathways, we asked whether the K78M mutant can inhibit the death of HT1080 cells induced by treatment with Fas, etoposide, or paclitaxel. HT1080 cells were transfected with a GFP control and the GFP-K78M LKB1 mutant, and 12 hr after transfection were treated with paclitaxel, etoposide, or Fas (7C11) together with cyclo-

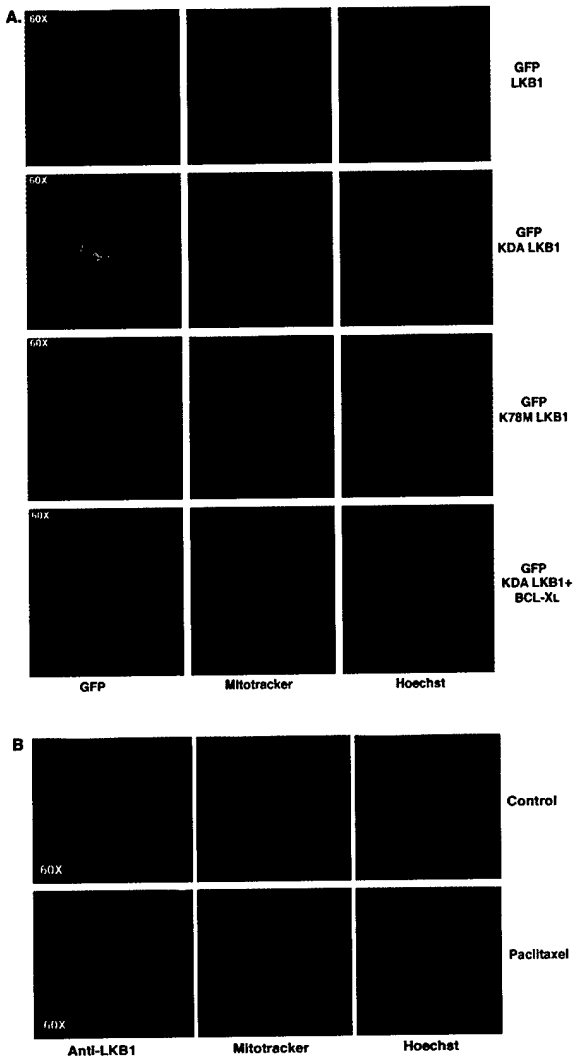

Figure 4. Mitochondrial Translocation of LKB1

(A) Subcellular localization of transfected LKB1. HT1080 cells were transfected with indicated expression plasmids. Twenty-four hr after transfection, the cells were stained with the mitochondrial-specific vital dye Mitotracker, and fixed and stained with Hoechst dye.

(B) Paclitaxel-induced LKB1 translocation in HT1080 cells. HT1080 cells were treated with paclitaxel (100 nM) for 16 hr and then stained with Mitotracker. Cells were fixed with 4% paraformaldehyde and processed for immunostaining with rat anti-LKB1 polyclonal antibody and goat anti-rat FITC-conjugated secondary antibody followed by Hoechst dye staining.

heximide. Cell death was assessed after 24 hr of treatment. Cells expressing the kinase-inactive LKB1 were much more resistant to apoptosis induced by paclitaxel than were control cells, but were equally sensitive to apoptosis induced by Fas or etoposide (Figure 3A). Fas-induced apoptosis does not require p53 (O'Connor et al., 2000), whereas apoptosis induced by paclitaxel has been proposed to be at least partially p53 dependent (Lanni et al., 1997). These results indicate that LKB1 may be involved in p53-dependent apoptosis pathways.

To further characterize the role of LKB1 in p53-dependent apoptosis, we infected HT1080 cells with a retrovirus expressing K78M LKB1, a dominant-negative p53 (p53.175H; Serrano et al., 1997) or vector. Cells were selected in hygromycin B for 4–6 days and their sensitivity to different apoptosis-inducing agents was determined. To establish that the dominant-negative p53 mutant was functioning, we checked for expression of p53 and p21. As expected, p53 expression was elevated, whereas p21 expression was absent in cells expressing the dominant-negative p53 mutant (Figure 3B). Western blot analysis showed that cells infected with the K78M LKB1 virus expressed the LKB1 mutant protein (Figure 3B). Control and HT1080 cells expressing K78M LKB1 or p53.175H were treated with different doses of 5-fluorouracil, doxorubicin, paclitaxel, or vincristine, and the loss of cell viability was measured 24 hr later by MTT assay (see Experimental Procedures). The cells expressing p53.175H exhibited considerable resistance to apoptosis induced by all four agents at the doses tested (Figure 3C). Interestingly, the cells expressing K78M LKB1 showed resistance to only paclitaxel and vincristine, the two agents that disrupt microtubule dynamics, but not to the DNA-damaging agents 5-fluorouracil or doxorubicin (Figure 3C). These results suggest that LKB1 is specifically required for the p53-dependent component of cell death induced by microtubule disruption.

Mitochondrial Translocation of LKB1 in Apoptosis

The mitochondrion is an important intracellular amplifier of apoptotic signals (Gross et al., 1999). Many types of apoptotic signals converge upon the mitochondria and cause the release of cytochrome c into the cytoplasm, which in turn activates caspase-9 by forming a complex with Apaf-1 (Li et al., 1997). In a small proportion of the HT1080 cells transfected with LKB1 and about half of the HT1080 cells transfected with KDA, we observed GFP-positive aggregates around the nuclei, which colocalized with cytochrome c (data not shown) and the mitochondrial-specific dye Mitotracker (Figure 4A, first and second row). Thus, overexpressed LKB1 KDA, and to a lesser extent, the full-length LKB1, are recruited to mitochondria. The efficiency of mitochondrial recruitment correlates with the apoptosis-inducing ability of LKB1 and KDA (compare Figures 2 and 4). This mitochondrial recruitment is evident before the appearance of nuclear condensation and appears to precede the onset of the morphological changes associated with cell death (Figure 4A, second row). To determine whether LKB1 kinase activity is required for the mitochondrial recruitment of LKB1, we transfected HT1080 cells with the kinase-dead mutant K78M LKB1. In contrast to LKB1 and KDA, K78M LKB1 is localized to both the cytoplasm and nucleus but not to mitochondria (Figure 4A, third row). Thus, the kinase activity of LKB1 appears to be required for LKB1 recruitment to the mitochondria.

To determine whether mitochondrial translocation of LKB1 is a cause or consequence of cell death, we cotransfected HT1080 cells with KDA and Bcl-x_L. Coexpression of Bcl-x_L strongly inhibited apoptosis induced by KDA (Figure 2A), but had no effect on the mitochondrial recruitment of KDA (Figure 4A, fourth row). This suggests that the mitochondrial recruitment of LKB1 is an early initiating event in LKB1-induced apoptosis.

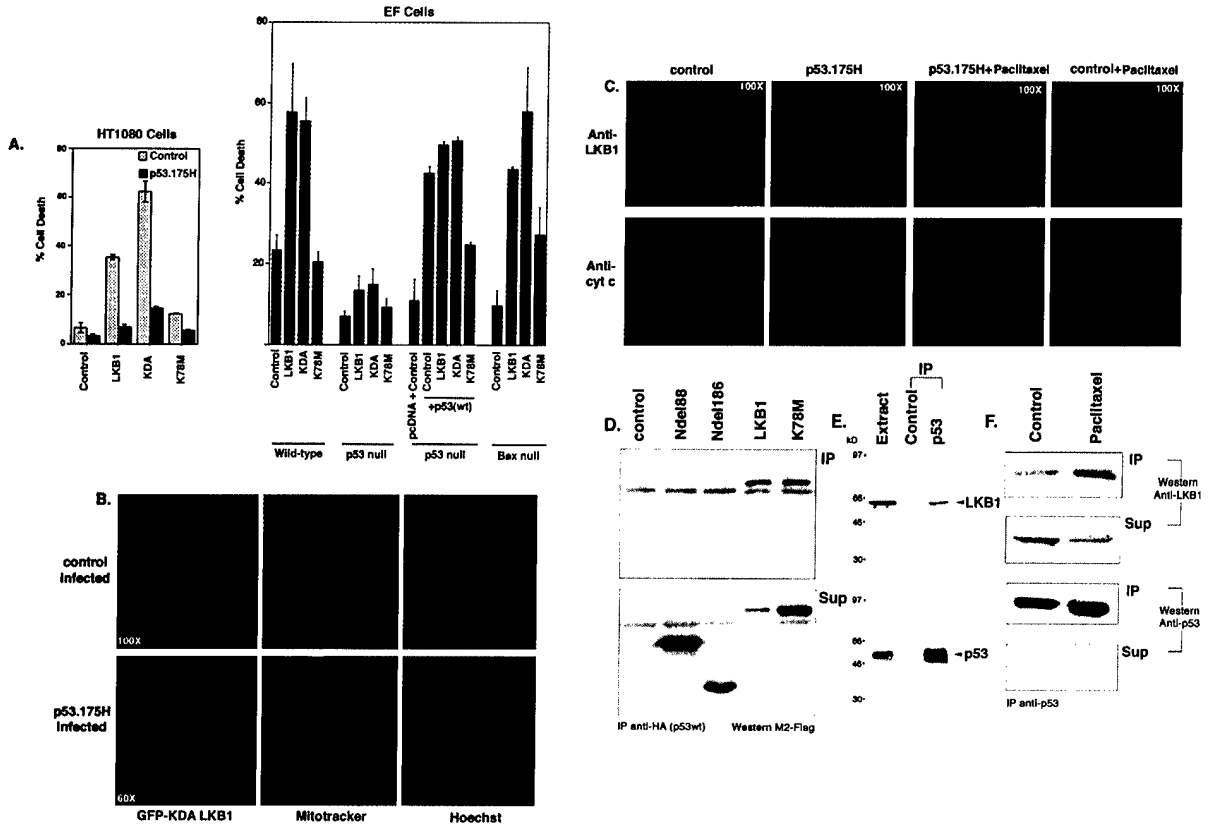

Figure 5. LKB1-Induced Apoptosis and Mitochondrial Translocation Require p53

(A) Loss of p53 function inhibits LKB1-induced apoptosis. HT1080 cells infected with control or p53.175H dominant-negative virus (pWZLHygro p53.175H) were transfected with 2 μg of indicated DNA. Or, MEF cells of equivalent early passage from p53 wild-type, p53 null, and $Bax^{-/-}$ mice were transfected with a total of 2 μg of DNA. p53 null EF cells were also complemented for p53 by cotransfecting an equivalent amount of HA-tagged wild-type p53 together with LKB1; a total of 2 μg of DNA was used. Cell death was assayed at 24 hr posttransfection. At least 100 cells were counted for each data point. All results are exhibited as the means ± s.e.m. from at least three experiments.

(B) p53 is required for mitochondrial translocation of LKB1 in HT1080 cells. Control or p53.175H virus-infected HT1080 cells were transfected with GFP-KDA LKB1 and 24 hr later stained with Mitotracker and Hoechst dye.

(C) Mitochondrial translocation of endogenous LKB1 is inhibited by the p53 dominant-negative retrovirus in HT1080 cells. Cells infected with control or p53.175H retrovirus were treated with paclitaxel (200 nM) for 12 hr and analyzed by rat anti-LKB1 and mouse anti-cytochrome c antibody with confocal microscopy. Magnification for (B) and (C) is as indicated in each first panel.

(D) Transfected LKB1 and p53 associate. HT1080 cells were transfected with HA-tagged wild-type p53 and indicated N-terminal Flag-tagged LKB1. The p53 immunocomplex precipitated by anti-HA was analyzed by Western blot using M2 anti-Flag.

(E) Endogenous p53 and LKB1 interact. Anti-p53 but not control antibody coimmunoprecipitates LKB1 from HT1080 cell lysates. The top panel shows an anti-LKB1 Western blot and the bottom panel is an anti-p53 Western blot.

(F) The interaction of endogenous p53 and LKB1 is stronger during paclitaxel-induced apoptosis. Control or paclitaxel (100 nM)-treated HT1080 cell lysates were immunoprecipitated by anti-p53, and the p53 immunocomplex was then analyzed by Western blot by anti-LKB1 or anti-p53.

To determine the subcellular localization of endogenous LKB1, we immunostained HT1080 cells with our polyclonal anti-LKB1 antibody (see Figure 1A). Endogenous LKB1 was present in both the cytoplasm and nucleus of HT1080 cells (Figure 4B, first row). Upon induction of apoptosis by paclitaxel, endogenous LKB1 translocated to the mitochondria (Figure 4B, second row). In contrast, the subcellular distribution of LKB1 did not change in apoptotic HT1080 cells induced by etoposide or UV (data not shown). Translocation of LKB1 to the mitochondria appears to be an early event in apoptosis, because a significant portion of cells with mitochondrial-localized LKB1 still exhibits normal nuclear and cell morphology (Figure 4B, second row). Thus, translocation of LKB1 to the mitochondria appears to represent an early step during paclitaxel-induced cell death.

Recruitment of LKB1 to Mitochondria and LKB1-Induced Cell Death Are Both p53 Dependent

As the inhibition of paclitaxel-induced cell death by K78M suggests that LKB1 functions in p53-dependent apoptotic pathways, we directly tested the requirement for wild-type p53 in LKB1-induced apoptosis. p53 in HT1080 cells was inactivated by retroviral transduction with p53.175H (Serrano et al., 1997). Control or p53.175H-infected HT1080 cells were then transfected with LKB1 or KDA expression constructs, and cell death was measured (Figure 5A, left panel). While control cells were still sensitive to apoptosis induced by LKB1, cells

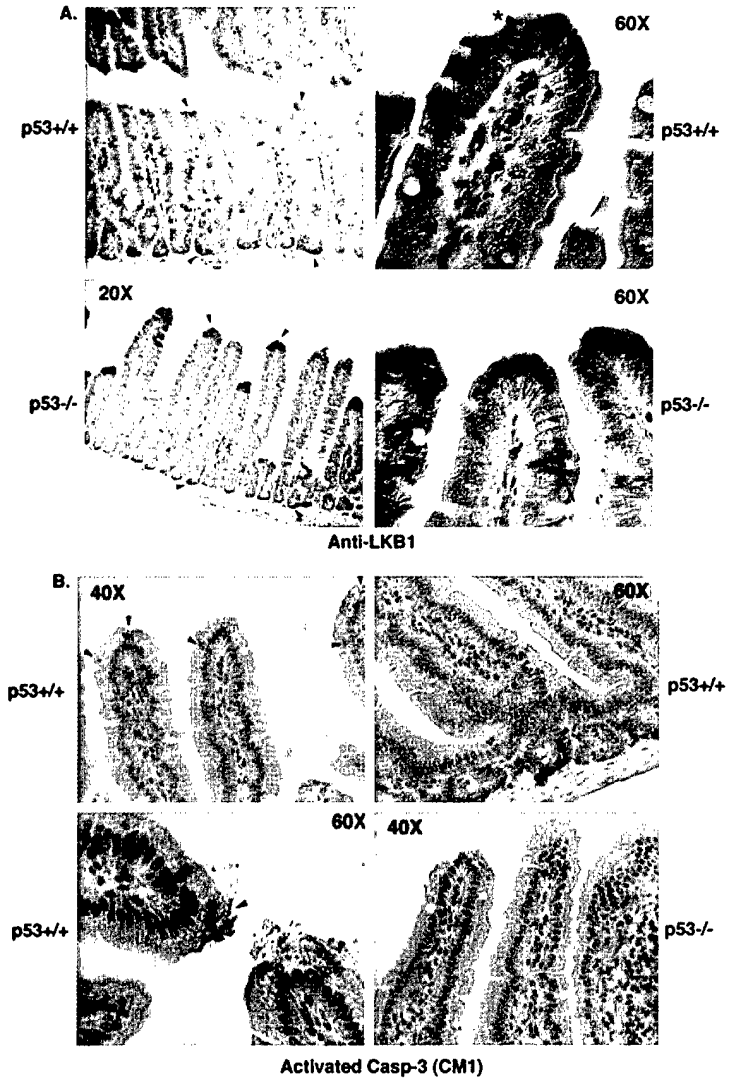

C.	p53+/+	p53-/-
# of villi counted (LKB1)	49	47
Average # of LKB1 (+) dead cells in the crypt	0.09 ± 0.04	0.04 ± 0.03
Average # of LKB1 (+) dead cells in the villus	1.1 ± 0.12*	0.17 ± 0.05*
# of villi counted (CM1)	49	49
Average # of CM1 (+) dead cells in the crypt	0.102 ± 0.04	0.04 ± 0.03
Average # of CM1 (+) dead cells in the villus	0.93 ± 0.14*	0.16 ± 0.05*

*The difference in apoptotic events between the villi of wild-type and that of p53-/- small intestine is significant (chi-square, $p < 0.00001$).

Figure 6. LKB1 Expression and Apoptosis in Mouse Small Intestine

(A) LKB1 immunostaining of wild-type and $p53^{-/-}$ mouse small intestine. The elevated LKB1 expression in the villus tips and crypts of mouse small intestine (arrowheads), a pyknotic cell in wild-type (*arrowhead), and goblet cells (arrows).

(B) CM1 staining of wild-type and $p53^{-/-}$ mouse small intestine. Arrowheads indicate CM1-positive dying cells.

(C) Quantitation of LKB1(+) and CM1(+) epithelial cells in wild-type and $p53^{-/-}$ mouse small intestine samples. Wild-type and $p53^{-/-}$ small intestinal sections were either immunostained with anti-LKB1 antibody or CM1 antibody (which recognizes activated caspase-3), and the number of apoptotic epithelial cells that exhibited elevated LKB1 expression or activated caspase-3 with pyknotic morphology in the villi and crypts were determined. As it was often difficult to distinguish between clusters of CM1(+) cells and single CM1(+) cells, we counted either of these in the villi/crypts to be one event.

expressing the dominant-negative p53 were resistant to LKB1-induced apoptosis (Figure 5A, left panel). These results suggest that wild-type p53 function is required for LKB1-induced apoptosis.

We next transfected wild-type and p53 null mouse embryonic fibroblast ($p53^{-/-}$ MEF) cells (Lowe et al., 1993) with the LKB1 expression constructs (Figure 5A, right panel). In contrast to the results in HT1080 cells, both wild-type LKB1 and KDA can induce apoptosis of wild-type MEFs with equal efficiency (Figure 5A, right panel). Since HT1080 cells are transformed cells, these results suggest that these cells may express an inhibitor of LKB1, which may not be present in nontransformed MEF cells. Consistent with HT1080 cells, wild-type LKB1 or KDA are incapable of inducing apoptosis of $p53^{-/-}$ MEF cells (Figure 5A, right panel).

To ask whether the inability of LKB1 to induce apoptosis in $p53^{-/-}$ MEF cells could be complemented by wild-type p53, $p53^{-/-}$ MEFs were cotransfected with LKB1 and wild-type p53. We found that the expression of wild-type p53 (cotransfected with control vector) was able to induce cell death, and that cotransfection of p53 with LKB1 or KDA does not significantly increase this level of apoptosis (Figure 5A, right panel). In addition, the expression of LKB1 K78M inhibited p53-induced cell death (Figure 5A, right panel). These data are consistent

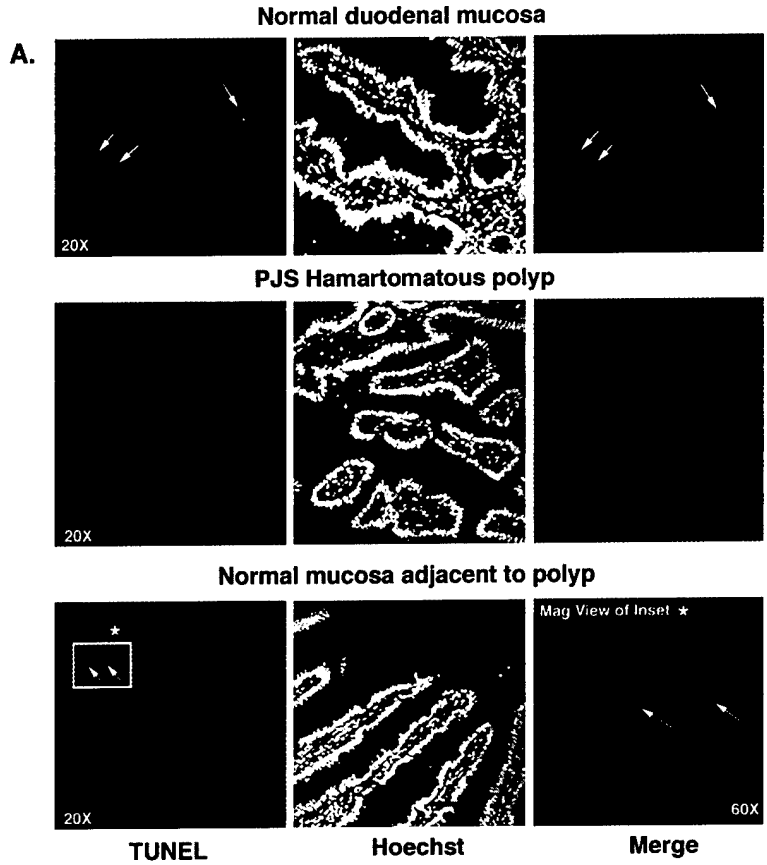

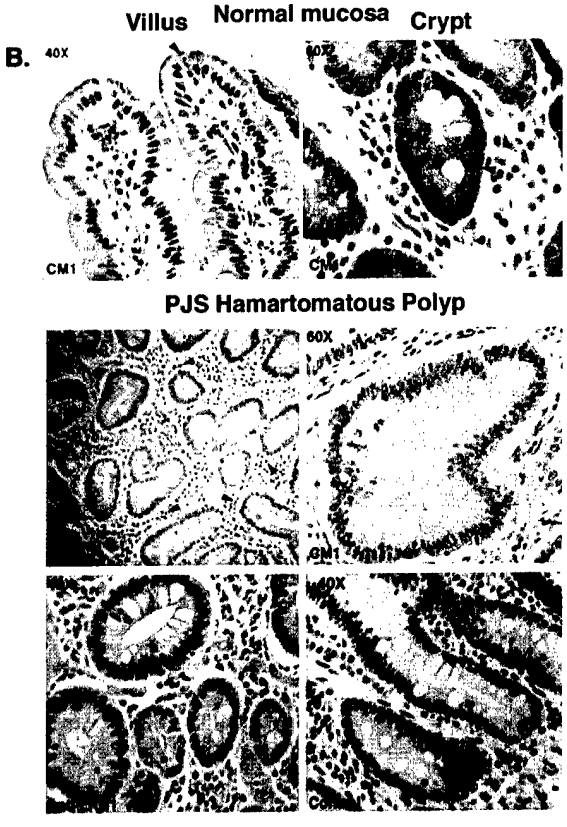

C.

	Peutz-Jeghers Polyp (n = 4 patients)	Normal Biopsies (n = 5 patients)
Mean # of epithelial cells counted	$4.1x10^4 \pm 5.6x10^3$	$1.05x10^4 \pm 3x10^3$
Mean % of apoptotic epithelial cells	$0.006 \pm 0.003^*$	$0.26 \pm 0.06^*$

*The difference between the mean percentage of apoptotic cells in the normal biopsies and the PJS hamartomas were statistically significant (Unpaired t-test $p<0.005$)

with the hypothesis that LKB1 and p53 act in the same pathway of apoptosis.

Since Bax has been proposed to be one of the downstream mediators of the p53 apoptosis pathway, we tested whether LKB1-induced apoptosis requires Bax. We transfected $Bax^{-/-}$ EF cells (Knudson et al., 1995) with LKB1 and its derivative constructs. $Bax^{-/-}$ EF cells were sensitive to LKB1- and KDA-induced apoptosis (Figure 5A, right panel). Taken together, we conclude that p53 but not Bax is essential for LKB1-induced apoptosis.

We next asked whether the mitochondrial recruitment of LKB1 during apoptosis requires p53. The subcellular localization of overexpressed KDA in control and p53.175H virally infected HT1080 cells was determined. Interestingly, transfected KDA was not recruited to the mitochondria in cells expressing p53.175H (Figure 5B), suggesting that wild-type p53 activity is needed for KDA translocation. In contrast, Bcl-x_L overexpression has no effect on the translocation of LKB1 to the mitochondria but blocks apoptosis by inhibiting a downstream event (Figure 4A).

To further confirm the role of p53 in mediating LKB1 mitochondrial translocation, we compared the paclitaxel-induced translocation of endogenous LKB1 in HT1080 cells that were infected with control or p53.175H retrovirus. After paclitaxel treatment, substantial mitochondrial recruitment of endogenous LKB1 was seen in the control virus-infected HT1080 cells (Figure 5C). As observed for overexpressed LKB1, endogenous LKB1 remained fairly diffuse throughout p53.175H-infected cells, even after paclitaxel treatment. These data establish that LKB1 mitochondrial translocation requires p53 function.

LKB1 and p53 Physically Associate

To examine the mechanism by which p53 regulates LKB1, we tested whether p53 physically interacts with LKB1. HT1080 cells were transfected with HA-tagged wild-type p53 and N-terminal Flag-tagged LKB1 constructs, and interactions were examined by immunoprecipitation (Figure 5D). We found that HA-tagged wild-type p53 can interact with Flag-tagged LKB1 and K78M LKB1; however, the efficiency of coimmunoprecipitation appeared to be higher with wild-type LKB1 than that of the K78M mutant (compare Sup/IP ratio), suggesting the LKB1 kinase activity may promote the interaction. The N-terminal kinase domain of LKB1 is required for its interaction with p53, as there is no detectable interaction between p53 and the two LKB1 N-terminal deletion mutants (NΔ88 and NΔ186; Figure 5D).

To determine whether endogenous p53 and LKB1 interact and whether the interaction is regulated by apoptosis, we examined the interaction of endogenous p53 and LKB1 in control and paclitaxel-treated HT1080 cell lysates (Figures 5E and 5F). In control HT1080 cells, immunoprecipitation by anti-p53 but not control antibody pulled down endogenous LKB1 (Figure 5E). After treatment with paclitaxel, a higher proportion of endogenous LKB1 was found in complex with p53 (Figure 5F, compare LKB1 immunoprecipitation levels in control versus paclitaxel lanes). In the paclitaxel-treated HT1080 cells, p53 levels were higher, but LKB1 levels did not change (Figure 5F and data not shown). Thus, p53 and LKB1 can interact physically in the basal state, and this interaction is enhanced in cells undergoing LKB1- and p53-dependent apoptosis.

Regulation of LKB1 Expression and Apoptosis by p53 in the Small Intestine

Since p53 is required for LKB1-induced apoptosis, we examined the possibility that p53 regulates the expression of LKB1 in vivo. We immunostained small intestinal samples of wild-type and $p53^{-/-}$ mice using the anti-LKB1 antibody. The basal expression gradient of LKB1 in wild-type and $p53^{-/-}$ mice (Figure 6A) is very similar to that seen in human tissue (Figure 1). As observed in human small intestine, LKB1 is expressed in both the nucleus and cytoplasm of mouse small intestine epithelial cells. The cytoplasm of older epithelial cells in the tips of villi and the nuclei of stem cells near the bottom of villi are highly positive for LKB1 expression. One difference in mouse LKB1 expression is that the cytoplasm of goblet cells is also positive for LKB1 staining (Figure 6A), whereas the LKB1 staining in the cytoplasm of human goblet cells is not above the basal level (Figure 1B). Similar to that of human small intestine, pyknotic mouse epithelial cells with elevated levels of LKB1 expression were detected in the crypts and tips of villi in the wild-type small intestine (Figure 6A). Interestingly, although the $p53^{-/-}$ small intestine contains only 2-fold fewer pyknotic cells with elevated LKB1 expression in the crypts than that of $p53^{+/+}$, they contain 6.5-fold fewer pyknotic cells with elevated LKB1 expression in the epi-

Figure 7. Apoptosis in Normal Human Small Intestine and PJS Polyps

(A) Confocal images of apoptosis in normal human duodenal biopsies, PJS hamartomatous polyps, and normal mucosa adjacent to polyps by TUNEL (left panels), Hoechst dye staining (middle panels), and merge (right panels). The enlargement of the boxed area is shown in the merged column to demonstrate the TUNEL positivity and nuclear fragmentation of apoptotic intestinal epithelial cells (arrows) in detail.

(B) CM1 staining of normal human small intestine and PJS polyps. Normal human small intestine and PJS polyps were immunostained by CM1. The arrowheads indicate pyknotic CM1-positive cells in normal mucosa. The arrowheads in the PJS polyp region show positive CM1 apoptotic lymphocytes. The same polyp region was immunostained by anti-LKB1 to assess LKB1 expression. Also shown is a section of normal small intestine control stained by secondary antibody alone.

(C) Quantitation of apoptotic epithelial cells in human small intestine and PJS hamartomas. The number of apoptotic epithelial cells from longitudinal sections of human small intestinal biopsies from five normal controls and four PJS patients was determined. At least ten equivalent fields of tissue per polyp were examined to obtain a representative picture of cell death events throughout the tissue. Apoptotic events in the submucosa and Brunner's glands were not taken into account. The mean numbers of cells counted (± s.e.m.) are derived from averaging the number of nuclei counted based on hematoxylin and Hoechst dye counterstaining of each sample. The absolute number of apoptotic cells per patient sample was counted and divided by the total number of epithelial cells examined in each sample to derive the percentage of apoptotic cells, which is then averaged to derive the average percentage of apoptotic cells. The difference between the mean percentage of apoptotic cells in the normal biopsies and the PJS hamartomas were statistically highly significant (unpaired t test $p < 0.005$).

thelial cells along the villi (Figures 6A and 6C). These results suggest that although p53 may not be critical for basal LKB1 expression in the crypts, it is required for induction or stabilization of LKB1 in mature epithelial cells.

A direct prediction of the above findings is that there would be a deficiency in apoptosis in the small intestine of $p53^{-/-}$ mice. To examine this possibility, we immunostained the wild-type and $p53^{-/-}$ small intestine with an antibody against activated caspase-3 (CM1; Srinivasan et al., 1998). We found evidence of spontaneous apoptosis resulting in CM1-positive epithelial cells in the wild-type small intestine epithelium, both in the tip of villi where older epithelial cells die and extrude into the intestinal lumen (Figure 6B) and in the crypts (data not shown). Interestingly, the $p53^{-/-}$ mouse small intestine contained CM1-positive cells in the crypts where intestinal epithelial stem cells are located, but they contained 6-fold fewer CM1-positive epithelial cells in the villi (Figures 6B and 6C). Our findings indicate that, although p53 is not required for spontaneous apoptosis of stem cells, it is required for apoptosis of mature differentiated intestinal epithelial cells. However, since the morphology of small intestine from 2-month-old $p53^{-/-}$ mice is not obviously different from that of wild-type, $p53^{-/-}$ epithelial cells may be eliminated through a caspase-independent mechanism.

Lack of Epithelial Apoptosis in Small Intestinal Polyps of Peutz-Jegher Patients

A prediction of the proposed model of LKB1 in regulating apoptosis is that intestinal polyposis in PJS patients may be caused by a deficiency in physiologic spontaneous apoptosis. To test this hypothesis directly, we examined biopsy and polypectomy samples from Peutz-Jegher patients for apoptosis. Apoptotic cells were scored as cells that are TUNEL positive with condensed pyknotic nuclear fragments when costained by Hoechst dye. In normal nonpolypoid intestinal samples, we observed apoptotic epithelial cells with pyknotic nuclei in almost every villus cross-section: there was an average of 0.95 apoptotic epithelial cells per villus, which was equivalent to about 0.26 $\pm$ 0.06% of the epithelial cells counted. This provides us with a representative snapshot of the rate of spontaneous apoptosis occurring in the normal intestinal mucosa at the moment of fixation (Figure 7A, top row and Figure 7C). In contrast, the spontaneous apoptosis rate was much lower in PJS polyps: there was an average of 0.05 apoptotic cells per equivalent area of polyp tissue examined, or about 0.006 $\pm$ 0.003% of epithelial cells counted in the hamartoma (Figure 7A, middle row and Figure 7C).

Apoptotic epithelial cells are found at a normal frequency in the areas of normal intestinal epithelium adjacent to or in between Peutz-Jegher polyps (Figure 7A, bottom row), consistent with the finding that LKB1 is expressed in these cells (Figure 1) and providing an important internal control for our analysis. Thus, there is an excellent correlation between the expression of LKB1 and the presence of apoptosis, suggesting that a severe deficiency of epithelial cell apoptosis in PJS polyps may play a causal role in benign hamartoma formation.

To confirm the lack of apoptosis in the polyps of Peutz-Jegher patients, we immunostained the human normal mucosa and PJS polyps with CM1 antibody (Figure 7B). The CM1 immunostaining patterns were very similar to those of TUNEL staining in normal and PJS polyps. Distinct CM1-positive cells can be found in the dying epithelial cells on the tips of villi as well as in the crypts. In contrast, far fewer CM1-positive cells can be found in the PJS polyps where LKB1 staining is absent (Figure 7B, PJS hamartomatous polyp section).

We also asked whether the hamartomatous polyps had lost the wild-type p53 allele, as a mutation in p53 might also explain the loss of apoptosis. Using a standard p53 immunostaining procedure (Walsh et al., 1999), we compared the p53 staining of Peutz-Jegher patient samples with that of the control. We found that p53 staining in Peutz-Jegher patient intestinal samples was indistinguishable from that of the normal control (data not shown), which suggests that the polyps from PJS patients most likely maintained wild-type p53 expression.

Discussion

The small intestine represents one of the most rapidly proliferating tissues of the body, with cell division occurring approximately every 5 min in each crypt. A consequence of such frequent cell division is that about one gram of tissue (10^9 cells) may be produced every 20 min or so in humans (Potten, 1992). Despite its high proliferation rate, cancers rarely develop in the small intestine, suggesting that this tissue contains an efficient mechanism for regulating cell proliferation, differentiation, and death. The epithelial cells of the small intestine are highly sensitive to apoptosis, whereas the epithelial cells in the colon are highly resistant; this has been proposed as a mechanism to explain why colon cancer is much more prevalent than cancers of the small intestine (Merritt et al., 1995). p53 is potently induced by radiation in stem cells of the small intestine but not in the colon. Thus, in the small intestine, p53 likely provides an important protective mechanism by eliminating damaged cells before they become neoplastic (Merritt et al., 1994). Our results suggest that LKB1 may be a key molecule in this highly sensitive apoptotic regulatory mechanism. Peutz-Jegher patients rapidly develop cancers of multiple tissue origins and die at a young age (Spigelman et al., 1989), suggesting that the tumor suppressor role of LKB1 is not limited to the epithelial cells of the small intestine. Mutations in LKB1 may remove the selection pressure on p53 mutation and allow cancer to develop by evading the apoptotic checkpoint regulated by p53 in a variety of cell types.

LKB1 has been demonstrated to have growth-suppressive ability in HeLa S3 cells, which have lost p53 function. Overexpression of LKB1 in HeLa S3 cells induced a G_1 cell cycle arrest, but not apoptosis (Tiainen et al., 1999). We propose that the presence of functional p53 is critical in determining LKB1-mediated apoptotic response, as overexpression of LKB1 induced apoptosis only in cells with functional p53. We have shown here that p53 and LKB1 can physically interact. However, another specific signal may be required to activate the LKB1 and p53 complex, as the interaction of endoge-

nous LKB1 and p53 can be detected under control conditions. Upon treatment with paclitaxel, we detect increased interaction of LKB1 and p53, and LKB1 undergoes mitochondrial translocation. These observations may represent two causally related events. Paclitaxel and the signal for homeostatic turnover of intestinal epithelial cells may serve as activators of LKB1/p53 interaction.

LKB1 is only required for a subset of p53-dependent apoptosis, as expression of K78M LKB1 only inhibits apoptosis induced by paclitaxel and vincristine but not 5-fluorouracil or doxorubicin. Paclitaxel is an effective chemotherapeutic agent (Rowinsky, 1997) that prevents the depolymerization of assembled microtubules. Paclitaxel-induced apoptosis is at least partially dependent on p53 (Lanni et al., 1997) and Bcl-2 (Haldar et al., 1996). The recent observation that a substantial portion of cytoplasmic p53 is associated with microtubules raises the interesting possibility that p53 functions as a sentinel of microtubule dynamics in the cells (Giannakakou et al., 2000). There is also a report demonstrating that p53 targets the mitochondrion in apoptosis (Marchenko et al., 2000). The physical interaction of p53 and LKB1 suggests that LKB1 may be a component in this p53-controlled sentinel for stress signals that result from the disruption of the microtubule network. Another possibility is that p53 and LKB1 can both be partners at the mitochondrial level to induce mitochondrial damage, although this is less likely because the interaction of LKB1 and p53 can be detected before LKB1 mitochondrial translocation. Since endogenous LKB1 interacts with p53 and most of the endogenous p53 is in the nuclear compartment, this complex may also form in the nucleus. The kinase-dead mutant of LKB1, which is mostly nuclear, can also interact with p53, supporting the notion that the interaction between p53 and LKB1 can occur in the nucleus. Our observation of mitochondrial localization of LKB1 upon paclitaxel treatment implies that paclitaxel can induce the activation of LKB1 kinase.

Microtubule-disrupting agents have been shown to activate c-Jun N-terminal kinase/stress-activated protein kinase (JNK/SAPK) as well as the apoptosis signal-regulating kinase (ASK1) and Ras signaling pathways. Ample evidence suggests that paclitaxel can induce apoptosis in a manner independent of its G_2/M arrest by activating these phosphoregulatory pathways (Blagosklonny et al., 1997; Haldar et al., 1995; Milas et al., 1995). There appear to be two phases of cell death in response to paclitaxel treatment. The early phase (up to 16 hr) can be inhibited by dominant-negative versions of ASK1, JNKK, and JNK (Wang et al., 1998). K78M LKB1 is most effective at inhibiting paclitaxel and vincristine in the first 24 hr, and time points at 48 hr show little protection (data not shown). The later phase of paclitaxel apoptosis has been shown to be independent of JNK/SAPK kinase activity and may be the result of eventual G_2/M arrest and catastrophic Cdk overactivation (Levkau et al., 1998). This result suggests that LKB1 may participate in stress kinase pathways mediated by ASK1, JNKK, and JNK.

Peutz-Jegher patients initially develop benign polyps. Since LKB1 is upregulated in dying mature epithelial cells as well as stem cells, the formation of PJS hamartomas is most likely due to a defect in the apoptosis of both proliferating as well as differentiated epithelial cells. Since $p53^{-/-}$ mice do not exhibit a defect in apoptosis of stem cells where LKB1 is clearly activated in dying cells, LKB1 may have a function in regulating stem cell survival independent of p53. This may be one of the reasons why $p53^{-/-}$ mice do not develop small intestinal polyps during their life span of 30 weeks or so before they succumb to other types of cancers. The function of LKB1 in regulating cell survival may play a critical role in malignant cancer formation later in the life of PJS patients.

Experimental Procedures

Kinase Assays

N-terminal Flag-tagged constructs were transiently transfected into HT1080 cells and harvested 18 hr posttransfection. Cells were lysed in 150 mM NaCl, 5 mM EDTA, 1 mM DTT, 10% glycerol, and 1% NP-40 in the presence of phosphatase and protease inhibitors and PKI. M2 α-Flag antibody-coupled agarose beads (Sigma) were used for immunoprecipitation, and the beads were washed four times with lysis buffer and once with kinase buffer (10 mM Tris [pH 7.4], 10 mM $MgCl_2$, 10 mM $MnCl_2$, and 1 mM DTT). The in vitro kinase assay was carried out in the presence of 20 μM cold ATP and 0.01 μCi [^{32}P]ATP at room temperature for 15–20 min and analyzed by autoradiography.

Retroviral Infection

The 293 GPG packaging cell line (generous gift of Richard Mulligan) was used to propagate high titre virus containing either vector alone or pWZL-Hygro p53(175H) dominant negative. HT1080 cells were then infected in the presence of 1 μg/ml of polybrene, and selected 16 hr postinfection by hygromycin B, 75 μg/ml, for 48–72 hr. The cell lines were then transiently transfected with GFP-tagged LKB1 constructs and assessed for cell death.

Immunocytochemistry and Mitochondrial Staining

Rat anti-LKB1 polyclonal antibodies were generated against purified recombinant LKB1 in pET28 expression vector (Novagen). To visualize mitochondrial translocated LKB1, control or apoptotic, transfected or nontransfected HT1080 cells were stained with Mitotracker (1 μM) for 15 min prior to fixation by 2% formaldehyde in PBS, and then immunostained by anti-LKB1 antibody. Paraffin-embedded, formalin-fixed tissue from human and mouse intestine or polyp was processed by automated high temperature antigen retrieval in Citra buffer (BioGenex) and stained with rat anti-LKB1 polyclonal (1/50 dilution) antibody and CM1 monoclonal antibody (processed caspase-3; 1/300 dilution) for 30 min. This was followed by incubation with secondary antibody and HRP labeling for 20 min each. The samples were then counterstained with hematoxylin.

Immunoprecipitation and Western Blot Analysis

Cells were lysed in hypotonic lysis buffer (0.2% Nonidet P-40, 100 mM Tris-HCl, 100 mM NaCl, 2 mM EDTA, and protease inhibitors) on ice for 30 min and then sonicated 3 × 10 s. After preclearing, an equal volume of binding buffer (20% glycerol, 200 mM NaCl, and 0.2% Nonidet P-40) was added prior to the addition of antibody. Immunoprecipitations were carried out with the anti-HA antibody (Roche Biosciences) and mouse anti-p53 monoclonal antibodies (Stressgen and Upstate Biotechnology). The beads were washed with wash buffer (equal volume of lysis and binding buffer) for four times before SDS-PAGE analysis.

TUNEL Staining

The ApoTag system (Oncor) was used to stain formaldehyde-fixed paraffin-embedded small intestinal biopsies obtained from both non-PJS normal-appearing small intestine and hamartomatous polyps from PJS patients. Epithelial cell apoptosis was quantified by counting the number of TUNEL-positive cells per villus. TUNEL positivity was checked against nuclear morphology using Hoechst dye

to rule out false-positive results. Equivalent high power fields of cells of normal and polyp-containing tissue were analyzed for consistency. TUNEL-positive cells in the submucosa and lymphocyte populations were excluded.

Acknowledgments

We thank Stanley Korsmeyer, Tyler Jacks, Richard Mulligan, Scott Lowe, and Frank McKeon for the generous gifts of reagents. We thank the skillful technical assistance by James Dilk at the Histopathology Core at the DHCC. We thank Frank McKeon, Mike Boyce, Katrin Chua, Honglin Li, Roberto Sanchez-Olea, and Lina Yoo for critical reading of this manuscript. This work was supported in part by grants to J.Y. from the NIH, the Army's Breast Cancer Program, the American Heart Established Investigatorship, an NIH fellowship to O.G., and the Overseas Graduate Scholarship and Singapore Cancer Society Grant to P.K.

Received August 2, 2000; revised April 24, 2001.

References

Bates, S., and Vousden, K.H. (1996). p53 in signaling checkpoint arrest or apoptosis. Curr. Opin. Genet. Dev. *6*, 12–18.

Blagosklonny, M.V., Giannakakou, P., el-Deiry, W.S., Kingston, D.G., Higgs, P.I., Neckers, L., and Fojo, T. (1997). Raf-1/bcl-2 phosphorylation: a step from microtubule damage to cell death. Cancer Res. *57*, 130–135.

Giannakakou, P., Sackett, D.L., Ward, Y., Webster, K.R., Blagosklonny, M.V., and Fojo, T. (2000). p53 is associated with cellular microtubules and is transported to the nucleus by dynein. Nat. Cell Biol. *2*, 709–717.

Giardiello, F.M., Welsh, S.B., Hamilton, S.R., Offerhaus, G.J., Gittelsohn, A.M., Booker, S.V., Krush, A.J., Yardley, J.H., and Luk, G.D. (1987). Increased risk of cancer in the Peutz-Jeghers syndrome. N. Engl. J. Med. *316*, 1511–1514.

Gross, A., McDonnell, J.M., and Korsmeyer, S.J. (1999). BCL-2 family members and the mitochondria in apoptosis. Genes Dev. *13*, 1899–1911.

Haldar, S., Jena, N., and Croce, C.M. (1995). Inactivation of Bcl-2 by phosphorylation. Proc. Natl. Acad. Sci. USA *92*, 4507–4511.

Haldar, S., Chintapalli, J., and Croce, C.M. (1996). Taxol induces bcl-2 phosphorylation and death of prostate cancer cells. Cancer Res. *56*, 1253–1255.

Hanahan, D., and Weinberg, R.A. (2000). The hallmarks of cancer. Cell *100*, 57–70.

Hanks, S.K., and Hunter, T. (1995). Protein kinases 6. The eukaryotic protein kinase superfamily: kinase (catalytic) domain structure and classification. FASEB J. *9*, 576–596.

Hemminki, A., Tomlinson, I., Markie, D., Jarvinen, H., Sistonen, P., Bjorkqvist, A.M., Knuutila, S., Salovaara, R., Bodmer, W., Shibata, D., et al. (1997). Localization of a susceptibility locus for Peutz-Jeghers syndrome to 19p using comparative genomic hybridization and targeted linkage analysis. Nat. Genet. *15*, 87–90.

Hemminki, A., Markie, D., Tomlinson, I., Avizienyte, E., Roth, S., Loukola, A., Bignell, G., Warren, W., Aminoff, M., Hoglund, P., et al. (1998). A serine/threonine kinase gene defective in Peutz-Jeghers syndrome. Nature *391*, 184–187.

Jeghers, H., McKusick, V.A., and Karz, K.H. (1949). Generalized intestinal polyposis and melanin spots of the oral mucosa, lips and digits: a syndrome of disgnostic significance. N. Engl. J. Med. *241*, 992–1005.

Jenne, D.E., Reimann, H., Nezu, J., Friedel, W., Loff, S., Jeschke, R., Muller, O., Back, W., and Zimmer, M. (1998). Peutz-Jeghers syndrome is caused by mutations in a novel serine threonine kinase. Nature *391*, 184–187.

Knudson, C.M., Tung, K.S., Tourtellotte, W.G., Brown, G.A., and Korsmeyer, S.J. (1995). Bax-deficient mice with lymphoid hyperplasia and male germ cell death. Science *270*, 96–99.

Labrecque, S., and Matlashewski, G.J. (1995). Viability of wild type p53-containing and p53-deficient tumor cells following anticancer treatment: the use of human papillomavirus E6 to target p53. Oncogene *11*, 387–392.

Lanni, J.S., Lowe, S.W., Licitra, E.J., Liu, J.O., and Jacks, T. (1997). p53-independent apoptosis induced by paclitaxel through an indirect mechanism. Proc. Natl. Acad. Sci. USA *94*, 9679–9683.

Levkau, B., Koyama, H., Raines, E.W., Clurman, B.E., Herren, B., Orth, K., Roberts, J.M., and Ross, R. (1998). Cleavage of p21Cip1/Waf1 and p27Kip1 mediates apoptosis in endothelial cells through activation of Cdk2: role of a caspase cascade. Mol. Cell *1*, 553–563.

Li, P., Nijhawan, D., Budihardjo, I., Srinivasula, S.M., Ahmad, M., Alnemri, E.S., and Wang, X. (1997). Cytochrome c and dATP-dependent formation of Apaf-1/caspase-9 complex initiates an apoptotic protease cascade. Cell *91*, 479–489.

Lowe, S.W., Schmitt, E.M., Smith, S.W., Osborne, B.A., and Jacks, T. (1993). p53 is required for radiation-induced apoptosis in mouse thymocytes. Nature *362*, 847–849.

Marchenko, N.D., Zaika, A., and Moll, U.M. (2000). Death signal-induced localization of p53 protein to mitochondria. A potential role in apoptotic signaling. J. Biol. Chem. *275*, 16202–16212.

Mehenni, H., Gehrig, C., Nezu, J., Oku, A., Shimane, M., Rossier, C., Guex, N., Blouin, J.L., Scott, H.S., and Antonarakis, S.E. (1998). Loss of LKB1 kinase activity in Peutz-Jeghers syndrome, and evidence for allelic and locus heterogeneity. Am. J. Hum. Genet. *63*, 1641–1650.

Merritt, A.J., Potten, C.S., Kemp, C.J., Hickman, J.A., Balmain, A., Lane, D.P., and Hall, P.A. (1994). The role of p53 in spontaneous and radiation-induced apoptosis in the gastrointestinal tract of normal and p53-deficient mice. Cancer Res. *54*, 614–617.

Merritt, A.J., Potten, C.S., Watson, A.J., Loh, D.Y., Nakayama, K., and Hickman, J.A. (1995). Differential expression of bcl-2 in intestinal epithelia. Correlation with attenuation of apoptosis in colonic crypts and the incidence of colonic neoplasia. J. Cell Sci. *108*, 2261–2271.

Milas, L., Hunter, N.R., Kurdoglu, B., Mason, K.A., Meyn, R.E., Stephens, L.C., and Peters, L.J. (1995). Kinetics of mitotic arrest and apoptosis in murine mammary and ovarian tumors treated with taxol. Cancer Chemother. Pharmacol. *35*, 297–303.

Nakagawa, H., Koyama, K., Miyoshi, Y., Ando, H., Baba, S., Watatani, M., Yasutomi, M., Matsuura, N., Monden, M., and Nakamura, Y. (1998). Nine novel germline mutations of STK11 in ten families with Peutz-Jeghers syndrome. Hum. Genet. *103*, 168–172.

O'Connor, L., Harris, A.W., and Strasser, A. (2000). CD95 (Fas/APO-1) and p53 signal apoptosis independently in diverse cell types. Cancer Res. *60*, 1217–1220.

Olschwang, S., Markie, D., Seal, S., et al. (1998). Peutz-Jeghers disease: most, but not all, families are compatible with linkage to 19p13.3. J. Med. Genet. *35*, 42–44.

Peutz, J.L. (1921). On a very remarkable case of familial polyposis of the mucous membrane of the intestinal tract and nasopharynx accompanied by peculiar pigmentation of the skin and mucous membrane. Ned. Tijdschr. Geneeskd. *10*, 134–146.

Potten, C.S. (1992). The significance of spontaneous and induced apoptosis in the gastrointestinal tract of mice. Cancer Metastasis Rev. *11*, 179–195.

Potten, C.S. (1997). Epithelial cell growth and differentiation. II. Intestinal apoptosis. Am J. Physiol. *273*, G253–G257.

Rowinsky, E.K. (1997). The development and clinical utility of the taxane class of antimicrotubule chemotherapy agents. Annu. Rev. Med. *48*, 353–374.

Serrano, M., Lin, A.W., McCurrach, M.E., Beach, D., and Lowe, S.W. (1997). Oncogenic ras provokes premature cell senescence associated with accumulation of p53 and p16INK4a. Cell *88*, 593–602.

Smith, D.P., Spicer, J., Smith, A., Swift, S., and Ashworth, A. (1999). The mouse Peutz-Jeghers syndrome gene Lkb1 encodes a nuclear protein kinase. Hum. Mol. Genet. *8*, 1479–1485.

Spigelman, A.D., Murday, V., and Philips, R.K. (1989). Cancer and the Peutz-Jeghers syndrome. Gut *30*, 1588–1590.

Srinivasan, A., Roth, K.A., Sayers, R.O., Shindler, K.S., Wong, A.M., Fritz, L.C., and Tomaselli, K.J. (1998). In situ immunodetection of activated caspase-3 in apoptotic neurons in the developing nervous system. Cell Death Differ. *5*, 1004–1016.

Su, J.Y., Erikson, E., and Maller, J.L. (1996). Cloning and characterization of a novel serine/threonine protein kinase expressed in early *Xenopus* embryos. J. Biol. Chem. *271*, 14430–14437.

Tiainen, M., Ylikorkala, A., and Makela, T.P. (1999). Growth suppression by Lkb1 is mediated by a G(1) cell cycle arrest. Proc. Natl. Acad. Sci. USA *96*, 9248–9251.

Walsh, S.V., Loda, M., Torres, C.M., Antonioli, D., and Odze, R.D. (1999). P53 and β catenin expression in chronic ulcerative colitis—associated polypoid dysplasia and sporadic adenomas: an immunohistochemical study. Am. J. Surg. Pathol. *23*, 963–969.

Wang, T.H., Wang, H.S., Ichijo, H., Giannakakou, P., Foster, J.S., Fojo, T., and Wimalasena, J. (1998). Microtubule-interfering agents activate c-Jun N-terminal kinase/stress-activated protein kinase through both Ras and apoptosis signal-regulating kinase pathways. J. Biol. Chem. *273*, 4928–4936.

Identification of small-molecule inhibitors of interaction between the BH3 domain and Bcl-x_L

Alexei Degterev*†‡, Alexey Lugovskoy§¶‡, Michael Cardone#, Bradley Mulley*, Gerhard Wagner§, Timothy Mitchison*† and Junying Yuan*,

*Department of Cell Biology, Harvard Medical School, 240 Longwood Avenue, Boston, Massachusetts 02115, USA
†Institute of Chemistry and Cell Biology, Harvard Medical School, 240 Longwood Avenue, Boston, Massachusetts 02115, USA
§Committee on Higher Degrees in Biophysics, Harvard University, Cambridge, Massachusetts 02138, USA
¶Department of Biochemistry and Molecular Pharmacology, Harvard Medical School, 240 Longwood Avenue, Boston, Massachusetts 02115, USA
#Department of Biology, Massachusetts Institute of Technology, 77 Massachusetts Ave., Cambridge, MA 02138, USA
‡These authors contributed equally to the paper.
**e-mail: junying_yuan@hms.harvard.edu.

To study the role of the BH3 domain in mediating pro-apoptotic and anti-apoptotic activities of Bcl-2 family members, we identified a series of novel small molecules (BH3Is) that inhibit the binding of the Bak BH3 peptide to Bcl-x_L. NMR analyses revealed that BH3Is target the BH3-binding pocket of Bcl-x_L. Inhibitors specifically block the BH3-domain-mediated heterodimerization between Bcl-2 family members *in vitro* and *in vivo* and induce apoptosis. Our results indicate that BH3-dependent heterodimerization is the key function of anti-apoptotic Bcl-2 family members and is required for the maintenance of cellular homeostasis.

Apoptosis is a highly regulated, energy-dependent programme of cellular suicide triggered by internal or external cellular stimuli. Most apoptotic signalling pathways converge on the mitochondrion, which releases cytochrome *c*, leading to the activation of the caspase-9/caspase-3 cascade[1]. The response of mitochondria to upstream apoptotic signals is a crucial control point for the regulation of apoptosis. The Bcl-2 family proteins regulate these responses, but their precise mechanism of action, and, in particular, the way in which the pro-apoptotic and anti-apoptotic activities of the different family members are balanced is still controversial[1–3].

Much of the discussion on the regulation of apoptosis by Bcl-2 family members has concentrated on the relative importance of homodimerization and heterodimerization of family members and of pore formation by multimers of these proteins[4,5]. NMR structural analysis of the Bcl-x_L/Bak BH3 peptide complex showed that the Bak BH3 domain binds to the hydrophobic cleft formed by the BH1, BH2 and BH3 domains of Bcl-x_L[6]. Several lines of evidence indicate that BH3-domain-mediated homodimerizations and heterodimerizations have a key role in regulating apoptotic functions of the Bcl-2 family[5]. Site-directed mutagenesis studies showed a correlation between dimer formation *in vitro* and the ability of mutant proteins to regulate apoptosis[4,7]. Furthermore, short peptides encompassing the BH3 domains of various pro-apoptotic Bcl-2 family members are sufficient to induce apoptosis in both cells and cell-free systems[8,9].

Additionally, both anti-apoptotic and pro-apoptotic multi-BH-domain Bcl-2 family members can form channels in the mitochondrial membrane[10–13]. However, the exact contribution of pore formation *in vivo* to apoptosis regulation by Bcl-2 family members remains controversial[14].

Small-molecule inhibitors are useful tools for the elucidation of the mechanisms of cellular processes[15]. They are more stable than peptide inhibitors, are often cell-permeable, and it is easy to compare *in vivo* the activity of the analogues that have a range of activities *in vitro*[16]. The use of small-molecule inhibitors of protein–protein interactions is particularly helpful, because intracellular signalling pathways are controlled primarily by protein–protein interactions. Unfortunately, most of the currently available cell-permeable inhibitors are mechanism-based enzyme inhibitors, and there are very few examples of protein–protein interactions inhibitors acting inside cells[17,18].

To dissect further the functions of Bcl-2 family members, we wished to probe the effects of interfering with BH3-mediated dimerization in a variety of biological situations through the development of cell-permeable small molecules disrupting BH3-domain binding to Bcl-x_L. We identified two classes of novel small-molecule cell-permeable inhibitor of the BH3-domain-mediated dimerization and demonstrated that BH3Is induce apoptosis by preventing BH3 domain-mediated interaction between pro-apoptotic and anti-apoptotic members of the Bcl-2 family.

Results

Identification of the small-molecule inhibitors of Bak BH3–Bcl-x_L interaction. To identify small-molecule inhibitors of the Bcl-x_L–BH3 domain interaction, we developed a high-throughput screen based on fluorescence polarization (FP)[19]. This assay monitors the displacement of a fluorescently labelled BH3 domain of Bak[6] from a recombinant glutathione-*S*-transferase (GST)–Bcl-x_L fusion protein (Fig. 1a, b). A library consisting of 16,320 chemicals (ChemBridge Corp.) was screened, and three compounds (two close homologues (BH3I-1 and BH3I-1′) and an unrelated compound (BH3I-2); Fig. 1c) showing the highest potency in disrupting BH3–Bcl-x_L interaction were selected for further analyses. Because these compounds disrupted BH3 interactions they were termed BH3 inhibitors (BH3Is). Additional homologues of the BH3I-1s (BH3I-1″ and BH3I-1‴) and BH3I-2 (BH3-2′ and BH3I-2″) were also analysed in the study (Fig. 1c). According to the results of FP assays, the affinity of the inhibitors was in the low micromolar range, with affinities decreasing in the following order: BH3I-1>BH3I-1′>BH3I-2′>BH3I-2>BH3I-2″>BH3I-1″. We were not able to assess the affinity of BH3I-1‴ with FP assay owing to its intrinsic fluorescence.

BH3Is inhibit Bcl-x_L heterodimerization *in vitro*. To test the possibility that BH3Is might target the Oregon Green moiety of the

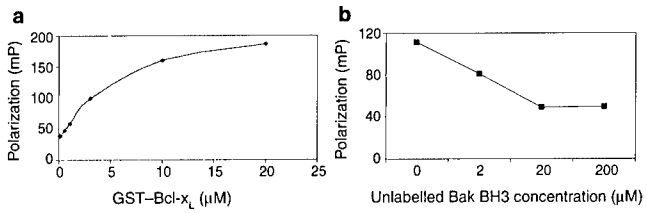

c **Bak BH3 peptide**: K_d=378±10 nM; K_i=576±179 nM

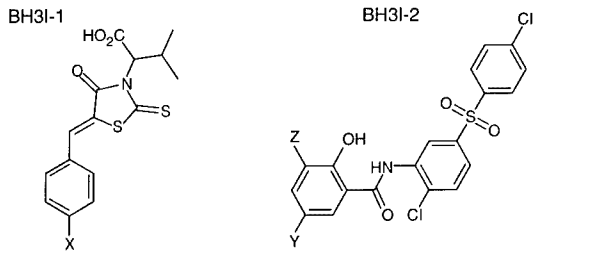

5-Benzylidene-α-isopropyl-4-oxo-2-thioxo-3-thiozolidineacetic acid

3-Bromo-5-chloro-*N*-{2-chloro-5-[(4-chlorophenyl) sulphonyl]phenyl}-2-hydroxybenzamide

	K_i by FP	K_i by NMR
BH3I-1: X=Br;	2.4±0.2 μM	7.8±0.9 μM
BH3I-1': X=Cl;	3.6±0.3 μM	8.4±0.5 μM
BH3I-1'': X=H;	12.5±0.9 μM	13.0±0.7 μM
BH3I-1''': X=N(CH$_3$)$_2$;	n.d.	15.6±0.7 μM

	K_i by FP
BH3I-2: Y=Cl; Z=Br;	4.1±0.4 μM
BH3I-2': Y=Cl; Z=I;	3.3±0.3 μM
BH3I-2'': Y=I; Z=I;	6.4±1.2 μM

Figure 1 Selection of small-molecule inhibitors of Bak BH3–Bcl-x$_L$ interaction. **a**, Titration of Bak BH3 peptide (KGGGQVGRQLAIIGDDINR) labelled with Oregon Green with increasing amounts of GST–Bcl-x$_L$ protein. Binding of the peptide is accompanied by an increase in polarization. mP, millipolarization. **b**, Competition of the fluorescently labelled Bak BH3 peptide ('tracer') with increasing amounts of the unlabelled BH3 peptide ('competitor') for binding to GST–Bcl-x$_L$. **c**, The structures and chemical names of the compounds selected through the screening. K_i values (means ± s.d.) for the inhibition of Bak/Bcl-x$_L$–His$_6$ interaction determined with FP and NMR titration assays are shown. n.d., not determined.

fluorescently labelled BH3 peptide, we designed a novel BH3/Bcl-x$_L$ binding assay with unlabelled BH3 peptide. In this assay Bcl-x$_L$ was covalently attached to a surface-enhanced laser desorption/ionization (SELDI) chip, and binding of the unlabelled BH3 peptide to immobilized protein was monitored by mass spectrometry. BH3 peptide bound to the Bcl-x$_L$-modified surface in a dose-dependent fashion (Fig. 2a). The addition of BH3I-1 or BH3I-2 resulted in a decrease in BH3 binding. Interestingly, BH3I-2 had a higher activity than BH3I-1 in this assay. As with the FP results, BH3I-1'' showed a lower potency than BH3I-1 in this assay. In addition, BH3Is disrupted BH3–Bcl-2 interaction, suggesting that these chemicals could target multiple anti-apoptotic Bcl-2 family members (Fig. 2b).

Next, we determined whether BH3Is could disrupt the heterodimerization of Bcl-x$_L$ with pro-apoptotic proteins from the Bcl-2 family, such as truncated Bid (tBid). Truncation of Bid by caspase-8 activates it and markedly increases its affinity for anti-apoptotic Bcl-2 family members[20]. *In vitro*-translated tBid bound specifically to His-tagged Bcl-x$_L$ immobilized on Ni^{2+} beads (Fig. 2c). The addition of either BH3I-2 (Fig. 2c) or BH3I-1 (Fig. 2d) resulted in a dose-dependent decrease in the tBid binding. BH3I-1 showed lower activity than BH3I-2 (Fig. 2d), and the activity of BH3I-1'' was even lower (data not shown).

The results of tBid pulldown and SELDI assays indicated that the use of Oregon Green moiety in FP assays could have resulted in an overestimation of the K_i values of the BH3I-1s relative to BH3I-2s. To verify this conclusion we performed NMR titrations of Bcl-x$_L$ with BH3I-1s (see below) and determined their K_i values (Fig. 1c). The results of NMR titrations show that the relative order of affinities of BH3I-1s was: BH3I-1>BH3I-1'>BH3I-1''>BH3I-1'''. Moreover, the NMR-derived K_i for BH3I-1 was lower than the fluorescence-polarization-derived K_i for BH3I-2. We were unable to verify the K_i for BH3I-2 by NMR titrations owing to the intermediate exchange rate of this compound. In contrast with FP data, the K_i values for BH3I-1s obtained by NMR approach agree with the results of both pulldown and SELDI analyses. The order of affinities of BH3Is is therefore BH3I2'>BH3I-2>BH3I-2''>BH3I-1>BH3I-1'>BH3I-1''>BH3I-1'''.

BH3Is are selective inhibitors of Bcl-2 family proteins. To determine the specificity of BH3Is, we tested their ability to inhibit other protein–protein interactions. Neither BH3I-1 nor BH3I-2 affected the interaction between splicing factors U2AF^{35} and U2AF^{65} (ref. 21; Fig. 2e). BH3Is (80 μM) also had no effect on interaction between the Apaf-1 CARD domain fragment and caspase-9 in a SELDI assay (data not shown).

Because NMR spectroscopy allows the detection of low-affinity (up to a K_d of 1 mM) interactions, we used it to confirm the absence of inhibition of the control protein–protein interactions by BH3Is. BH3Is did not affect the interactions between CIDE-N domains of CIDE-B and DFF40 or DFF45 (ref. 22; data not shown). Despite close structural homology between full-length Bid and Bcl-x$_L$[23,24], BH3Is failed to bind Bid (data not shown) and therefore demonstrated a high degree of specificity.

BH3Is induce apoptosis. Because Bcl-2 proteins are central to the regulation of apoptosis, we investigated whether BH3Is induce apoptosis. Treatment of JK cells with BH3Is resulted in positivity in a TdT-mediated dUTP nick end labelling (TUNEL) assay, indicating that BH3Is induced DNA fragmentation (Fig. 3A). In addition, a significant portion of cells treated with BH3Is displayed a sub-G1 DNA content indicative of apoptosis (Fig. 3B). Finally, BH3Is induced the appearance of Annexin V binding without an increase in staining with propidium iodide (PI) (Fig. 3C). On the basis of these results we concluded that BH3Is induce apoptosis.

Next, we examined whether BH3Is induce the release of cytochrome *c* from mitochondria. Immunostaining with cytochrome *c* antibody and fractionation experiments showed that BH3I-1 (Fig. 3D, E) and BH3I-2 (Fig. 3E, and data not shown) induced cytochrome *c* release, whereas staining with 3,3'-dihexyloxacarbocyanine iodide ($DiOC_6$) failed to demonstrate a decrease in mitochondrial membrane potential in the cells treated with BH3Is for 48 h (data not shown).

To demonstrate the activation of caspases by BH3Is, we measured the activation of caspases by using the preferred caspase-3 and caspase-9 fluorogenic substrates Asp-Glu-Val-Asp-(7-amino-4-methylcoumarin) (DEVD.AMC) and Leu-Glu-His-Asp-AMC (LEHD.AMC). Treatment of JK cells with either BH3I-1 or BH3I-2 resulted in an increase in caspase-3-like (Fig. 3F) and caspase-9-like (Fig. 3G) activities. The activation of both caspases followed an essentially identical time course and reached a maximum 12 h after the addition of BH3Is. If BH3Is induce apoptosis through mitochondrial pathway, caspase-9 should be activated before caspase-8, because the latter is a mediator of the death receptor pathway at the plasma membrane[25]. We therefore compared levels of caspase-9/caspase-8 activity by measuring LEHD.AMC/Ile-Glu-Thr-Asp-AMC (IETD.AMC) cleavage activities. BH3Is failed to induce the activation of caspase-8-like activity after 12 and 24 h of treatment when caspase-9-like activity was elevated (Fig. 3H). These data indicate that BH3Is induce the activation of caspases in the mitochondrial pathway.

BH3Is induce apoptosis through disruption of BH3 domain interactions. Because BH3Is induce apoptosis, we investigated whether they act through the disruption of BH3 domain interactions. First, we reasoned that if apoptosis induced by BH3Is is BH3 dependent, their cytotoxicity should correlate with their ability to disrupt BH3 domain interactions *in vitro*. To examine this possibility we treated JK cells with BH3Is and determined the cell death by assay with MTS (see Methods) and uptake of PI (Fig. 4a). We found that the

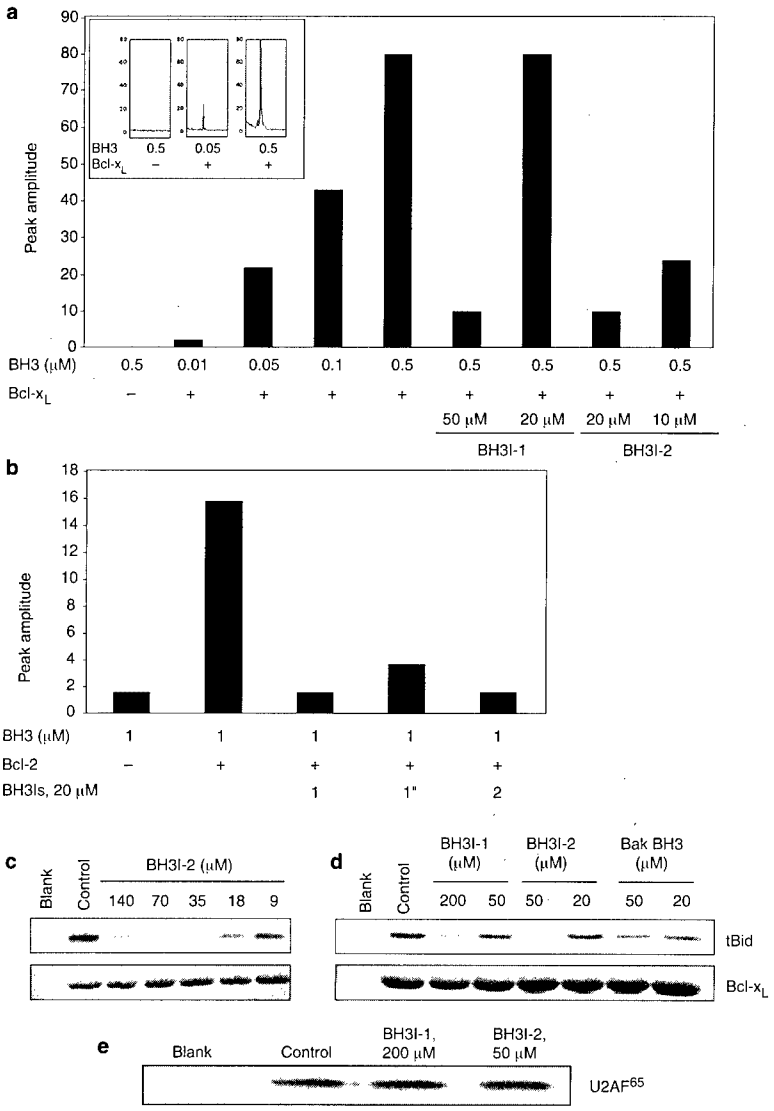

Figure 2 Inhibition of BH3–Bcl-x_L interaction by BH3Is *in vitro*. **a**, Binding of increasing amounts of Bak BH3 peptide to the SELDI surfaces modified with 2 pmol of Bcl-x_L–His_6 in the presence or absence of the indicated amounts of BH3Is. The inset shows examples of mass spectrometry data. **b**, Bak BH3 peptide was incubated with the SELDI surface modified with 5 pmol of GST–Bcl-2 in the presence or absence of the indicated concentrations of BH3Is. As a negative control Bak BH3 peptide was incubated with the SELDI surface without Bcl-x_L/Bcl-2 proteins (–). **c–e**, For pull-down experiments, Bcl-x_L–His_6 (**c**, **d**) or $U2AF^{35}$–His_6 (**e**) containing agarose beads were preincubated with the indicated concentrations of BH3I-2 (**c–e**), BH3I-1 (**d**, **e**) and Bak BH3 peptide (**d**) and then with ^{35}S-labelled *in vitro*-translated tBid (**c**, **d**) or $U2AF^{65}$ (**e**). Ni-NTA (Qiagen) beads without protein were used as a negative control (blank). Autoradiographs of tBid and $U2AF^{65}$ and Coomassie Blue images of Bcl-x_L are shown.

cytotoxicity of BH3Is followed the order BH3I-2′>BH3I-2>BH3I-2″>BH3I-1>BH3I-1′>BH3I-1″>BH3I-1‴, which paralleled the order of their K_i values determined in Bcl-x_L binding assays *in vitro* (Fig. 4b, c). Similar data were obtained with a trypan blue exclusion assay (data not shown). These results suggest that the ability to inhibit the BH3 domain interaction is critical for the BH3I-mediated induction of cell death.

Second, we determined whether BH3Is disrupt the heterodimerization of Bcl-2 family proteins *in vivo*. Dimerization of Bcl-2 in immunoprecipitation experiments might represent post-lysis events induced by detergents[26]. We therefore focused on assaying Bcl-x_L dimerization status in intact cells. The interaction between Bax and Bcl-2 has been studied recently in intact living cells by fluorescent resonance energy transfer (FRET) measurements between fusion proteins with green fluorescent protein (GFP)[27]. We used this approach to monitor the effects of BH3Is on Bcl-x_L/Bax heterodimerization in intact cells. We co-transfected HEK-293 cells with the expression vectors Bax fused to yellow fluorescent protein (YFP) and Bcl-x_L fused to cyan fluorescent protein (CFP) and treated them with BH3Is. The extent of FRET between CFP and YFP was determined as the ratio between the fluorescence at 527 nm and that at 475 nm after excitation at 433 nm. Co-transfection of Bax–YFP and Bcl-x_L–CFP resulted in an increase in the FRET ratio from 1.0 (when two proteins were expressed separately) to 1.7 (Fig. 5a), indicative of interaction between Bax and Bcl-x_L in cells. The addition of BH3Is resulted in changes in the FRET ratio consistent with the activities of the compounds *in vitro*: BH3I-2>BH3I-1>BH3I-1″. YFP 513/527 nm fluorescence is not affected by FRET and can serve as an accurate indicator of the Bax–YFP levels and a rough index of cell death. The effects on YFP fluorescence reduction was also in the order BH3I-2>BH3I-1>BH3I-1″ (Fig. 5a). These results are consistent with previous cell viability studies

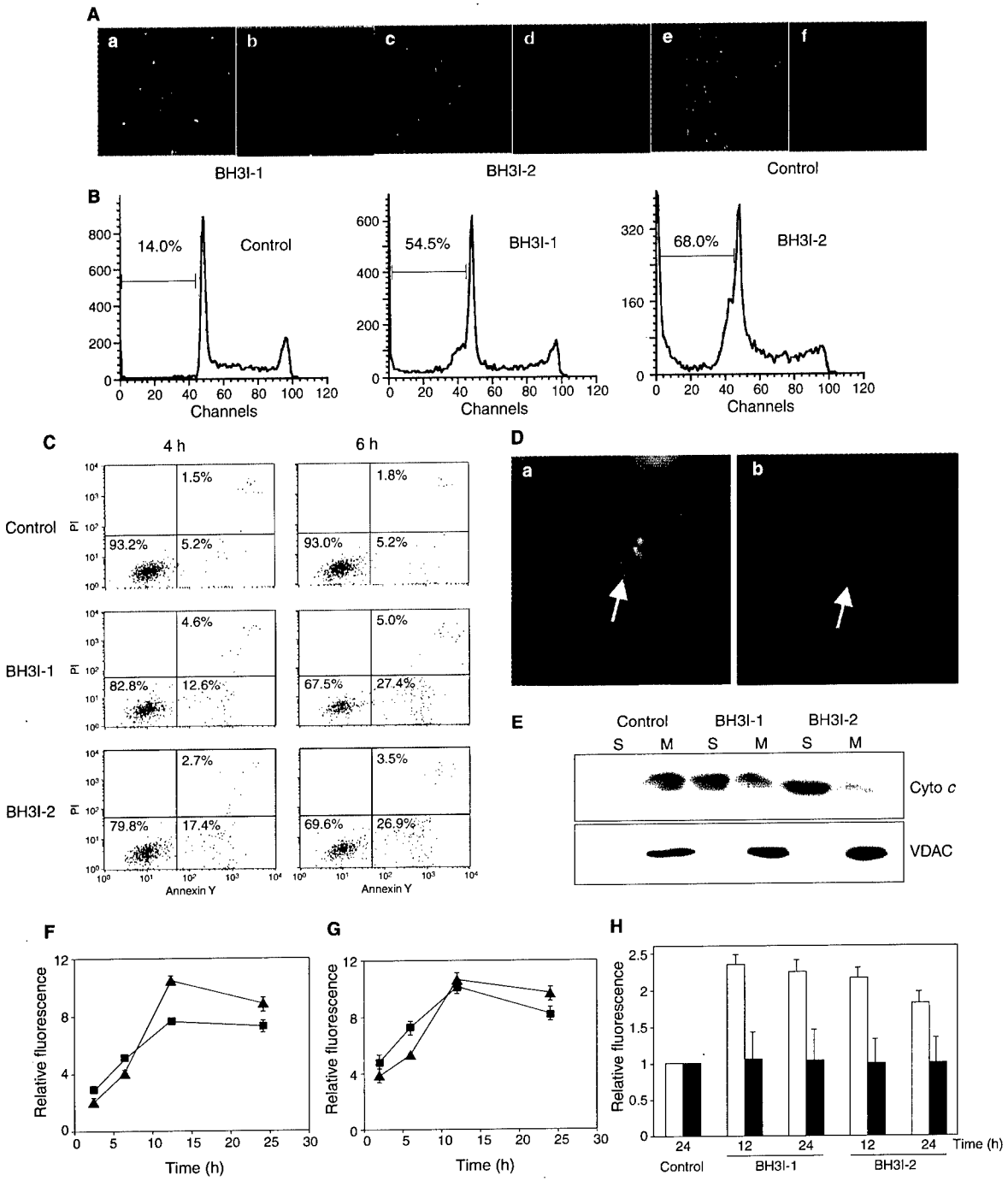

Figure 3 Induction of apoptosis by BH3Is. **A**, TUNEL assays of JK cells treated with BH3Is. JK cells were treated with BH3I-1 (100 μM) (**a**, **b**), BH3I-2 (30 μM) (**c**, **d**) and DMSO (**e**, **f**) for 48 h and stained with Hoechst dye (**a**, **c**, **e**) and a FragEL TUNEL kit (Oncogene Research Products; **b**, **d**, **f**). **B**, DNA fragmentation analysis of JK cells. JK cells were treated with BH3I-1 (100 μM) and BH3I-2 (30 μM) and 72 h later they were fixed and stained with PI. Samples were analysed by FACS. Percentages of sub-G1 DNA are shown. **C**, Annexin V staining of JK cells. JK cells were treated with BH3I-1 (100 μM) and BH3I-2 (30 μM) and stained 4 or 6 h later with Annexin V-EGFP/PI. Cells were analysed by FACS and relative amounts of live, apoptotic and late apoptotic/necrotic cells are shown. **D**, Cytochrome *c* release induced by BH3Is. HeLa cells were treated with 100 μM BH3I-1 for 48 h and stained with Hoechst dye (**a**) or antibody against cytochrome *c* (**b**). The arrow indicates the position of the apoptotic cell. **E**, Western blot analyses of cytochrome *c* release. JK cells were treated with BH3I-1 (100 μM) and BH3I-2 (50 μM) for 48 h; they were then fractionated and soluble (S) and heavy membrane (M) fractions were subjected to western blot analyses with antibodies against cytochrome *c* (PharMingen) and VDAC (Calbiochem). **F**, **G**, Time courses of caspase activation in JK cells. Cells were treated with 100 μM BH3I-1 (triangles) and 50 μM BH3I-2 (squares) for 2, 6, 12 and 24 h. Fluorescence-based assays of caspase-3 (Ac-DEVD-AMC) (**F**) and caspase-9 (Ac-LEHD-AMC) (**G**) activity were performed with a QuantiPak kit (Biomol) in accordance with the manufacturer's instructions. Results are relative AMC fluorescence in each sample compared with the value obtained with untreated JK cells incubated for 24 h, which was set at 1. Error bars indicate s.d. Equal protein amounts in the samples and timing of caspase-3 activation were confirmed by western blot analyses with antibodies against tubulin and the caspase-3 substrate poly (ADP-ribose) polymerase (PARP) (data not shown). **H**, Comparison of caspase-9 (Ac-LEHD-AMC) (open bars) and caspase-8 (Ac-IETD-AMC) (filled bars) activation 12 and 24 h after treatment of JK cells with BH3Is.

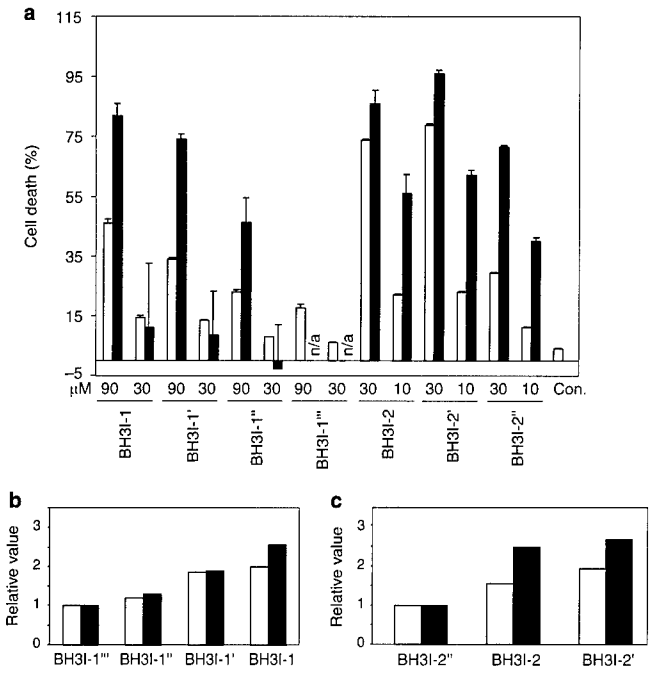

Figure 4 Cytotoxicity of BH3Is. **a**, Titrations of BH3Is. JK cells were treated for 48 h with BH3Is and their cytotoxicity was determined with PI (open bars) and MTS (filled bars) assays. Numbers are percentages cell death. In MTS assays the numbers were normalized by subtracting values for DMSO-treated control, which was set at 0% cell death. Error bars indicate s.d. The cytotoxicity of BH3I-1''' was determined using only PI staining because the highly coloured nature of this compound interfered with MTS assays. **b**, **c**, Relative cytotoxicities (filled bars) of 90 μM BH3I-1s (**b**) and 30 μM BH3I-2s (**c**), determined by the PI staining method used in (**a**) compared with their affinities (open bars) as determined in Fig. 1. Cytotoxicities and affinities were normalized to the values for BH3I-1''' and BH3I-2".

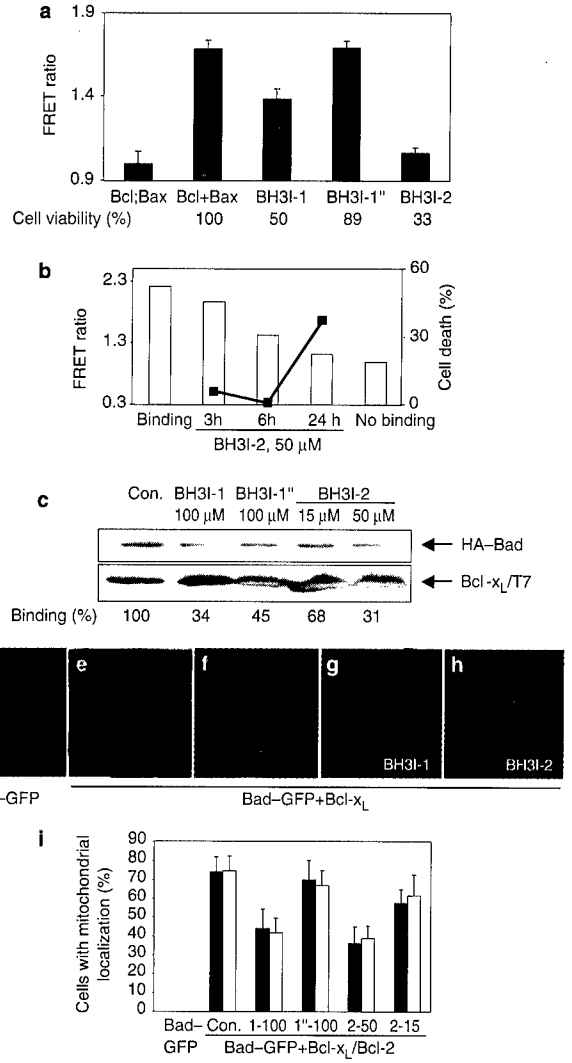

Figure 5 Disruption of Bcl-2 heterodimerization by BH3 inhibitors in intact cells. **a**, **b**, FRET analysis of Bax/Bcl-x_L binding. **a**, HEK-293 cells were transfected with 5 μg of Bcl-x_L–CFP and Bax–YFP expression vectors, both together and separately, and treated for 48 h with the indicated chemicals 24 h after transfection. Cells were harvested in PBS and analysed immediately in a C60 fluorimeter. Results are FRET ratios normalized to the FRET value obtained for the separate expression of Bax–YFP and Bcl-x_L–CFP, which was set at 1.0. The index of cell viability normalized relative to the DMSO-treated Bcl-x_L–CFP and Bax–YFP co-transfected cells, which were set at 100% viability, is also shown. **b**, Time course of changes in FRET values (histogram) and cell death (graph) induced by 50 μM BH3I-2. Cytotoxicity was determined with the PI staining method. **c–i**, BH3Is effect on Bad mitochondrial tethering. **c**, HEK-293 cells were co-transfected with HA–Bad and Bcl-x_L/T7. After 48 h, cells were harvested; isolated mitochondria were treated with BH3Is for 2 h. After the treatments, mitochondria were pelleted by centrifugation and subjected to western blot analysis with anti-HA and anti-T7 antibodies. **d–i**, BH3I's effects on Bad localization in intact cells. BSC-1 cells were transfected with 5 μg of Bad–GFP expression vector alone (**d**, **i**) or co-transfected with 5 μg of Bad–GFP and 5 μg of Bcl-x_L–T7 (**e–i**). At 24 h after transfection, cells were treated with 100 μM BH3I-1 (**g**) or 50 μM BH3I-2 (**h**) for 6 h. The GFP signal in the fixed cells is shown (**d**, **f–h**). To determine mitochondrial localization, cells were prestained with MitoTracker Red CMXRos for 30 min before fixation (**e**). In **i**, values are relative numbers of BSC-1 cells transfected with Bad–GFP or co-transfected with Bad–GFP and Bcl-x_L–T7 (filled bars) or Bcl-2–Flag (open bars) showing granular mitochondrial localization of Bad–GFP after treatment with the BH3 inhibitors. At least 100 transfected cells per sample were counted. Transfection was repeated three times. Error bars indicate s.d. All cells were pretreated with 100 μM zVAD-FMK to decrease the detrimental effects of overexpression of pro-apoptotic Bcl-2 proteins on cell viability. 1-100, 1"-100, 2-50 and 2-15 represent 100 μM BH3I-1, 100 μM BH3I-1", 50 μM BH3I-2 and 15 μM BH3I-2, respectively.

and demonstrate that the ability of the BH3Is to disrupt the interaction between Bax and Bcl-x_L in intact cells correlates directly with their cytotoxicity in the same samples. We also performed a time course experiment that demonstrated that the disruption of FRET preceded cell death (Fig. 5b).

Bad is a pro-apoptotic member of the Bcl-2 family whose apoptosis-promoting activity and mitochondrial targeting depends on heterodimerization with anti-apoptotic Bcl-2 family members[28]. Transfection of BSC-1 cells with Bad expression vector resulted in a predominantly cytoplasmic localization of Bad (Fig. 5d), whereas co-transfection with Bcl-x_L (Fig. 5e, f) resulted in a mitochondrial localization of Bad. BH3Is disrupted the mitochondrial association of Bad, but not that of Bcl-x_L, after *in vitro* treatment of the mitochondria isolated from the cells co-transfected with Bad and Bcl-x_L (Fig. 5c). The relative activities of the BH3Is in this assay (BH3I-2>BH3I-1>BH3I-1") were consistent with the previous results. Treatment of cells with either BH3I-1 or BH3I-2 resulted in an increase in cells with the cytosolic redistributed Bad–GFP (Fig. 5g, h). Quantification of cells with mitochondrial and cytosolic localizations of Bad–GFP indicated that BH3I-1 and BH3I-2 efficiently disrupted mitochondrial targeting and heterodimerization of Bad–GFP with either Bcl-2 or Bcl-x_L in intact cells (Fig. 5i). Again, the order of the activities in these assays was BH3I-2>BH3I-1>BH3I-1". No cell death was detectable at the time of measurement (Fig. 5g, h), suggesting that in this system the disruption of BH3 interactions also precedes cell death.

Third, we reasoned that if BH3Is act through inhibiting the function of anti-apoptotic members of the Bcl-2 family, the overexpression of Bcl-x_L should provide certain protection against

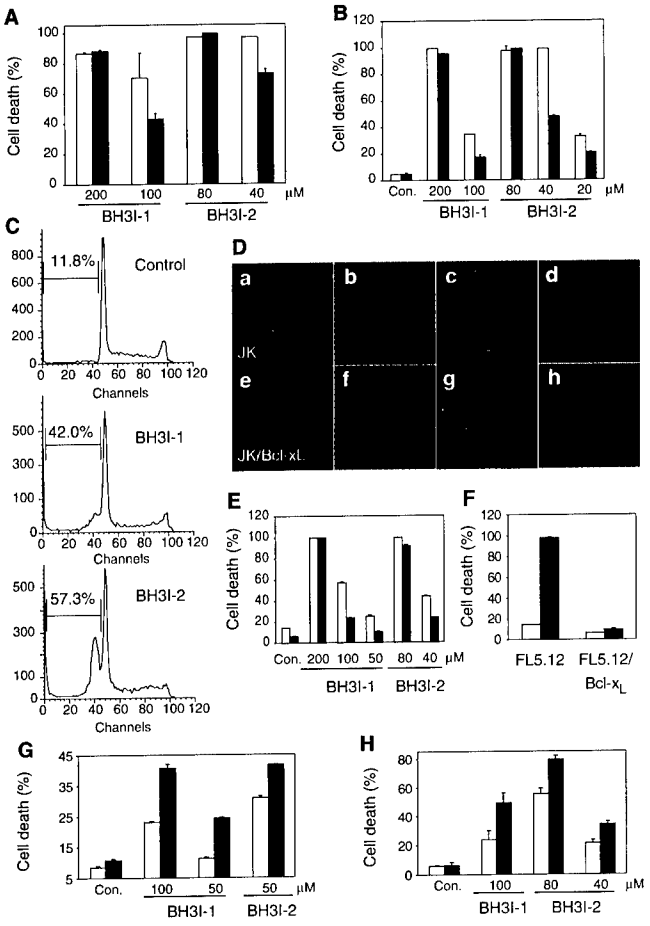

Figure 6 Attenuation of the cytotoxicity of BH3Is by overexpression of Bcl-x_L. **A, B**, Attenuation of cytotoxicity of BH3Is by Bcl-x_L overexpression. JK (open bars) or JK/Bcl-x_L (filled bars) cells were treated with BH3I-1 or BH3I-2 for 48 h. Cell death was determined by MTS assay (**A**) or PI staining (**B**). Numbers are percentages cell death. In the MTS assays the numbers were normalized to the DMSO-treated control, which was set at 100% viability. Error bars indicate s.d. **C**, DNA fragmentation analysis of JK/Bcl-x_L cells. Cells were treated with BH3I-1 (100 μM) and BH3I-2 (30 μM); 72 h later they were fixed and stained with PI. Samples were analysed by FACS. Experiments were performed in parallel with studies in Fig. 3B. **D**, Caspase activation in JK/Bcl-x_L cells treated with BH3Is. JK (**a–d**) and JK/Bcl-x_L (**e–h**) cells were treated with BH3I-1 (200 μM) and BH3I-2 (80 μM) and stained live with Hoechst dye (**a, c, e, g**) or the cell-permeable fluorescent active caspase marker FAM-VAD-FMK (**b, d, f, h**) (CaspaTag Fluorescein Caspase activity kit; Intergen). **E, F**, Attenuation of cell death in FL 5.12 cells by Bcl-x_L overexpression. FL 5.12 or FL 5.12/Bcl-x_L cells were subjected to IL-3 deprivation (**F**; open bars, with IL-3; filled bars, without IL-3) or treated with BH3I-1 and BH3I-2 (**E**; open bars, FL 5.12; filled bars, FL 5.12/Bcl-x_L) for 48 h. Cell death was determined by PI staining. Numbers are percentages cell death. Error bars indicate s.d. **G, H**, Inactivation of anti-apoptotic activity of Bcl-x_L by BH3Is. FL 5.12/Bcl-x_L cells were incubated with BH3I-1 and BH3I-2 in the presence (open bars) or absence (filled bars) of IL-3 for 48 h (**H**) or 72 h (**G**). Cell death was determined by PI staining (**G**) and by counting cells with activated caspases (**H**) (CaspaTag Fluorescent Caspase Activation Assay, Intergen).

BH3Is that can be overcome by an increased amount of BH3Is. Furthermore, cells overexpressing Bcl-x_L should still undergo apoptosis when treated with a high enough dose of BH3Is to overcome the protection by Bcl-x_L. Overexpression of Bcl-x_L provides some protection for JK cells from lower doses of BH3Is (up to 40 μM BH3I-2 and up to 100 μM BH3I-1), but gives no protection after treatment with 80 μM BH3I-2 or 200 μM BH3I-1 (Fig. 6A, B). Treatment with BH3Is (100 μM BH3I-1 or 30 μM BH3I-2) induces the appearance of sub-G1 DNA indicative of apoptosis (Fig. 6C). To determine whether caspases are activated in JK/Bcl-x_L cells treated with high doses of BH3Is, indicating that the cells were undergoing apoptosis rather than necrosis, we stained cells with the carboxyfluorescein derivative of Val-Asp-Ala fluoromethyl ketone (FAM-VAD-FMK), which binds to the active caspases and allows the detection of caspase activation in intact cells (Fig. 6D). We found that caspases are activated in Hoechst-positive dying cells after treatment with high doses of BH3Is. No Hoechst/caspase-positive cells were seen in untreated control cells (data not shown).

FL5.12 cells undergo apoptosis in response to deprivation of interleukin-3 (IL-3), which is efficiently blocked by overexpression of Bcl-x_L[29] (Fig. 6F). Overexpression of Bcl-x_L attenuated killing by BH3Is and this effect could be overcome by a higher dose of the inhibitors (Fig. 6E). Inactivation of Bcl-x_L by BH3Is should result in increased sensitivity of FL5.12/Bcl-x_L cells to BC3Is after IL-3 deprivation. The cytotoxicity of BH3I-1 and BH3I-2 was indeed significantly increased upon IL-3 deprivation of the Bcl-x_L-overexpressing cells, whereas IL-3 deprivation alone did not induce significant cell death (Fig. 6G). Moreover, staining cells with FAM-VAD-FMK demonstrated increased caspase activation induced by combined treatment with BH3Is and deprivation of IL-3 in Bcl-x_L/FL5.12 cells (Fig. 6H), demonstrating an enhancement of apoptosis in these cells in response to Bcl-x_L inactivation.

Finally, if inhibition of the BH3 domain interaction results in the release of pro-apoptotic members of Bcl-2 family, pro-apoptotic activity of BH3Is should mimic that of pro-apoptotic members of the Bcl-2 family. We therefore compared the pro-apoptotic activity of BH3Is with that of Bax. Cell death induced by either the treatment of HeLa cells with BH3Is or transfection with Bax is only partly dependent on caspase activity (Fig. 7A). MTS (Fig. 7B) and PI exclusion (data not shown) assays of BH3Is/zVAD-treated JK cells confirmed this conclusion.

To characterize further the role of caspases in apoptosis induced by BH3Is, we stained HeLa cells that had been treated with BH3Is in the presence of zVAD-FMK with Hoechst dye and antibody against cytochrome *c*. The addition of zVAD-FMK completely protected cells from BH3I-induced nuclear fragmentation, but not from nuclear condensation or cytochrome *c* release induced by BH3I-1 (compare Figs 7C and 3D) and BH3I-2 (data not shown). This conclusion was confirmed by sub-G1 analysis, showing that zVAD-FMK prevented the appearance of fragmented DNA in the cells treated with BH3Is (Fig. 7D). Therefore, although BH3Is induce some events that require caspase activation, similarly to Bax-induced cell death[30,31], eventual cellular demise is only partly dependent on caspase activity.

Taking these results together, we conclude that BH3Is induce apoptosis by disrupting interactions, mediated by the BH3 domain, between pro-apoptotic and anti-apoptotic members of the Bcl-2 family.

Neither Bak BH3 peptide nor BH3Is affect pore formation by Bcl-x_L. Because Bcl-x_L forms pores in membrane, which might have a role in its ability to regulate apoptosis[10,11,13,32], we tested whether BH3Is affect pore formation by Bcl-x_L. We found that BH3Is and BH3 peptide did not affect the Bcl-x_L-mediated release of carboxyfluorescein encapsulated in artificial liposomes (data not shown). This result suggests that Bcl-x_L pore formation is independent of BH3-mediated homodimerization and that pro-apoptotic activity of BH3Is reflects a critical role of BH3-dependent heterodimerization in mediating cell survival.

BH3Is interact with the BH3-peptide-binding pocket of Bcl-x_L. We employed NMR titration[33] to examine whether BH3Is interact with the binding pocket of Bcl-x_L in a manner similar to Bak BH3 peptide (Fig. 8).

First, we analysed changes in the two-dimensional $^{15}N/^{1}H$

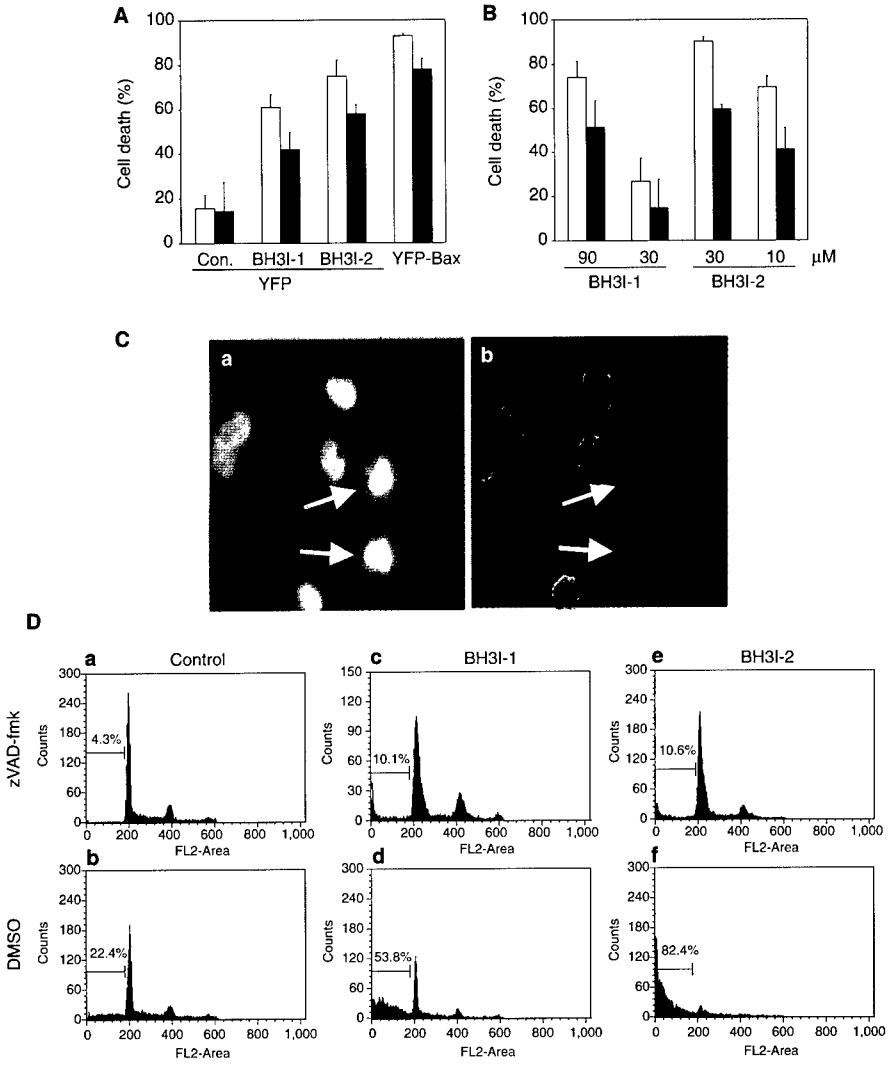

Figure 7 The requirement of caspases for cytotoxicity of BH3Is is similar to that of Bax. **A**, Comparison of cell death induced by BH3Is and Bax. HeLa cells were transfected with Bax–YFP or pEYFP-C1 for 48 h in the absence (open bars) or presence (filled bars) of 100 μM zVAD-FMK. YFP-transfected cells were also treated with BH3I-1 (100 μM) and BH3I-2 (50 μM) for 48 h. Cell viability was determined by PI staining and a microscopic examination of PI/YFP-positive cells. Numbers show the percentage of PI-positive cells in the YFP-positive population. Error bars indicate s.d. **B**, Attenuation of cytotoxicity of BH3Is by the pan-caspase inhibitor zVAD-FMK. JK cells were treated with BH3I-1 and BH3I-2 in the presence (open bars) or absence (filled bars) of 100 μM zVAD-FMK for 48 h. Cell death was determined by MTS assay. Numbers represent percentages cell death. In the MTS assays the numbers were normalized to the DMSO-treated control, which was set at 100% viability. Error bars indicate s.d. **C**, Nuclear fragmentation, but not the release of cytochrome *c*, induced by BH3Is require caspases. HeLa cells were treated with 100 μM BH3I-1 and 100 μM zVAD-FMK for 48 h, then stained with Hoechst dye (**a**) or antibody against cytochrome *c* (**b**). The arrows indicates the positions of the dying cells. **(D)** DNA fragmentation analysis of JK cells treated with BH3Is and zVAD-FMK. Cells were treated with DMSO (blank) (**a**, **b**), BH3I-1 (100 μM) (**c**, **d**) and BH3I-2 (30 μM) (**e**, **f**) in the presence (**a**, **c**, **e**) or absence (**b**, **d**, **f**) of zVAD-FMK for 72 h, then fixed and stained with PI. Samples were analysed by FACS. Percentages of sub-G1 DNA are shown.

heteronuclear single-quantum correlation (HSQC) spectrum of ^{15}N-labelled Bcl-x_L on the addition of the Bak BH3 peptide. Addition of Bak BH3 peptide primarily affected residues in the BH1–BH3 hydrophobic cleft and especially residues at the BH1/BH2 interface (Fig. 8a, b), which is consistent with the published structure of the Bak/Bcl-x_L complex[6] (Fig. 8c).

Next, we analysed changes in Bcl-x_L structure after the addition of increasing amounts of BH3Is. We found that all the BH3Is induced significant changes in Bcl-x_L structure, targeting the hydrophobic cleft formed by the BH1, BH2 and BH3 domains on the surface of the Bcl-x_L protein, and bound primarily to the area formed by the BH1 and BH2 domains (Fig. 8d, e, and data not shown). The NMR data suggest that BH3I-2s have slower dissociation rates than BH3I-1s as judged by the intermediate exchange kinetics of BH3I-2s binding compared with the fast exchange shown by BH3I-1s.

Because BH3I-1 differs from BH3I-1″ by a single substitution, we compared the changes induced by these chemicals in the ^{15}N/^{1}H HSQC spectra of Bcl-x_L[34]. The primary area differentially affected by BH3I-1 and BH3I-1″ is in the middle of the BH2 domain (residues N100, G102, I104, A106, F110, G111 and G112) (Fig. 8f, g). The only other differentially affected residue is R55, which lies in the BH3 domain (Fig. 8f, g). A similar comparative analysis of BH3I-2 and BH3I-2′ resulted in the mapping of A164, A165, R168, located carboxy-terminal to the BH1 domain, and F110 in the BH2 domain. This suggests that BH3I-2s target a more upstream part of

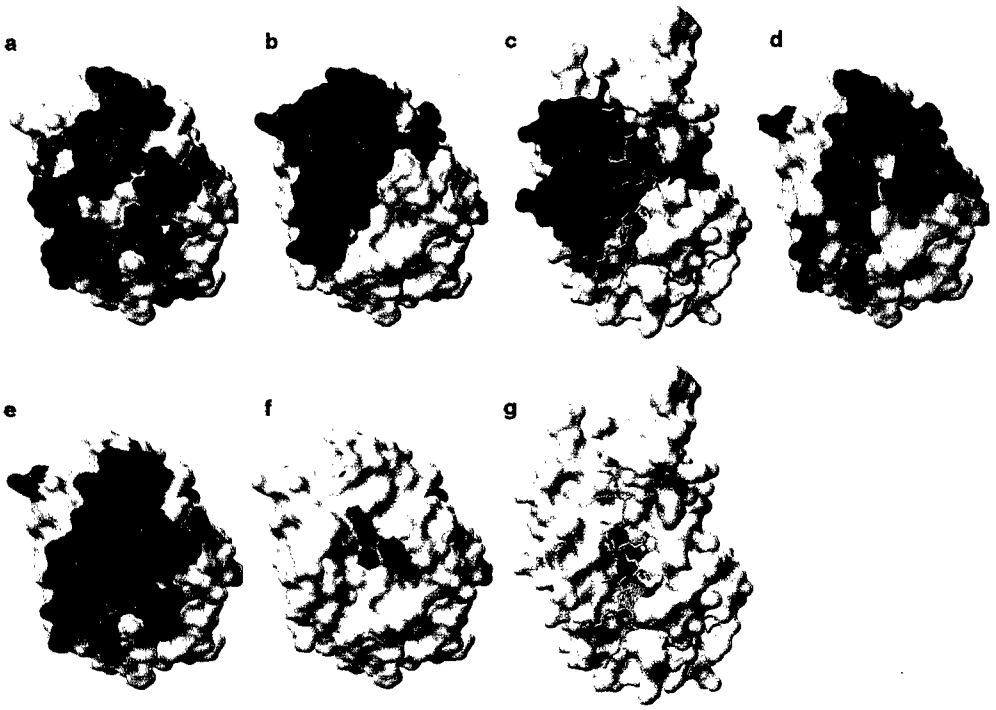

Figure 8 NMR analyses of the BH3 inhibitors binding to Bcl-x_L. Areas perturbed by the binding of chemicals and a BH3 peptide are mapped on the surface of the structure of free Bcl-x_L[35] (**a**, **b**, **d–f**) and the Bcl-x_L complex with the Bak BH3 peptide[6] (**c**, **g**). **a**, Residues affected by the binding of the Bak BH3 peptide. Residues displaying fast exchange kinetics are shown in blue and intermediate exchange kinetics (tighter binding) in red. **b**, Structure of free Bcl-x_L[35]. The location of the hydrophobic cleft is shown: dark blue, BH1; green, BH2; red, BH3. **c**, Structure of Bcl-x_L in complex with the Bak BH3 peptide[6]. The locations of BH1, BH2 and BH3 domains are shown: dark blue, BH1; green, BH2; red, BH3. **d**, Residues affected by the binding of BH3-1. **e**, Residues affected by the binding of BH3I-2. **f**, **g**, Differential mapping of the analogues of BH3I-1 and BH3I-2. Residues differentially affected by the binding of BH3I-1 and BH3I-1″ are shown in green. Y65 and F107, forming a direct contact with BH3I-1, are shown in red. Residues differentially affected by the binding of BH3I-2 and BH3I-2′ are shown in gold. F110, which is differentially affected by either BH3I-1 and BH3I-1″ or by BH3I-2 and BH3I-2′ is shown in cyan. Residues F107 (red), F110 (cyan), A164, A165 and R168 (gold) are buried in the structure of free Bcl-x_L[35] (**f**) and are exposed in the structure of the Bcl-x_L complex with the Bak BH3 peptide (**g**).

the Bcl-x_L hydrophobic groove than BH3I-1s.

Additionally, we observed magnetization transfer between the benzene-ring protons of BH3I-1 and the amide protons of Y65 and F107 in a nuclear Overhauser effect (NOE) spectrum, indicative of direct contact between BH3I-1 and these residues (Fig. 8f, g). Interestingly, residue F107, as well as residues F110, A164, A165 and R168 (identified in a differential mapping analysis), are buried in the structure of free Bcl-x_L (Fig. 8f)[35] but are surface-exposed in the structure of the Bcl-x_L/Bak complex (Fig. 8g)[6]. In this complex, Y65, F107 and F110 form direct contacts with the side-chain of the leucine residue of the Bak BH3 peptide, which is essential for binding[6]. This observation suggests that, on binding BH3I-1, Bcl-x_L undergoes a conformational change similar to that induced by the Bak BH3 peptide.

Overall, the results of the NMR analyses demonstrate that BH3Is target the hydrophobic cleft on the surface of Bcl-x_L, which is a docking site for the BH3 domain of Bak and therefore mediates the dimerization of Bcl-2 family members. Binding of BH3Is to the hydrophobic pocket of Bcl-x_L affects the conformation of Bcl-x_L in a fashion similar to Bak BH3 peptide binding. This suggests a similarity between the modes of action of BH3Is and Bak BH3 peptide.

Discussion

Our results indicate that BH3Is act as 'BH3 mimetics' because they induce apoptosis similarly to Bak BH3 peptide[8] and bind to the same area of Bcl-x_L as Bak BH3 peptide. Moreover, the characteristic features of BH3I-induced cell death closely parallel those caused by the overexpression of pro-apoptotic Bcl-2 family proteins[20,31,36,37].

BH3Is might induce apoptosis via several distinct mechanisms. Bid triggers a conformational change in Bax, which induces its oligomerization and pore formation[38]. However, the addition of BH3Is or Bak BH3 peptide was not sufficient to induce Bax insertion into mitochondrial membrane, nor did they affect Bax membrane insertion induced by tBid (data not shown). Thus, the BH3 domain alone is not sufficient to induce Bax oligomerization. Interestingly, a recent mutagenesis study has suggested that tBid-induced Bax oligomerization, membrane insertion and cytochrome *c* release are BH3-dependent[39]. It is possible that even transient interaction of tBid with Bax is sufficient to induce Bax membrane insertion, which explains why this process cannot be efficiently inhibited by reversible inhibitors such as BH3Is. Overall, these results indicate that BH3Is are unlikely to induce apoptosis by directly inducing Bax oligomerization and mitochondrial insertion.

Another possibility is that BH3Is act directly on the anti-apoptotic Bcl-2 family members. Bcl-2 and Bcl-x_L were proposed to inhibit apoptosis through two major mechanisms: heterodimerization and pore formation[13]. Although we found that BH3Is inhibited heterodimerization between Bcl-x_L and pro-apoptotic members of Bcl-2 family, BH3Is had no effect on pore formation by Bcl-x_L. We therefore conclude that BH3Is induce apoptosis by inhibiting the heterodimerization of Bcl-x_L/Bcl-2 and releasing pro-apoptotic Bcl-2 family members, which in turn initiate downstream apoptotic events. Overall, our findings underscore the crucial role of the BH3-mediated heterodimerization in the anti-apoptotic function of Bcl-2/Bcl-x_L, and its constitutive requirement for the mainte-

nance of cellular homeostasis.

Mitochondria in general, and Bcl-2 proteins in particular, are promising new targets in cancer therapy owing to their central role in the regulation of apoptosis as well as their importance in the development of resistance to chemotherapy[40,41]. It has been shown the inhibition of the activity of anti-apoptotic Bcl-2 family proteins specifically kills transformed cells and sensitizes tumour cells to chemotherapy[42–44]. The chemical inhibitors developed in this study should circumvent the upstream anti-apoptotic barriers in transformed cells *in vitro* and might be used to explore the feasibility of anti-apoptotic agents as novel anti-cancer therapies. □

Methods

Cell culture and cell lines

Jurkat cells overexpressing Bcl-x_L were generated by stably transfecting Jurkat cells with Bcl-x_L/T7 expression vector. FL 5.12 and FL 5.12/Bcl-x_L cells were a gift from Dr Craig Thompson (University of Pennsylvania, Philadelphia, PA). All other cell lines were obtained from ATCC (Manassas, VA) and maintained in accordance with the supplier's instructions.

Plasmid construction

Bax–YFP, Bad–GFP, Bcl-x_L–CFP and Bcl-2–CFP expression vectors were generated by subcloning corresponding cDNAs into the pEYFP-N1, pEGFP-N1 and pECFP-N1 vectors, respectively (Clontech). Bacterial GST–tBid–Flag (where Flag is $(EYKEEEK)_2$) expression vector was prepared by the insertion of the Flag-coding region into the GST–tBid expression vector[20]. Protein was cleaved by Precision protease (Pharmacia) to separate tBid from GST. Bcl-x_L–His_6 bacterial expression vector was generated as described[6]. GST-Bcl-x_L vector has been previously described[20].

Immunocytochemistry

HeLa cells were seeded into four-chamber glass slides (Lab Tech) and treated with BH3Is for 48 h. Cells were then fixed in 4% paraformaldehyde and stained with monoclonal antibody against cytochrome *c* (Pharmingen) and Hoechst dye.

FP assays

Bak BH3 peptide (Research Genetics) was labelled with succinimidyl Oregon Green (Molecular Probes) and purified by HPLC. For the initial screening assays, 33 nM labelled BH3 peptide, 2 μM GST–Bcl-x_L protein, 0.1% bovine γ-globulin (Sigma) and 1 mM dithiothreitol mixed with PBS, pH 7.2 (Gibco), were added to 384-well black plates (Lab Systems) with Multidrop (Lab Systems). Small molecules (5 mg ml^{-1} in DMSO; Chembridge) were transferred by using plastic 384-pin arrays (Genetix). The plates were incubated for 1–2 h at 25 °C, and FP values were determined with an Analyst plate reader (LJL Biosystems). Reactions containing 16.65 nM labelled BH3 peptide and 4.2 μM Bcl-x_L–His_6 fusion protein, used previously to characterize BH3/Bcl-x_L binding[6], were used for the further FP analyses. K_d and K_i determinations were performed as described previously[19] with a GraphPad Prism software package (GraphPad). Chemicals for further testing were obtained from Chembridge, except for BH3I-1′′′, which was obtained from Chemical Diversity.

Mass spectrometry

Purified recombinant GST–Bcl-2 and Bcl-x_L–His_6 were coupled through their primary amines to SELDI chip surfaces derivatized with carbonyldiimidazole (Ciphergen). Bak BH3 peptide was incubated in the total volume of 1 μl for 12 h at 4 °C in a humidified chamber to allow binding to each spot of the SELDI chip, then washed with alternating high-pH and low-pH buffers (0.1 M sodium acetate containing 0.5 M NaCl, followed by 0.01 M HEPES, pH 7.3). The samples were embedded in α-cyano-4-hydroxycinnamic acid matrix and analysed for mass by matrix-assisted laser desorption ionization time-of-flight (MALDI-TOF) mass spectrometry. The data presented are averages of 100 laser shots at a constant setting collected over 20 spots in each sample.

In vitro binding assays

Translation of tBid and U2AF[65] *in vitro* was performed with TNT Coupled Reticulocyte or Wheat Germ Lysate (Promega) Systems respectively. Bcl-x_L, U2AF[35] or corresponding amounts of original Ni-NTA agarose beads (blank) were preincubated with the BH3 inhibitors or peptide in 100 μl of PBS for 30 min at 25 °C and then 1 μl of ^{35}S-labelled tBID or U2AF[65] was added and incubations were continued for 2 h at 4 °C. Beads were washed three times with PBS containing 10 mM imidazole, 1 mM EDTA and corresponding BH3Is. The samples were subjected to SDS–PAGE, Coomassie Blue staining and autoradiography.

Cytotoxicity assays

Cells (5×10^4 cells per well) were seeded into white 96-well plates (Costar) and treated with various concentrations of the compounds for 48 h. For zVAD-FMK protection experiments, cells were preincubated with 100 μM zVAD-FMK (Bachem or Alexis) for 1 h before the addition of chemicals. Cell viability was determined with an MTS (3-(4,5-dimethylthiazol-2-yl)-5-(3-carboxymethoxyphenyl)-2-(4-sulphophenyl)-2H-tetrazolium salt) assay (CellTiter 96 Assay; Promega) with a Victor plate reader (Wallac). For PI staining experiments, cells were grown in 24-well plates and then incubated with 2 μg ml^{-1} PI (Boehringer Mannheim). Cell death was determined by FACS analysis in a FACSCalibur machine (Beckton Dickinson).

For the determination of cytotoxicity in HeLa cells, cells were transfected with 2 μg of Bax–YFP or pEYFP-C1 (Clontech) vectors by using TransLT-1 reagent (PanVera). Some sample cells were pretreated with 100 μM zVAD-FMK. At 48 h after transfection, cells were harvested by trypsinization, combined with floating cells recovered by centrifugation from culture medium and resuspended in PBS (pH 7.2) supplemented with 1% fetal bovine serum (FBS) and 2 mg ml^{-1} PI. Numbers of PI/YFP-positive cells were determined by fluorescence microscopy.

Apoptotic assays

Annexin V/PI staining was performed with an Annexin V-EGFP Apoptosis Detection kit (PanVera). For sub-G1 staining, cells were harvested, resuspended in PBS supplemented with 2% FBS and fixed in a 10-fold excess of ice-cold ethanol. Cells were recovered by centrifugation at 1000 *g* for 5 min at 4 °C, washed once in PBS, 2% FBS, 0.2% Triton X-100, incubated in the same medium supplemented with 50 mg ml^{-1} PI and 50 μg ml^{-1} of RNase A for 30 min at 37 °C, and analysed in FACSCalibur. TUNEL assays were performed with a Fluorescent FragEL kit (Oncogene Research Products). Staining of the cells with active caspases was performed with a CaspaTag kit (Intergen).

Cell-based FRET assays

HEK-293 cells were transfected with Bcl-x_L–CFP and Bax–YFP expression vectors by using LipofectAMINE Plus (Gibco) or TransLT-1 (PanVera); 24 h later they were treated with BH3 chemicals. For the dose–response experiment, cells were pretreated with 100 μM zVAD-FMK for 1 h before transfection, to decrease cell death induced by the expression of Bax–YFP. Cells were harvested in PBS supplemented with BH3 inhibitors, and fluorescence was determined with a C-60 fluorimeter (PTI) or a Wallac plate reader. Fluorescence in the samples separately overexpressing Bax and Bcl-x_L was added together and used to estimate the FRET value in the absence of dimerization.

Bad localization assays

HEK-293 cells were transfected with 5 μg of haemagglutinin (HA)–Bad expression vector alone or in combination with 5 μg of Bcl-x_L/T7, with the calcium phosphate procedure. At 48 h after transfection, cells were harvested and mitochondria were isolated[45]. A 50 μg sample of mitochondria was incubated with BH3I for 2 h at 25 °C and then pelleted by centrifugation at 10000 *g* for 15 min at 4 °C. Mitochondrial pellets were subjected to western blotting with anti-HA (Roche) and anti-T7 (Novagen) antibodies. For the fluorescence microscopy study, BSC-1 cells were transfected with 5 μg of Bad–GFP and 5 μg of Bcl-x_L/T7 or Bcl-2/Flag (a gift from S Korsmeyer, Dana Farber Cancer Institute, Boston, MA) by using the calcium phosphate procedure. Cells were treated with BH3Is for 6 h and fixed; the relative numbers of cells with mitochondrial localization of Bad–GFP were determined by fluorescence microscopy.

Cytochrome *c* release assay

JK cells were incubated with BH3Is for 48 h. Cell fractionation was performed as described previously[45]. Soluble fraction proteins (50 μg) and an equivalent amount of heavy membrane proteins were subjected to SDS–PAGE and analysed by western blotting with antibodies against cytochrome *c* (Pharmingen) and voltage-dependent anion channel (VDAC) (Calbiochem).

Pore formation assays

Liposomes containing 20 mM 5,6-carboxyfluorescein were prepared as described previously[12]. For Bcl-x_L pore formation, 5 μM Bcl-x_L–His_6 was preincubated with BH3I-2 or Bak BH3 peptide in 50 μl of 5 mM sodium citrate, 150 mM NaCl (pH 4.0) buffer for 10 min at 25 °C, followed by addition of 5 μl of undiluted liposomes. Before determination of the fluorescence, the pH was adjusted by the addition of 10 μl of 1.5 M Tris–HCl, pH 7.5.

NMR spectroscopy

Sequential assignments were achieved as described previously[22]. $^1H/^{15}N$ HSQC spectra were recorded by adding different amounts of BH3Is and Bak BH3 peptide into 300 μM ^{15}N-labelled Bcl-x_L/His_6. The determination of the K_i values of BH3Is was performed as described previously[46]. NOE transfers between BH3I-1 and Bcl-x_L were observed in the ^{14}N-filtered ^{15}N-edited NOESY-HSQC spectra recorded on 100% deuterated Bcl-x_L in water in accordance with ref. 47, with the exception that the ^1H evolution period was replaced with a semi-constant time[48] element and the phase of the second proton 90° pulse was adjusted to select protons that were not coupled to ^{15}N.

RECEIVED 5 JUNE 2000; REVISED 7 AUGUST 2000; ACCEPTED 13 SEPTEMBER 2000; PUBLISHED 17 JANUARY 2001.

1. Gross, A., McDonnell, J. M. & Korsmeyer, S. J. BCL-2 family members and the mitochondria in apoptosis. *Genes Dev.* **13**, 1899–1911 (1999).
2. Vander Heiden, M. G. & Thompson, C. B. Bcl-2 proteins: regulators of apoptosis or of mitochondrial homeostasis? *Nature Cell Biol.* **1**, E209–E216 (1999).
3. Tsujimoto, Y. & Shimizu, S. Bcl-2 family: life-or-death switch. *FEBS Lett.* **466**, 6–10 (2000).
4. Zha, J. *et al.* BH3 domain of BAD is required for heterodimerization with Bcl-x_L and pro-apoptotic activity. *J. Biol. Chem.* **272**, 24101–24104 (1997).
5. Diaz, J. L. *et al.* A common binding site mediates heterodimerization and homodimerization of Bcl-2 family members. *J. Biol. Chem.* **272**, 11350–11355 (1997).
6. Sattler, M. *et al.* Structure of Bcl-x_L–Bak peptide complex: recognition between regulators of apoptosis. *Science* **275**, 983–986 (1997).
7. Chang, B. S. *et al.* The BH3 domain of Bcl-x(S) is required for inhibition of the antiapoptotic function of Bcl-x(L). *Mol. Cell. Biol.* **19**, 6673–6681 (1999).
8. Holinger, E. P., Chittenden, T. & Lutz, R. J. Bak BH3 peptides antagonize Bcl-x_L function and induce apoptosis through cytochrome *c*-independent activation of caspases. *J. Biol. Chem.* **274**, 13298–13304 (1999).
9. Cosulich, S. C., Worrall, V., Hedge, P. J., Green, S. & Clarke, P. R. Regulation of apoptosis by BH3 domains in a cell-free system. *Curr. Biol.* **7**, 913–920 (1997).
10. Minn, A. J. *et al.* Bcl-x(L) forms an ion channel in synthetic lipid membranes. *Nature* **385**, 353–357 (1997).
11. Schendel, S. L. *et al.* Channel formation by antiapoptotic protein Bcl-2. *Proc. Natl Acad. Sci. USA* **94**, 5113–5118 (1997).

12. Antonsson, B. *et al.* Inhibition of Bax channel-forming activity by Bcl-2. *Science* **277,** 370–372 (1997).
13. Minn, A. J. *et al.* Bcl-x_L regulates apoptosis by heterodimerization-dependent and -independent mechanisms. *EMBO J.* **18,** 632–643 (1999).
14. Conus, S. *et al.* Bcl-2 is a monomeric protein: prevention of homodimerization by structural constraints. *EMBO J.* **19,** 1534–1544 (2000).
15. Schreiber, S. L. Chemical genetics resulting from a passion for synthetic organic chemistry. *Bioorg. Med. Chem.* **6,** 1127–1152 (1998).
16. Thompson, L. A. & Ellman, J. A. Synthesis and applications of small molecule libraries. *Chem. Rev.* **96,** 555–600 (1996).
17. McMillan, K. *et al.* Allosteric inhibitors of inducible nitric oxide synthase dimerization discovered via combinatorial chemistry. *Proc. Natl Acad. Sci. USA* **97,** 1506–1511 (2000).
18. Young, K. *et al.* Identification of a calcium channel modulator using a high throughput yeast two-hybrid screen. *Nature Biotechnol.* **16,** 946–950 (1998). (erratum, *Nature Biotechnol.* **16,** 1074 (1998)).
19. Dandliker, W. B., Hsu, M. L., Levin, J. & Rao, B. R. Equilibrium and kinetic inhibition assays based upon fluorescence polarization. *Methods Enzymol.* **74,** 3–28 (1981).
20. Li, H., Zhu, H., Xu, C. J. & Yuan, J. Cleavage of BID by caspase 8 mediates the mitochondrial damage in the Fas pathway of apoptosis. *Cell* **94,** 491–501 (1998).
21. Zhang, M., Zamore, P. D., Carmo-Fonseca, M., Lamond, A. I. & Green, M. R. Cloning and intracellular localization of the U2 small nuclear ribonucleoprotein auxiliary factor small subunit. *Proc. Natl Acad. Sci. USA* **89,** 8769–8773 (1992).
22. Lugovskoy, A. A. *et al.* Solution structure of the CIDE-N domain of CIDE-B and a model for CIDE-N/CIDE-N interactions in the DNA fragmentation pathway of apoptosis. *Cell* **99,** 747–755 (1999).
23. Chou, J. J., Li, H., Salvesen, G. S., Yuan, J. & Wagner, G. Solution structure of BID, an intracellular amplifier of apoptotic signaling. *Cell* **96,** 615–624 (1999).
24. McDonnell, J. M., Fushman, D., Milliman, C. L., Korsmeyer, S. J. & Cowburn, D. Solution structure of the proapoptotic molecule BID: a structural basis for apoptotic agonists and antagonists. *Cell* **96,** 625–634 (1999).
25. Cryns, V. & Yuan, J. Proteases to die for. *Genes Dev.* **12,** 1551–1570 (1998). (erratum, *Genes Dev.* **13,** 371 (1999)).
26. Hsu, Y. T. & Youle, R. J. Nonionic detergents induce dimerization among members of the Bcl-2 family. *J. Biol. Chem.* **272,** 13829–13834 (1997).
27. Mahajan, N. P. *et al.* Bcl-2 and Bax interactions in mitochondria probed with green fluorescent protein and fluorescence resonance energy transfer. *Nature Biotechnol.* **16,** 547–552 (1998).
28. Zha, J., Harada, H., Yang, E., Jockel, J. & Korsmeyer, S. J. Serine phosphorylation of death agonist BAD in response to survival factor results in binding to 14-3-3 not BCL-X(L). *Cell* **87,** 619–628 (1996).
29. Vander Heiden, M. G., Chandel, N. S., Schumacker, P. T. & Thompson, C. B. Bcl-x_L prevents cell death following growth factor withdrawal by facilitating mitochondrial ATP/ADP exchange. *Mol. Cell* **3,** 159–167 (1999).
30. Xiang, J., Chao, D. T. & Korsmeyer, S. J. BAX-induced cell death may not require interleukin 1β-converting enzyme-like proteases. *Proc. Natl Acad. Sci. USA* **93,** 14559–14563 (1996).
31. Gross, A., Jockel, J., Wei, M. C. & Korsmeyer, S. J. Enforced dimerization of BAX results in its translocation, mitochondrial dysfunction and apoptosis. *EMBO J.* **17,** 3878–3885 (1998).
32. Matsuyama, S., Schendel, S. L., Xie, Z. & Reed, J. C. Cytoprotection by Bcl-2 requires the pore-forming α5 and α6 helices. *J. Biol. Chem.* **273,** 30995–31001 (1998).
33. Hajduk, P. J., Meadows, R. P. & Fesik, S. W. Discovering high-affinity ligands for proteins. *Science* **278,** 497–499 (1997).
34. Hajduk, P. J. *et al.* High-throughput nuclear magnetic resonance-based screening. *J. Med. Chem.* **42,** 2315–2317 (1999).
35. Muchmore, S. W. *et al.* X-ray and NMR structure of human Bcl-x_L, an inhibitor of programmed cell death. *Nature* **381,** 335–341 (1996).
36. Shimizu, S. & Tsujimoto, Y. Proapoptotic BH3-only bcl-2 family members induce cytochrome *c* release, but not mitochondrial membrane potential loss, and do not directly modulate voltage-dependent anion channel activity. *Proc. Natl Acad. Sci. USA* **97,** 577–582 (2000).
37. Finucane, D. M., Bossy-Wetzel, E., Waterhouse, N. J., Cotter, T. G. & Green, D. R. Bax-induced caspase activation and apoptosis via cytochrome *c* release from mitochondria is inhibitable by Bcl-x_L. *J. Biol. Chem.* **274,** 2225–2233 (1999).
38. Eskes, R., Desagher, S., Antonsson, B. & Martinou, J. C. Bid induces the oligomerization and insertion of Bax into the outer mitochondrial membrane. *Mol. Cell. Biol.* **20,** 929–935 (2000).
39. Kudla, G. *et al.* The destabilization of lipid membranes induced by the C-terminal fragment of caspase 8-cleaved Bid is inhibited by the N-terminal fragment. *J. Biol. Chem.* **275,** 22713–22718 (2000).
40. Decaudin, D., Marzo, I., Brenner, C. & Kroemer, G. Mitochondria in chemotherapy-induced apoptosis: a prospective novel target of cancer therapy. *Int. J. Oncol.* **12,** 141–152 (1998).
41. Reed, J. C. Bcl-2: prevention of apoptosis as a mechanism of drug resistance. *Hematol. Oncol. Clin. North Am.* **9,** 451–473 (1995).
42. Miayake, H., Tolcher, A. & Gleave, M. E. Chemosensitization and delayed androgen-independent recurrence of prostate cancer with the use of antisense Bcl-2 oligodeoxynucleotides. *J. Natl Cancer Inst.* **92,** 34–41 (2000).
43. Jansen, B. *et al.* Bcl-2 antisense therapy chemosensitizes human melanoma in SCID mice. *Nature Med.* **4,** 232–234 (1998).
44. Baba, M., Iishi, H. & Tatsuta, M. *In vivo* electroporetic transfer of bcl-2 antisense oligonucleotide inhibits the development of hepatocellular carcinoma in rats. *Int. J. Cancer* **85,** 260–266 (2000).
45. Kluck, R. M., Bossy-Wetzel, E., Green, D. R. & Newmeyer, D. D. The release of cytochrome *c* from mitochondria: a primary site for Bcl-2 regulation of apoptosis. *Science* **275,** 1132–1136 (1997).
46. Johnson, P. E., Tomme, P., Joshi, M. D. & McIntosh, L. P. Interaction of soluble cellooligosaccharides with the N-terminal cellulose-binding domain of *Cellulomonas fimi* CenC 2. NMR and ultraviolet absorption spectroscopy. *Biochemistry* **35,** 13895–13906 (1996).
47. Talluri, S. & Wagner, G. An optimized 3D NOESY-HSQC. *J. Magn. Reson. B* **112,** 200–205 (1996).
48. Grzesiek, S. & Bax, A. Amino acid type determination in the sequential assignment procedure of uniformly $^{13}C/^{15}N$-enriched proteins. *J. Biomol. NMR* **3,** 185–204 (1993).

ACKNOWLEDGEMENTS
We thank C. Thompson, S. Korsmeyer, R. Reed and L. Bergeron for their gifts of the cells and expression vectors; R. Fathi, J. D. Gross, J. Tuttle, A. Fahmy and G. Heffron for experimental assistance; and R. King, B. Antonsson, A. Sinskey, P. Sorger, R. Ward, O. Gozani and N. Moerke for helpful discussions. A.D. is a recipient of a postdoctoral fellowship from the American Cancer Society. This work was supported in part by the American Heart Association Established Investigatorship and NIH grants to J.Y., by an NIH grant to G.W. and by a research grant from Biomeasure to M.C. The Institute of Chemistry and Cell Biology is supported by NIH, Merck & Co. Inc. and Merck KGaA, Darmstadt, Germany. Acquisition and maintenance of the spectrometers and computers are supported by the Giovanni Armenise-Harvard Foundation for Advanced Scientific Research.
Correspondence and requests for materials should be addressed to J.Y.